Sedimentologika

Research article

Tectonic, eustatic and climate controls on facies architecture during the transition to the Neoproterozoic icehouse in the Adelaide Superbasin, Australia

Georgina M. Virgo[1]*, Alan S. Collins[1], Morgan L. Blades[1], Kathryn J. Amos[2]

[1] Tectonics and Earth Systems (TES) and Mineral Exploration CRC, Discipline of Earth Sciences, The University of Adelaide, SA 5005, Australia
[2] Discipline of Earth Sciences, School of Physics, Chemistry and Earth Sciences (PCES), The University of Adelaide, SA 5005, Australia

*corresponding author: Georgina M. Virgo (georgina.virgo@adelaide.edu.au)

doi: 10.57035/journals/sdk.2023.e11.1083

Editors: Giovanna Della Porta and Or Bialik
Reviewers: Paula Castillo and John Counts
Copyediting, layout and production: Romain Vaucher, Farid Saleh and Sophie Hage

Submitted: 07.02.2022
Accepted: 27.06.2023
Published: 26.07.2023

Abstract | The Tonian to Cryogenian (ca. 1000–635 Ma) marks a crucial turning point in Earth's history, where tectonic reorganisation and fluctuating oceanic and atmospheric geochemistry plunged the globe into icehouse conditions. This was followed by a postglacial warming period that delivered large volumes of nutrients to the oceans and stimulated eukaryotic evolution. The Adelaide Superbasin in South Australia hosts a thick repository of Neoproterozoic and lower Cambrian sedimentary successions that preserve the depositional conditions during this unique time. In this study, detailed sedimentological data were collected from over 8,350 m of measured section at seven locations across the northern Flinders Ranges. Tonian deposits reveal a carbonate platform setting, where deposition was controlled by basin geometry and proximity to uplifted source areas. In the early Cryogenian, sedimentary successions were affected by the Sturtian glaciation, characterised by two glacial advance-retreat phases that coincide with climatically driven regression. The end of the Sturtian glaciation was marked by basin subsidence and widespread transgression into a more distal subaqueous environment. Despite the lithostratigraphic and sequence stratigraphic similarity between Tonian–Cryogenian successions globally, their correlation remains contentious. The influence of local tectonic regimes during the Tonian created a potential oceanic restriction between developing basins, which challenges the chemostratigraphic correlation between these deposits. Further, limited geochronological ages and opposing interpretations of glacial cyclicity puts into question the timing and extent of the Sturtian glaciation. Conversely, the post glacial transgression appears to be the most globally consistent as it results from climatically controlled sea level rise that was driven by melting ice sheets.

Lay summary | This study establishes a sequence stratigraphic framework and facies architecture for between ca. 800 and 650 Ma in the northern Flinders Ranges, South Australia. Seven major stratigraphic sequences were characterised and coincide with changes in tectonic regimes, climate, eustacy and sediment input into the basin. Deposition in carbonate platform environments during the Tonian was largely controlled by basin geometry and proximity to sediment sources. Two glacial advance-retreat cycles recorded in syn-glacial successions correspond to climatically driven changes in eustacy in a glaciomarine setting. Fine-grained post-glacial successions represent a widespread transgression to more distal subaqueous settings associated with melting of continental ice sheets following the Sturtian glaciation.

Keywords: Neoproterozoic, sedimentology, sequence stratigraphy, Adelaide Rift Complex

1. Introduction

The Neoproterozoic (ca. 1000 to 539 Ma) was one of the most dynamic eras in Earth's history and is marked by significant tectonic, biological, atmospheric, and climatic events. These include a supercontinent cycle, with the breakup of Rodinia and amalgamation of Gondwana (Li et al., 2008; Merdith et al., 2017; 2019; 2021); evolution from a prokaryote- to a eukaryotic-dominated biosphere (Butterfield, 2011; Lenton et al., 2014; Brocks et al., 2017);

the Neoproterozoic Oxygenation Event (Shields-Zhou & Och, 2011); and vast low-latitude glaciations that have been referred to as "Snowball Earth" (Kirschvink, 1992; Hoffman et al., 1998; 2017b). These global shifts facilitated the development of a suite of depositional settings under vastly contrasting conditions, from warm shallow carbonate-rich seas to cold, ice-covered continents (Hoffman et al., 1998; 2017b; Halverson et al., 2009; Brocks et al., 2017). Palaeoenvironments varied not only on a global scale, but also at a local level within the confines of sedimentary basins. The Adelaide Superbasin in South Australia (Lloyd et al., 2020), preserves thick successions of these Neoproterozoic sedimentary rocks, recording the temporal and spatial variability and distribution of environments through the Tonian (ca. 1000–720 Ma), Cryogenian (ca. 720–635 Ma), Ediacaran (ca. 635–539 Ma), and Cambrian (ca. 539–485 Ma).

Literature from early studies in South Australia provide a foundation for the stratigraphy and tectonic evolution of the Adelaide Superbasin (e.g., Howchin, 1929; Segnit, 1939; Mawson & Sprigg, 1950; Preiss, 1987; Preiss et al., 1993), while contemporary sedimentological research presents more detailed analyses of specific formations and locations within the basin (Hill & Walter, 2000; McKirdy et al., 2001; Frank & Fielding, 2003; Giddings et al., 2009; Giddings & Wallace, 2009a, 2009b; Preiss et al., 2009, 2011; Fromhold & Wallace, 2011, 2012; Grey et al., 2011; Hood et al., 2011, 2016, 2018; Hood & Wallace, 2012, 2014, 2015; Le Heron et al., 2011, 2011a, 2014; Busfield & Le Heron, 2014; Lechte & Wallace, 2015, 2016; Wallace et al., 2015; Counts et al., 2016; Cox et al., 2018; Corkeron & Slezak, 2020; O'Connell et al., 2020; Virgo et al., 2021). In addition, advances in understanding the chronostratigraphy and provenance of the superbasin have established a firmer temporal framework and tectonic setting for the evolving basin (Cox et al., 2018; Armistead et al., 2020; Lloyd et al., 2020; 2022). Although these studies have contributed immensely to our understanding of Neoproterozoic palaeoenvironments and stratigraphic evolution through this time, they have not captured the wider facies architecture across the basin. In particular, basin-scale architecture within the context of sequence stratigraphic changes related to active rifting and climatically driven sea level fluctuations, which resulted from the breakup of Rodinia and the Cryogenian glaciations.

Further, there have been a number of notable studies through Neoproterozoic strata at other sites globally, including Namibia (Frimmel et al., 1996; Hoffman & Halverson, 2008; Le Heron et al., 2013; Miller, 2013; Hood et al., 2015; Lechte & Wallace, 2016; Hoffman et al., 2017a; 2021; Lamothe et al., 2019), northern Ethiopia (Alene et al., 2006; Avigad et al., 2007; Miller et al., 2009; 2011; Swanson-Hysell et al., 2015; Park et al., 2020), Scotland (Spencer & Spencer, 1972; Glover & Winchester, 1989; Smith et al., 1999; Anderson et al., 2013; Stephenson et al., 2013; Fairchild et al., 2017; Ali et al., 2018), Svalbard (i.e., Norway, Halverson et al., 2004; 2011; 2017; 2022; Maloof et al., 2006; Hoffman et al., 2012; 2017a; Kunzmann et al., 2015; Fairchild et al., 2016; 2016a; Millikin et al., 2022), western USA (Link et al., 1994; Crittenden et al., 1983; Lund et al., 2003; Fanning & Link, 2004; Link & Christie-Blick, 2011; Keeley et al., 2012; Balgord et al., 2013; Busfield & Le Heron, 2016; Le Heron & Busfield, 2016; Le Heron et al., 2020; Nelson et al., 2020; 2021), northern Canada (Chartrand & Brown, 1985; Park & Jefferson, 1991; Eisbacher, 1985; Narbonne et al., 1994; Narbonne & Aitken, 1995; Batten et al., 2004; Long & Turner, 2013; Milton et al., 2017) and south China (Wang & Li, 2001; Li et al., 2003; Zhang et al., 2008; Zhang et al., 2011; Lan et al., 2015; Lan et al., 2015; Busigny et al., 2018). These studies have investigated the lithostratigraphic variation across each respective basin, and the subsequent relationship with shifting climate and tectonic regimes. Although many of these changes are local, global climatic fluctuations and tectonic reorganisation could also be responsible for the major temporal and spatial variability in stratigraphy, potentially providing a platform from which these sections may be correlated globally.

In this study, we use detailed sedimentological data collected from multiple sites across the northern Flinders Ranges to construct a sequence stratigraphic framework and correlate facies across the width of the Adelaide Superbasin during the Neoproterozoic. This is achieved through extensive analyses of grain sizes, sedimentary structures, bedding thicknesses, and palaeocurrent directions, followed by lithostratigraphic correlations and the interpretation of sequence stratigraphic boundaries and palaeoenvironmental settings. The temporal and spatial distributions of depositional environments can subsequently be correlated to other basins across the globe in order to better differentiate local vs. global influence in tectonic and palaeoclimatic regimes during the Tonian and Cryogenian. As one of the most well-preserved and understudied Precambrian basins in the world, the Adelaide Superbasin therefore provides a window into an important and unique time in Earth's past.

2. Geological setting

The Adelaide Rift Complex (Figure 1) lies within the Adelaide Superbasin and forms a thick repository of sedimentary rocks that preserve a record of Earth surface systems throughout the Neoproterozoic and early Cambrian. The northern part of this ~750 km north–south trending basin started as a half graben fault-controlled rift basin that initiated during the breakup of Rodina as Laurentia rifted from Australia-east Antarctica (Merdith et al., 2019). The basin then developed into an aulacogen (continentward of a passive margin) during the late Proterozoic (Lloyd et al., 2022). Tonian sediments were transported into the basin from the surrounding rift shoulders, which were focused at the time along a NW–SE rift valley that formed the present day Willouran Ranges (Figure 1; Preiss, 2000; Lloyd et al., 2020). The start of the Cryogenian was characterised by widespread erosion

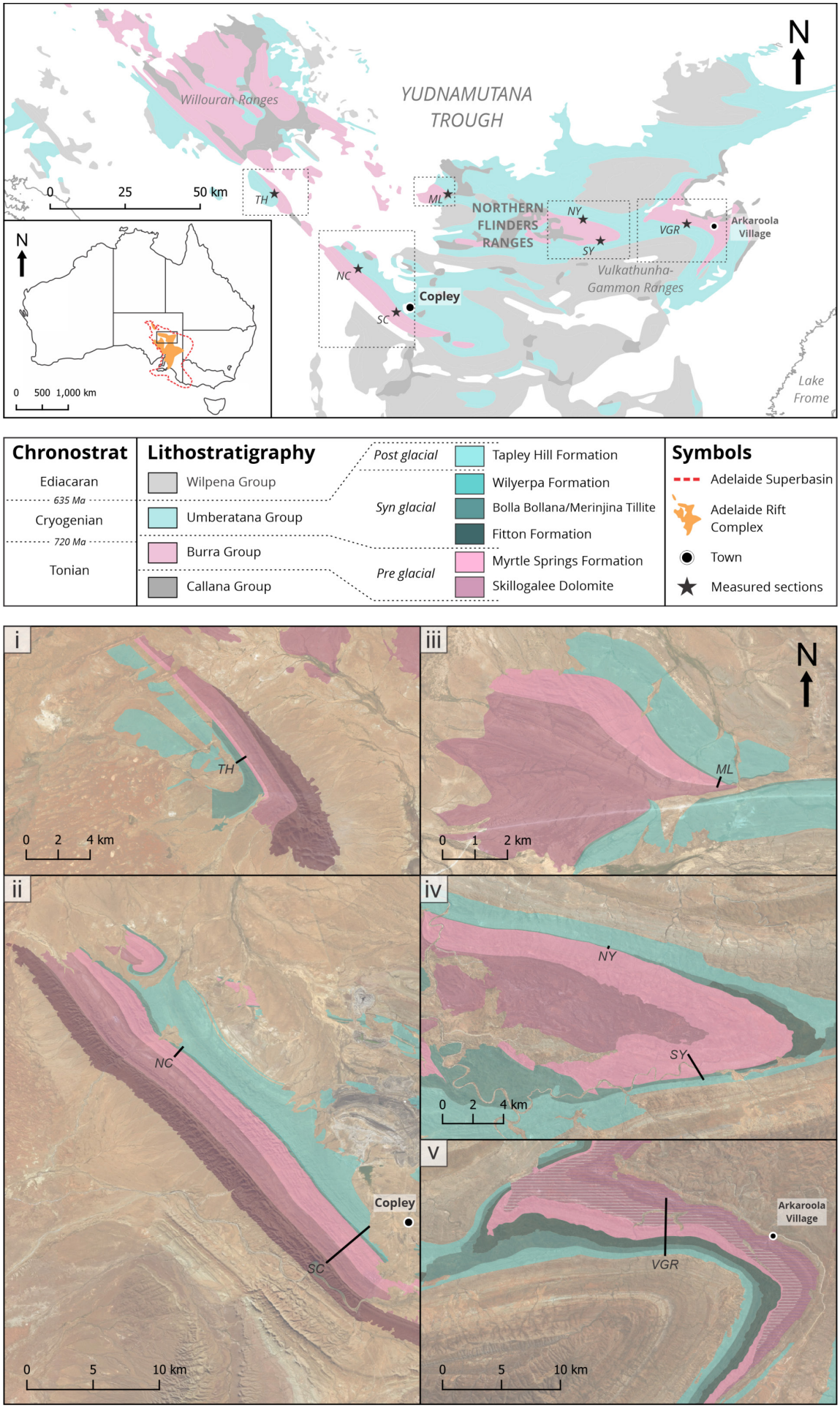

Figure 1 | Geological map of Neoproterozoic lithostratigraphic groups in the Adelaide Rift Complex, northern Flinders Ranges, South Australia. Insert shows position of Adelaide Rift Complex within Australia. Satellite images of fieldwork locations overlain by stratigraphic formations. Black line denotes the location of the section measured. (i) TH = Termination Hill (ii) NC = North Copley, SC = South Copley (iii) ML = Mount Lyndhurst (iv) NY = North Yankaninna, SY = South Yankaninna (v) VGR = Vulkathunha-Gammon Ranges.

across the basin during the Sturtian glaciation, followed by a second period of sedimentation focused in the northwest and sourced from the reactivated rift shoulders (Lloyd et al., 2020). Deposition was terminated at the onset of the Delamerian Orogeny (ca. 514 Ma; Preiss, 2000; Foden et al., 2006; 2020), and the subsequent folding, uplift and erosion exposed the Neoproterozoic rocks as the modern Flinders Ranges of South Australia (Figure 1).

The Neoproterozoic sedimentary rocks are divided lithostratigraphically into the Callana, Burra, Umberatana, and Wilpena groups (Thomson et al., 1964; Preiss et al., 1998; Preiss & Cowley, 1999; Preiss, 2000; Preiss et al., 2011; Lloyd et al., 2020), where deposits of the Tonian and Cryogenian periods correspond to the Burra and Umberatana groups, respectively (Figure 1; Mawson & Sprigg, 1950; Thomson et al., 1964; Lloyd et al., 2020). Formation nomenclature varies across the basin and largely arises from the locally derived classification of type sections (Preiss & Cowley, 1999). Overall, the Burra Group in the northern Flinders Ranges can be subdivided into three units. There is a basal quartzite, which has several designations that corresponds to the location of the measured sections and reflects an overall deltaic environment (Preiss, 1987). This transitions into the Skillogalee Dolomite, a carbonate (magnesite and dolomite) dominated succession with minor clastic interbeds that is interpreted to represent a paralic/marginal marine setting (Belperio, 1990; Frank & Fielding, 2003). The top of the Burra Group in the northern Flinders Ranges is marked by the Myrtle Springs Formation, a dominantly fine-grained clastic unit with minor carbonate interbeds, which reflect deposition in a subtidal to marginal marine environment (Preiss, 1987, 2000). The base of the Umberatana Group corresponds to the Sturtian glaciation and is represented by diamictite successions that are separated by finer-grained clastic beds that represent an overall glaciomarine setting (Link and Gostin, 1981; Young & Gostin 1988; 1990; 1991). Several of these diamictite successions have tillite nomenclature that are in the process of being synthesized and reclassified to the Sturt Formation (Lloyd et al., 2023). This is overlain by the Wilyerpa/Lyndhurst Formation, which defines the onset of deglacial conditions and is dominated by fine-grained clastic lithofacies that are dropstone rich, reflecting deposition in a proglacial setting. This is succeeded by an extensive post-glacial carbonate and shale unit that is termed the Tapley Hill Formation and represents a shift to a slope to basinal environment (Preiss, 1987). This formation includes a basal shale member, Tindelpina Shale Member, which directly overlies glaciogenic rocks (Thomson et al., 1964; Preiss, 1987). The Tapley Hill Formation and its basal member are widespread and were deposited not only in the northern Flinders Ranges but across the basin.

Chronostratigraphic constraints are provided by U–Pb zircon ages from tuffs and volcanic units as well as from the youngest zircons preserved in detrital successions. Age constraints on the Tonian succession are provided by a maximum depositional age (MDA) of 893 ± 9 Ma from the basal sequence in the Callana Group (Lloyd et al., 2022). This complements the 802 ± 10 Ma depositional age of the Rook Tuff in the Willouran Ranges (Fanning et al., 1986), which sits stratigraphically below the Burra Group (Preiss et al., 2009; Lloyd et al., 2020). Igneous zircon grains from the base of the overlying Burra Group have been dated and provide depositional ages of 788 ± 6 Ma (Boucaut Volcanics, Armistead et al., 2020) and 794 ± 4 Ma (Kooringa Member, Preiss et al., 2009). These are stratigraphically equivalent to the base of the Skillogalee Dolomite Formation in this study (Lloyd et al., 2020). In the Cryogenian, a new in-situ Rb-Sr age of 684 +/- 37 Ma dates deposition of the interglacial shales within the Sturt Formation (Lloyd et al. 2023). The Wilyerpa Formation of the Umberatana Group is constrained from a precise tuff age of 663.03 ± 0.76 Ma (zircon U–Pb CA-ID-TIMS; Cox et al., 2018) collected from the South Copley section. The base of the Wilpena Group is constrained by an MDA of 654 ± 11 Ma (Seacliff Sandstone, van der Wolff, pers. comms., 2020) from the Southern Mount Lofty Ranges, which is stratigraphically equivalent to the "cap carbonate" (Nuccaleena Formation) of the Marinoan glaciation in the northern Flinders Ranges (Lloyd et al., 2020). Up-section, an MDA of 630 +/- 16 Ma (ABC Range Quartzite, Lloyd et al., 2020) collected from the Willouran Ranges defines the middle of the Wilpena Group.

3. Methods

This study encompasses several field sites located across the northern Flinders Ranges (Figure 1). Site selection was based on previous geological mapping (Coats, 1973), access to site location, geographic spread, and stratigraphic thickness. Coordinates for each section were recorded with a handheld GPS and the stratigraphy was measured bed by bed at approximately one metre-resolution using a tape measure. Detailed descriptions of grain size, sedimentary structures, bedding thicknesses and palaeocurrent direction were recorded (Supplementary Figures 1–7).

Sedimentary logs produced in the field were digitised using EasyCore software and palaeocurrent data were analysed with the software Stereonet. Lithofacies were classified based on grain size and sedimentary structures (Table 1). The lithofacies were then grouped into facies associations (Table 2), which were determined by the stacking pattern of facies. Each facies association represents multiple depositional processes in a genetically related interval (Catuneanu, 2006). All these elements were used together to interpret the depositional environments throughout each section. Lithofacies, facies associations and interpreted depositional environment are presented within the sedimentary logs in Supplementary Figures 1–7.

The spatial and temporal distribution of depositional environments across the northern Flinders Ranges was incorporated into a sequence stratigraphic model based on lithofacies stacking patterns and stratigraphic

Lithofacies	Descriptions	Depositional Processes	Occurrence
LF1 Laminated mudstone	Fresh medium grey to dark brown/blue; weathered red, pink, purple, blue green and white; planar and wavy laminated (mm to cm scale); occasional inverse grading, mud to very fine silty mud; occasionally dolomitic (SY, VGR); rare crude laminations (mm scale) to massive (SC, SY); rare dropstones (gravel to cobble clasts), soft sediment deformation (convolute, simple load cast and flame structures), subcritical (15° climb) climbing ripples (~20 cm stoss, 5 cm foresets) (SC)	Fine grained material - settled out of suspension, lower flow regime, slow sedimentation rate (Boggs, 2014; Yawar & Schieber, 2017); ice-rafted debris - transported in floating ice and deposited as rainout (e.g., Link & Gostin, 1981; Young & Gostin, 1988; 1991; Powell, 2002; Eyles et al., 2007; Preiss et al., 2011; Boggs, 2014; Le Heron et al., 2013; 2014; 2021; Le Heron & Busfield, 2016); soft sediment deformation - liquefaction induced from rapid sedimentation (Postma, 1983; Stromberg & Bluck, 1998; Moretti et al., 2001); convolute laminations - bottom current reworking (Shanmugam, 1997), earthquakes (Shanmugam, 2017), or submarine slumping (Stow & Mayall, 2000; Strachan, 2008); simple load casts and flame structures - formed in response to differential sediment densities or lateral loading during liquefaction (Owen, 2003); subcritical climbing ripples - deceleration of turbulent current activity and net deposition (high sediment supply and rapid sedimentation rate), stoss-side erosion and bedform migration (Ashley et al., 1982; Young & Gostin, 1988; Baas et al., 2000; Jobe et al., 2012; Boggs, 2014; Le Heron & Busfield, 2016; Maciaszek et al., 2019)	SC, NY, SY, VGR
LF2 Laminated siltstone	Fresh light grey/blue/purple to dark brown; weathered white, yellow, orange, pink, red; planar and wavy laminated (mm to cm scale); occasionally crude planar laminated (mm scale) and massive; occasional normal and inverse grading, silt to very fine sandy silt; occasionally dolomitic; soft sediment deformation (convolute, load and fold and drag structures) (SC, VGR); rare gravel lags in base of bed (SC); rare shrinkage cracks, connected branches and polygons (NC); debrite breccia, randomly orientated angular boulder clasts of well-laminated silt	Fine grained material – same as LF1; soft sediment deformation – same as LF1; gravel lag - winnowing unidirectional flows, high sediment supply and rapid deposition (Boggs, 2014); connected branches and polygons - subaqueous shrinkage of cohesive sediment caused by compaction during burial, filled with overlying coarse sediment (Plummer & Gostin, 1981; Tanner, 1998; Pflueger, 1999; McMahon et al., 2017); breccia – gravitational debris flow (Thomson et al., 2014; Wallace et al., 2015; Thorie et al., 2020)	All sections
LF3 Rippled and cross-stratified siltstone	Light grey/purple to green; very fine silt; thin laminations (mm to cm scale), occasionally black minerals (VGR); occasionally dolomitic (NC, SY, VGR); concave-down (hummock) and concave-up (swale) ripple cross laminations (1 cm to 15 cm scale foresets), cross sets marked by curved erosional surfaces, occasionally bimodal (SY); occasional reactivation surfaces (SY, VGR) and mud drapes (SY); rare supercritical (60° climb) climbing ripples (~3 cm stoss, 5 cm foresets) (NC); rare straight crested symmetrical ripples (cm scale wavelengths) (VGR), and shrinkage cracks, connected branches and polygons (NC), and branching spindles (VGR)	Hummocky and swaley cross stratification - suspended load, decreasing flow regime (storm activity), waning combined unidirectional and oscillatory flow (Nottvedt & Kreisa, 1987; Arnott & Southard, 1990; Cheel, 1991; Duke et al., 1991; Cheel & Leckie, 1993; Dumas & Arnott, 2006; Reading, 2009; Basilici et al., 2012; Boggs, 2014); bimodal ripple cross lamination – lower flow regime, unidirectional tidal flow, downcurrent migration of small sinuous and catenary ripples (Ashley, 1990; Colquhoun, 1995; Chakrabarti, 2005; Reading, 2009; Daidu, 2013; Davis, 2013; Boggs, 2014; Thomson et al., 2014; Momta et al., 2015; Jorissen et al., 2018); reactivation surfaces – foreset erosion due to changing flow conditions (Mowbray & Visser, 1984; Daidu, 2013; Davis, 2013); mud drapes - settle out of suspension during slackwater (Reineck & Wunderlich, 1968; Bhattacharya, 1997; Daidu, 2013; Davis, 2013; Boggs, 2014); supercritical climbing ripples – same as LF1, stoss-side preservation, increasing rate of suspension sedimentation and decreasing bedform migration (Jobe et al., 2012); symmetrical ripples - traction transport as bedload, lower flow regime, oscillatory flow (Reading, 2009; Boggs, 2014; Counts et al., 2016); connected branches and polygons - desiccation during exposure (Plummer & Gostin, 1981; Boggs, 2014); branching spindles – same as LF2 (Donovan & Foster, 1972)	SC, NC, ML, SY, VGR
LF4 Heterolithic siltstone and sandstone	Fresh light grey/yellow/brown; weathered white, orange, purple to dark brown/red/black; feldspathic and quartzitic; normal and inverse grading, silt and fine sand; bifurcated wavy connected and disconnected mud flasers, mm thickness (flaser bedding), concavely and convexly bowed, fill sand ripple troughs and overlie sand ripple crests (CQ), both curve crested current ripples and bidirectional ripples (SY); mud layer drapes complete sand ripples (wavy bedding) (SY, VGR); mud layer drapes discontinuous and continuous bidirectional sand ripples, cm thickness (lenticular bedding) (VGR); mud layer drapes connected unidirectional sand ripples, up to 3 cm thickness (SY); rare shrinkage cracks, partially connected branches and rectangular to hexagonal polygons, multiple generations (SY, VGR)	Bedload and suspended load, alternating high and low energy flows, rippled sand deposited from energetic turbulent flow, mud drapes settle out of suspension during slackwater (Reineck & Wunderlich, 1968; Bhattacharya, 1997; Daidu, 2013; Davis, 2013; Boggs, 2014; Maciaszek et al., 2019); flaser bedding – highest energy flows, unidirectional and bidirectional (tidal and wave currents); wavy bedding – moderate energy flows, unidirectional (tidal current); lenticular bedding – lowest energy flows, bidirectional and unidirectional (tidal and wave currents); partially connected branches and polygons – same as LF3	SY, VGR
LF5 Laminated sandstone	Fresh light grey/yellow/brown; weathered white, orange, green, purple to dark brown/red/black; feldspathic and quartzitic; normal and inverse grading, very fine to fine sand; planar and wavy laminated (mm to cm scale), occasional thin black laminations (NC); occasional crude laminations to massive; rare small (5 cm to 15 cm scale) scour and fill structure (SY, VGR); rare dropstones (pebble to boulder clasts) (SY, VGR); soft sediment deformation (convolute, simple load cast structures) (VGR); rare gravel lags in base (VGR); rare shrinkage cracks, partially connected branches (VGR)	Planar laminated - traction transport as bedload, upper flow regime, unidirectional laminar flow (Cheel, 1990; Bridge, 2009; Boggs, 2014; Jorissen et al., 2018); wavy laminations - bedload and suspended load, lower flow regime, unidirectional flow (Colquhoun, 1995; Bridge, 2009; Boggs, 2014; Momta et al., 2015; Jorissen et al., 2018); scour and fill structure - erosion from high velocity flow, filled by coarse material during waning stage of flow (Fielding, 2006; Bridge, 2009; Boggs, 2014); ice-rafted debris – same as LF1; soft sediment deformation – same as LF1; gravel lags - same as LF2; partially connected branches - same as LF3	All sections
LF6 Rippled and cross-stratified sandstone	Light grey/yellow/orange/brown to dark brown; weathered white, orange, purple to dark brown/red; feldspathic and quartzitic; normal and inverse grading, very fine to coarse sand; occasional thin black laminations (NC, SY, VGR); concave-down (hummock) and concave-up (swale) ripple cross laminations (10 cm foresets), cross sets marked by curved erosional surfaces, occasional mud drapes on foresets (10 cm foresets) (NC, SC, VGR); occasional small trough cross stratification (cm scale foresets), occasionally bimodal (NC, SY, VGR); occasional sand lenses (cm scale), rare tabular cross stratified (40 cm foresets) (VGR); rare symmetrical rippled (~10 cm scale wavelengths) and shrinkage cracks (SY, VGR); rare interference rippled (cm scale wavelengths), symmetrical and asymmetrical (SC)	Hummocky and swaley cross stratification – same as LF3; ripple cross lamination and mud drapes – same as LF3; trough - bedload and suspended load, lower flow regime, unidirectional flow, downcurrent migration of small scale ripples (Ashley, 1990; Bridge, 2009; Boggs, 2014; Momta et al., 2015); tabular - traction transport as bedload, lower flow regime, unidirectional flow, downcurrent migration of straight crested dunes (Ashley, 1990; Bridge, 2009; Boggs, 2014; Momta et al., 2015); symmetrical ripples – same as LF3; straight to bifurcating and terminating crests - decreasing flow velocities (Nelson & Voulgaris, 2014); interference ripples - lower flow regime, bidirectional and unidirectional flow (Colquhoun, 1995; Bridge, 2009; Boggs, 2014; Momta et al., 2015; Jorissen et al., 2018), two sets of current directions intersecting at high angles (Gough, 2020)	SC, NC, SY, VGR
LF7 Massive sandstone	Light grey/yellow/brown/blue to dark red; quartzitic; occasionally immature, lithics, angular to sub-rounded, fine sand to gravel; massive; occasional thin planar and wavy laminations; rare normal and inverse grading, very fine to coarse sand; rare scoured base (SC); rare thin, heavy mineral trough cross-laminations (SC); rarely dolomitic with silty matrix (TH)	Hyperconcentrated debris flows, rapid deposition; normal grading – high density turbidity current (Lowe, 1982; Kneller, 1995; Shanmugam, 2000; Winsemann et al., 2009; Talling et al., 2012; Le Heron & Busfield, 2016), inverse grading – kinetic sieving (Legros, 2002; Talling et al., 2012; Le Heron et al., 2014); scoured base – same as LF5; cross-laminations – same as LF3 OR low density turbidity current (Shanmugam, 1997; Talling et al., 2012)	SC, NC, TH, NY, SY, VGR
LF8 Ortho-conglomerate	Fresh light grey/brown/grey/green/blue, weathered dark grey/blue/black; clast supported (50% to 80% clasts); very coarse sand to cobble clasts (sub-angular to well-rounded), granite/quartzite/carbonate boulders, quartzite cobbles, carbonate pebbles; medium to coarse sand matrix; massive, inverse and normal grading; occasionally interlaminated or interbedded with silt (SY, NY); occasionally pierces top surface (SC); rare scoured base (SY)	Subaqueous hyperconcentrated debris flows, rapid deposition, non-cohesive, laminar flows (Lowe, 1982; Kneller, 1995; Shanmugam, 2000; Winsemann et al., 2009; Talling et al., 2012; Le Heron & Busfield, 2016); scoured base – same as LF5	SC, NC, NY, SY, VGR
LF9 Stratified diamictite	Light blue/purple/green/brown/red; thin (cm scale) planar laminations; silt to fine sand matrix; often clast-poor (<15% clasts); quartzite/carbonate/conglomerate boulder, quartzite/carbonate/basaltic cobbles and quartzite/sand gravel, casts; occasionally clast-rich (30-60% clasts), granite/quartzite boulders/cobbles, carbonate pebbles and sand pebbles/cobbles, casts (SC, NY, VGR); rare inverse and normal grading (SC, VGR); rare scoured base (NY, SY); rarely carbonaceous (TH)	Subaqueous sediment gravity flow (Young & Gostin, 1988; Anderson, 1989; Eyles et al., 2007; Le Heron et al., 2013; 2014); stratification - sorting through clast settling (Anderson, 1989) OR current reworking (Boggs, 2014); scoured base – same as LF7	SC, TH, NY, SY, VGR

Table 1 | Lithofacies and their subsequent characteristics and depositional processes and occurrence throughout the measured section. LF = lithofacies. SC = South Copley, NC = North Copley, TH = Termination Hill, ML = Mount Lyndhurst, NY = North Yankaninna, SY = South Yankaninna, VGR = Vulkathunha-Gammon Ranges.

LF10 Massive diamictite	Light grey/green/yellow/brown/red; matrix to clast supported (<5% - 60% clasts); quartzite/granite/carbonate/sandstone boulders (up to 1.5 m), quartzite/carbonate/sandstone/granite cobbles/pebbles, conglomerate fragments, and casts; mud to fine sand matrix; inverse and normal grading; occasionally dolomitic (VGR, TH)	Slow deposition directly from the ice as melt-out (Link & Gostin, 1981; Young & Gostin, 1988; Preiss et al., 2011) OR cohesive debris flows, moderate to high strength (Talling et al., 2012); rapid deposition (Young & Gostin, 1988; Anderson, 1989; Eyles et al., 2007; Le Heron et al., 2013; 2014), kinetic sieving during flows (Legros, 2002; Talling et al., 2012; Le Heron et al., 2014)	All sections
LF11 Massive dolostone	Fresh brown/blue/grey, weathered white/yellow/pink/red; elephant skin weathering style; occasional laminated weathering style (NC, TH, SY); rarely ferruginous (SY); rare shrinkage cracks, multiple generations (NC)	Authigenic precipitation from the water column, due to chemical, salinity or temperature fluctuations (Tucker, 1982; Tucker & Wright, 2009; Flügel, 2010) OR syn-sedimentary dolotimisation (mimetic replacement), carbonates retain primary textures and water column geochemical signatures (Hood et al., 2011; 2018; Hood & Wallace, 2012; 2014; Shuster et al., 2018); shrinkage cracks – same as LF3	SC, NC, TH, SY, VGR
LF12 Laminated dolostone	Fresh light yellow/brown/blue/grey, weathered white/yellow/orange/pink/red; fine crystalline texture; elephant skin weathering style; normal and inverse grading, thinly (mm to cm scale) planar laminated with fine (mud to silt) clastic material; occasionally wavy laminated and massive; small (cm scale) tepee structures, chert and breccia fills space under tepee crests (SC, VGR); rare thin black laminations (VGR); occasional soft sediment deformation (convolute structures) (VGR)	Dolostone material – same as LF11 OR secondary diagenetic recrystallisation (non-mimetic replacement), poorly preserves original carbonate textures (Tucker & Wright, 2009; Flügel, 2010); interlaminated clastic material - transported as suspended load, low energy tidal currents (O'Connell et al., 2020) or higher energy storm activity (Hoffman, 1976; Wanless et al., 1988; Tucker & Wright, 2009; Jahnert & Collins, 2012; Chiarella et al., 2017; Kunzmann et al., 2019; O'Connell et al., 2020); tepee structures - fracturing/crustal cracking, periods of desiccation (Asserto & Kendall, 1977; Kendall & Warren, 1987; Belperio, 1990; Frank & Fielding, 2003; Tucker & Wright, 2009; O'Connell et al., 2020); soft sediment deformation – same as LF1	All sections
LF13 Rippled and cross stratified dolostone	Grey/blue/black, weathered white/yellow/brown; thinly wavy laminated; fine crystalline texture; elephant skin weathering style; occasional dolostone layer drapes discontinuous and complete unidirectional sand ripples, cm thickness (lenticular and wavy bedding) (SY, VGR); rare large (8 cm wavelength, 3 cm height) (NY) and small (3 cm wavelength, 1 cm height) (NC) symmetrical ripples; rare ripple cross-laminations (5 cm foresets), obliquely stacked in opposing directions (NC, SC, ML); rare soft sediment deformation (convolute and buckled structures) (VGR); shrinkage cracks, partially connected branches (SY) and polygons (NC); shrinkage cracks, sinuous and curlicue cracks deposited in troughs of straight ripple sets (NC, VGR)	Dolostone material – same as LF11 and LF12; heterolithic stratification – same as LF4; symmetrical ripples – same as LF3; ripple cross-laminations – same as LF3; soft sediment deformation – same as LF1; partially connected branches and polygons – same as LF3; sinuous and curlicue cracks – same as LF2 (Gehling, 2000)	SC, NC, ML, SY, VGR
LF14 Massive dolostone	Fresh light blue/grey, weathered white/yellow/purple; crystalline texture; normal and inverse grading, fine to very coarsely crystalline; occasional thin (cm) planar laminated weathering style (SC, NC, ML); occasional faint wavy laminations (VGR); occasionally quartz rich and brecciated (VGR); rare concretions (nodular anhydrite?) (VGR); rare shrinkage cracks (NC)	Dolostone material – same as LF12; interlaminated clastic material – same as LF12; shrinkage cracks – same as LF2	SC, NC, TH, ML, SY, VGR
LF15 Layered microbialite	Fresh light blue/grey/yellow, weathered white; thin (mm to cm scale) stratiform and undulating dolomite laminations, interlaminated mud; rare thin black laminations (SY); occasional (1 cm to 10 cm scale) tepee structures (SY, TH, ML, VGR), brecciated material and chert replacement fills space under tepee crests (SC); occasional soft sediment deformation (convolute) (VGR), small (1 cm) load and flame structures (SC); occasional ripple cross-stratified and buckled (SY, ML); rare pseudocolumnar structures (SC); rare inverse grading, very finely to medium crystalline (SC, SY)	Microbial material - precipitated in-situ (authigenic) (Tucker, 1982; Tucker & Wright, 2009; Flügel, 2010); clastic material - trapped and bound by microbial material (Wright, 1984; Tucker & Wright, 2009; O'Connell et al., 2020); stratiform microbialite - suspended load, low flow regime, gentle current action (Hoffman, 1976; Wanless et al., 1988; Tucker & Wright, 2009; Jahnert & Collins, 2012; Chiarella et al., 2017; Kunzmann et al., 2019 O'Connell et al., 2020); small tepee structures – same as LF12; large tepee structures - crystallisation expansion in carbonate-supersaturated subaqueous conditions (Shinn, 1969; Kendall & Warren, 1987; O'Connell et al., 2020); soft sediment deformation – same as LF1; ripple cross-laminations – same as LF3	All sections
LF16 Microbialite buildup	Fresh light blue/grey to white/yellow; thin (cm scale) columnar and domical dolomite laminations, interlaminated (mud to silt) clastic material; hemispherical (SC, NC, ML), bulbous (ML) and nodular (SC, NC, TH, ML) domical buildup, cm scale; occasional domical and columnar bioherms (SC); rare columnar buildup, cm scale (SC); rare convex conical buildup (SC, ML), cm scale; rare brecciated material and chert replacement in domical buildups (SC); rarely mottled (SC, NC); rare inverse grading, very finely to medium crystalline (SC)	Microbial material – same as LF15; clastic material – same as LF15; microbialite buildup - suspended load, higher energy storm activity (Hoffman, 1976; Wanless et al., 1988; Tucker & Wright, 2009; Jahnert & Collins, 2012; Chiarella et al., 2017; Kunzmann et al., 2019 O'Connell et al., 2020)	SC, NC, ML
LF17 Magnesite mudstone	Light grey/cream to white; micritic; massive to laminated (cm scale); rare small (cm scale) tepee structures (SC); rare soft sediment deformation (convolute) (TH)	Magnesite material - precipitated in-situ, evaporative magnesium-rich water column (Mur & Urpinell, 1987; Warren, 1990; Melezhik et al., 2001); small tepee – same as LF12; soft sediment deformation – same as LF1	SC, TH
LF18 Intraclastic magnesite	Light grey/cream to white; massive to crudely laminated (cm scale); occasionally conglomerate (clast-rich), sub-angular to rounded clasts, mud to sand sized matrix; normal and inverse grading, gravel to very coarse-grained; rare undulating top surfaces and soft sediment deformation (convolute) (SC)	Magnesite material – same as LF17; conglomerate - reworked sedimentary magnesite (Uppill, 1980; Belperio, 1990; Preiss, 2000; Frank & Fielding, 2003; Counts, 2017); soft sediment deformation – same as LF1	SC, TH

Table 1 | (Continued)

relationships. Interpretations were then made as to the controls on sedimentary architecture within the basin (e.g., variations in accommodation and sediment input, driven by fluctuations in tectonism (i.e., subsidence or uplift), eustacy, and sediment supply; Catuneanu, 2006).

4. Results

4.1. Sedimentary logs

Summary graphic sedimentary logs for each of the measured sections are presented in Figure 2 and have a collective total stratigraphic thickness of 8,360 m. There are considerable variations in stratigraphic thicknesses and lithologies across the northern Flinders Ranges (Figure 2). However, the base of the measured sections was arbitrarily chosen, so thicknesses of the pre-glacial rocks do not reflect complete thicknesses of preserved stratigraphy.

On the western margin of the basin, the measured Skillogalee Dolomite intervals at Termination Hill (TH) and South Copley (SC) sections are 380 m and 925 m thick, respectively. This is represented by a carbonate-dominated succession of magnesite, dolomite and microbial lithologies with interbedded clastics. In the north-central zone of the basin at Mount Lyndhurst (ML), the stromatolite-dominated Skillogalee Dolomite unit is 48 m thick. In the east of the basin, in the Vulkathunha-Gammon Ranges (VGR), the 1040 m thick Skillogalee Dolomite unit records a shift to clastic-dominated deposition, characterised by siltstone and sandstone with minor dolostone and microbial carbonates. The overlying Myrtle Springs Formation varies in thickness from 80 m, 502 m, 966 m, 103 m, 21 m, and 848 m between the Termination Hill (TH), North

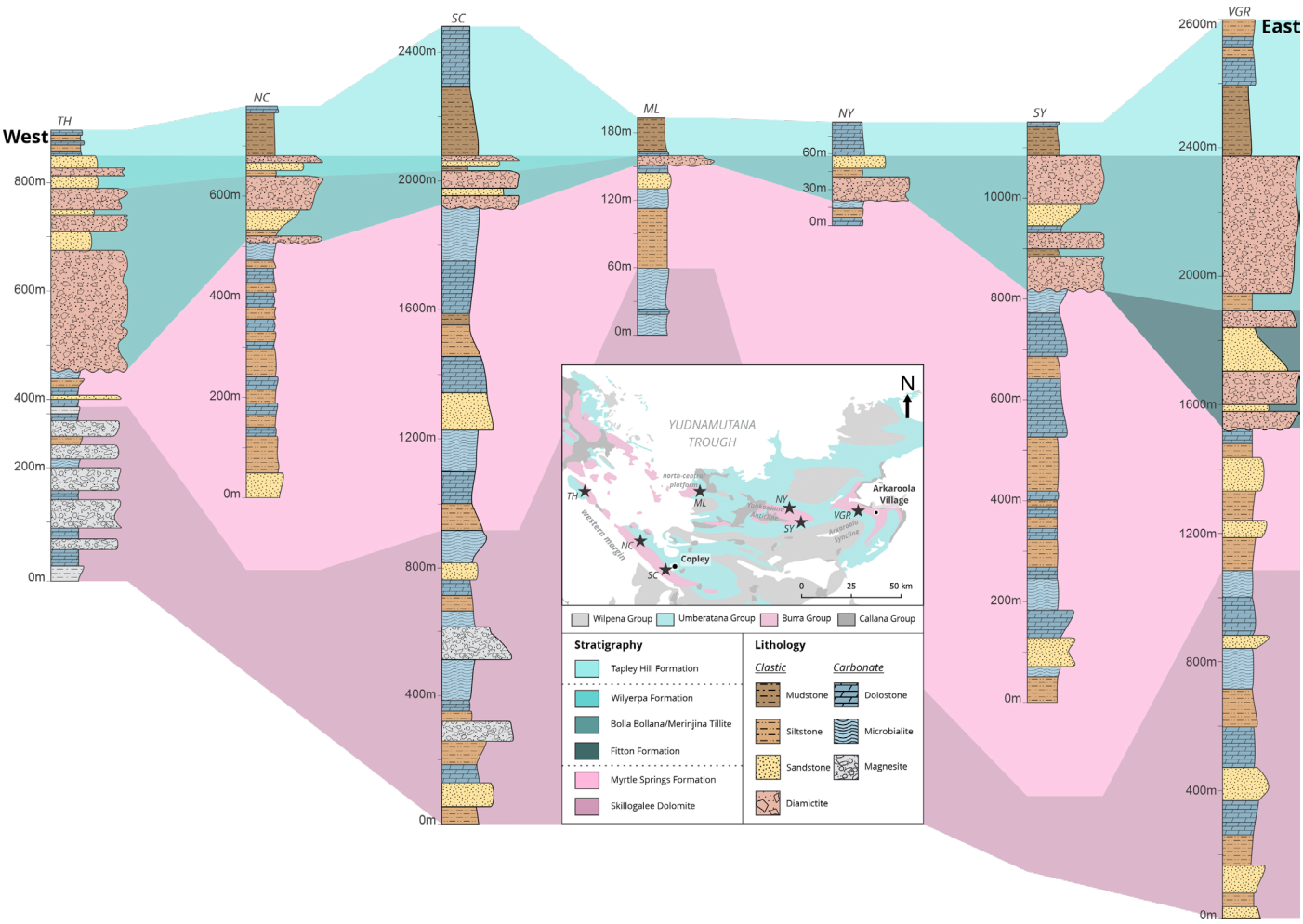

Figure 2 | Generalised sedimentary logs through Tonian–Cryogenian sections across the northern Flinders Ranges, South Australia. Coloured panels indicate correlation of stratigraphic formations between sections. TH = Termination Hill, NC = North Copley, SC = South Copley, ML = Mount Lyndhurst, NY = North Yankaninna, SY = South Yankaninna, VGR = Vulkathunha-Gammon Ranges.

Copley (NC), South Copley (SC), Mount Lyndhurst (ML), North Yankaninna (NY) and South Yankaninna (SY) sections, respectively. These are characterised by a suite of clastic and carbonate lithofacies, including siltstone, sandstone, dolostone and microbialites. In the Vulkathunha-Gammon Ranges (VGR), the Myrtle Springs Formation is marked by 477 m of interbedded siltstone and sandstone with minor dolostone lithofacies towards the top.

The measured syn-glacial successions unconformably overlie Tonian rocks and represent the true stratigraphic thicknesses throughout the region. The syn-glacial interval in the Vulkathunha-Gammon Ranges is divided into the 413 m thick Fitton Formation and 424 m thick Bolla Bollana Tillite, which is comprised of coarse-grained lithofacies, including diamictites with sandy and conglomeratic interbeds. In the south-central part of the basin, North Yankaninna (38 m) and South Yankaninna (256 m) sections are characterised by diamictites with mudstone and siltstone interbeds. At the Mount Lyndhurst section, towards the north-east, the equivalent Merinjina Tillite is incredibly thin (~5 m), and records only diamictite lithofacies. On the western margin, the Bolla Bollana Tillite thins towards the south from 324 m at Termination Hill, through 126 m at North Copley to 112 m at South Copley. These sections are represented by diamictites with thin siltstone, sandstone and conglomerate interbeds. The overlying Wilyerpa Formation consists of interbedded shale, siltstone and sandstone with frequent dropstones, and demonstrates the same pinching geometry to the south, from 57 m at Termination Hill, to 52 m at North Copley, to 44 m at South Copley.

The post-glacial intervals are lithologically consistent across the basin, recording deposition of fine clastic and carbonate lithofacies. A cap carbonate is exposed in the Termination Hill, Mount Lyndhurst and North Yankaninna sections. Conversely, the North Copley, South Copley, South Yankaninna and Vulkathunha-Gammon Ranges sections do not appear to have a carbonate cap but instead are clastic-dominated at the base of the post-glacial succession. This shale-dominated interval represents the Tindelpina Shale Member of the Tapley Hill Formation. The measured sections only capture the base of Tapley Hill Formation (between 30m and 400 m thick), while the entirety of this formation can reach stratigraphic thicknesses over 2000 m in the northern Flinders Ranges (Preiss, 1987).

Facies Association	Constituent lithofacies	Depositional environment
Carbonate Platform		
A – Inner platform	Major: LF2, LF5, LF12, LF13, LF14, LF15	A1 – Supratidal to intertidal
	Minor: LF3, LF4, LF6, LF7, LF17, LF18	A2 – Intertidal to subtidal
B – Outer platform	Major: LF2, LF12, LF16	B1 – Shallow subtidal
	Minor: LF1, LF5, LF13, LF14, LF15	B2 – Platform margin reef
C – Slope to basin	Major: LF1, LF2, LF12, LF13	C1 – Slope
	Minor: LF3, LF11, LF14	C2 – Basin
Glaciomarine		
D – Ice-margin	Major: LF10	D1 – Terrestrial to grounding zone
	Minor: LF9	D2 – Proximal subaqueous
E – Proximal proglacial	Major: LF2, LF5, LF6, LF7, LF10	E1 – Subaqueous glacial outwash
	Minor: LF3, LF8, LF9	E2 – Subaqueous channel
F – Distal proglacial	Major: LF1, LF2, LF14	F1 – Subaqueous fan
	Minor: LF5, LF6, LF7, LF8, LF9, LF10, LF12	

Table 2 | Facies associations and their constituent lithofacies and depositional environments. LF = lithofacies.

4.2. Lithofacies descriptions

Eleven clastic and seven carbonate facies were classified resulting in a total of 18 lithofacies (Table 1). The pre-glacial successions encompass a mix of both clastic and carbonate lithologies, while the syn-glacial successions comprise exclusively clastic lithofacies. The post-glacial sequences characterise a shift to interbedded clastic and carbonate lithologies. Three carbonate platform and three glaciomarine facies associations were interpreted (Table 2). Photographic excerpts from each facies association are presented in Figures 3 – 8, detailing the key lithofacies and sedimentary structures. Depositional processes within facies associations were used to identify eleven specific depositional environments throughout the section (Table 2; see also Supplementary Figures).

4.2.1. Inner platform

Inner platform deposits are characterised by mixed siliciclastic and carbonate lithologies, including laminated siltstone (LF2), laminated sandstone (LF5), laminated dolostone (LF12), cross-stratified dolostone (LF13) and massive dolostone (LF14), and layered microbialites (LF15). There are also minor cross-stratified siltstone (LF3), heterolithic strata (LF4), cross-stratified sandstone (LF6), massive sandstone (LF7), and micritic magnesite (LF17) and conglomeratic magnesite (LF18). Laminated beds are planar to wavy and range from millimetre- to centimetre-scale thicknesses. Shrinkage cracks are commonly recognised on bedding surfaces for both clastic and carbonate lithofacies, represented by partially connected branches, polygons (Figure 3A), branching spindles, and sinuous and curlicue cracks in ripple troughs (Figure 3B). Rippled beds are represented by straight-crested symmetrical (Figure 3B) and interference ripples while cross-stratified beds are represented by small (1 cm to 15 cm foresets) hummocky swaley cross-laminations, large (40 cm foresets) tabular cross-stratification, supercritical (60° climb angle) climbing ripples, and unimodal and bimodal ripple cross-laminations with rare reactivation surfaces and mud drapes. Heterolithic strata are marked by flaser, wavy and lenticular bedding that deposited bidirectional and unidirectional ripples (Figure 3C). Many carbonate lithofacies present tepee structures (Figure 3D; 1 cm to 10 cm) that occasionally comprise brecciated material and chert replacement in the space under tepee crests. Microbialite lithofacies are characterised by thin (mm- to cm-scale) stratiform and undulating laminations with rare pseudocolumnar structures. Intraformational conglomeratic magnesite beds (Figure 3E) are frequently graded (inverse and normal). Some of these beds show undulating top surfaces. Further, these inner platform lithofacies are also characterised by rare scour and graded fill structures with intraclasts, and soft sediment deformation structures expressed as convolute bedding, simple load casts and flame structures.

4.2.2. Outer platform

Laminated siltstone (LF2), laminated dolostone (LF12) and microbialite buildup (LF16) dominate the outer platform facies association. Minor lithofacies include laminated mudstone (LF1), laminated sandstone (LF5), cross-stratified dolostone (LF13), massive dolostone (LF14) and layered microbialite (LF15). The frequent thinly (mm to cm thick) laminated lithofacies are commonly planar with minor wavy laminae (Figure 4A), forming both inverse and normally graded beds. Occasionally, these beds contain soft sediment deformation (convolute) structures (Figure 4B). Microbialite lithofacies are frequently represented by domical (hemispherical, bulbous, nodular) buildups (Figure 4C), domical and columnar bioherms (Figure 4D), with rare columnar and conical (convex) buildups (Figure 4E and 4F). These beds, as well as massive dolostone

Figure 3 | Key lithofacies and sedimentary structures in inner platform setting. (A) Laminated siltstone, LF2. Polygonal shrinkage cracks on bedding surface. North Copley section. (B) Rippled dolostone, LF13. Bedding surface with curlicue shrinkage cracks deposited in troughs of straight ripple sets. North Copley section. (C) Heterolithic siltstone and sandstone, LF4. Lenticular bedding with discontinuous and continuous sandstone ripples. South Yankaninna section. (D) Layered microbialite, LF15. Undulating dolomite and mudstone laminations with tepee structures. Mount Lyndhurst section. (E) Intraclastic magnesite and laminated dolostone, LF18 and LF12. Crudely (convolute) interbedded carbonate layers. South Copley section.

successions, are commonly inverse graded, coarsening from a fine to coarse crystalline texture.

4.2.3. Slope to basin

Slope to basinal successions are mainly comprised of laminated mudstone (LF1), siltstone (LF2), dolostone (LF12)

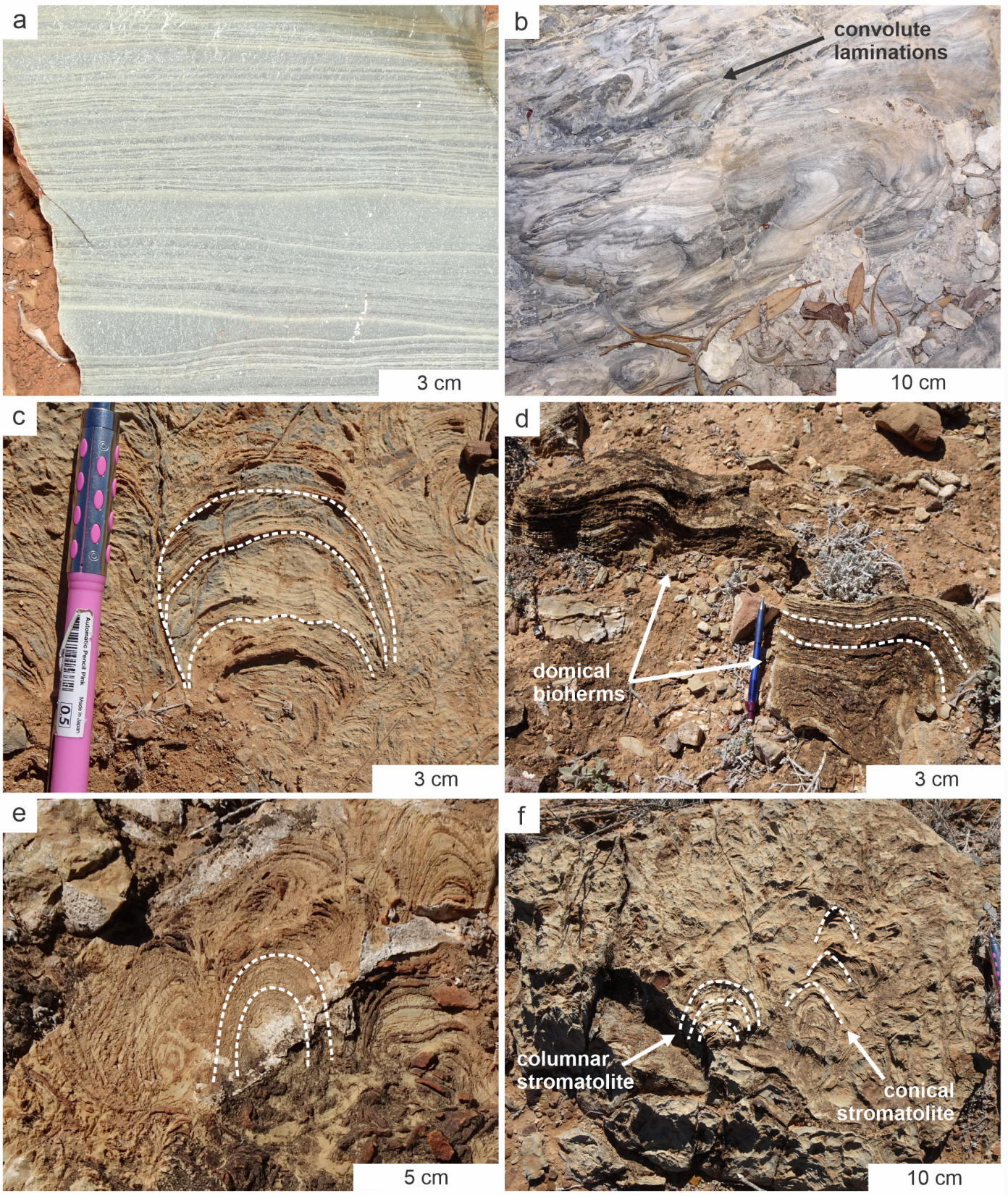

Figure 4 | Key lithofacies and sedimentary structures in outer platform setting. (A) Laminated siltstone, LF2. Very thinly (mm scale) planar laminated. South Copley section. (B) Laminated siltstone, LF2. Convolute soft sediment deformation. South Copley section. (C) Stromatolitic microbialite, LF16. Hemispherical domical buildup. Mount Lyndhurst section, (D) Stromatolitic microbialite, LF16. Domical bioherm. South Copley section. (E) Stromatolitic microbialite, LF16. Columnar buildup. South Copley section. (F) Stromatolitic microbialite, LF16. Columnar buildup and convex conical buildup. Mount Lyndhurst section.

and cross-stratified dolostone (LF13). Cross-stratified siltstone (LF3), massive dolostone (LF11) and laminated dolostone (LF14) occur as minor lithofacies. Ripple cross laminations (Figure 5A) and small (15 cm foresets) hummocky swaley cross laminations (Figure 5B) are common in cross-stratified successions. Slope packages are also characterised by convolute beds (Figure 5C) and associated rare breccia beds of randomly oriented, boulder-sized angular blocks comprising well-laminated rocks (Figure 5D. Fine-grained deposits are massive (Figure 5E)

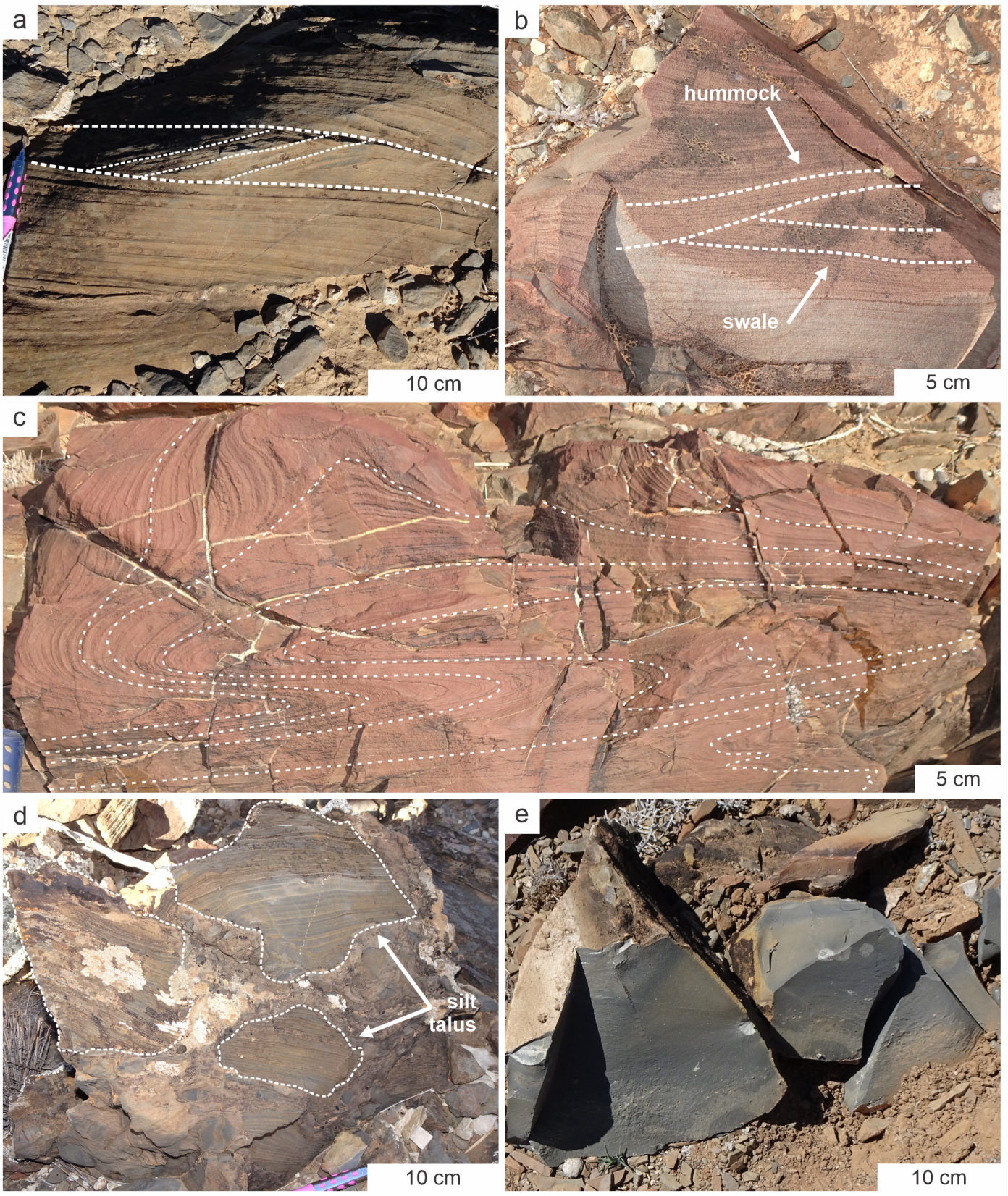

Figure 5 | Key lithofacies and sedimentary structures in slope to basin setting. (A) Cross stratified siltstone, LF3. Unidirectional ripple cross lamination. Vulkathunha-Gammon Ranges section. (B) Cross stratified siltstone, LF3. Hummock (concave-down) and swale (concave-up) ripple cross lamination. South Copley section. (C) Laminated siltstone, LF2. Convolute soft sediment deformation. Vulkathunha-Gammon Ranges section. (D) Laminated siltstone, LF2. Debrite breccia with randomly oriented angular boulder clasts of well-laminated siltstone. Vulkathunha-Gammon Ranges section. (E) Massive dolostone, LF11. South Copley section.

or planar to wavy laminated at millimetre to centimetre scale.

4.2.4. Ice margin

Massive diamictite (LF10) lithofacies dominate the grounded ice-margin facies association, with minor deposition of stratified diamictite (LF9). Both diamictite

Figure 6 | Key lithofacies and sedimentary structures in ice-margin setting. (A) Massive diamictite, LF10. Clast-rich diamictite with rounded quartzite bounder in mudstone matrix. South Yankaninna section. (B) Massive diamictite, LF10. Clast-rich diamictite with carbonate cobble from underlying bed. Termination Hill section. (C) Massive diamictite, LF10. Clast-rich diamictite with pebble to cobble sized clasts in mudstone matrix. Vulkathunha-Gammon Ranges section. (D) Massive diamictite, LF10. Clast-rich diamictite with pebble sized clasts in mudstone matrix. South Yankaninna section. (E) Massive diamictite, LF10. Clast-poor diamictite with angular quartzite boulder in mudstone matrix. Vulkathunha-Gammon Ranges section. (F) Stratified diamictite, LF9. Clast-poor diamictite with quartzite cobble. South Copley section.

lithofacies are inverse and normally graded. The massive diamictites are matrix supported (<5% to 20% clasts), incorporating sub-angular to well-rounded pebble to boulder-sized clasts. These include sandstone, quartzite, carbonate, granite and conglomerate fragments (Figure 6A–E). The matrix is mudstone to fine-grained sandstone

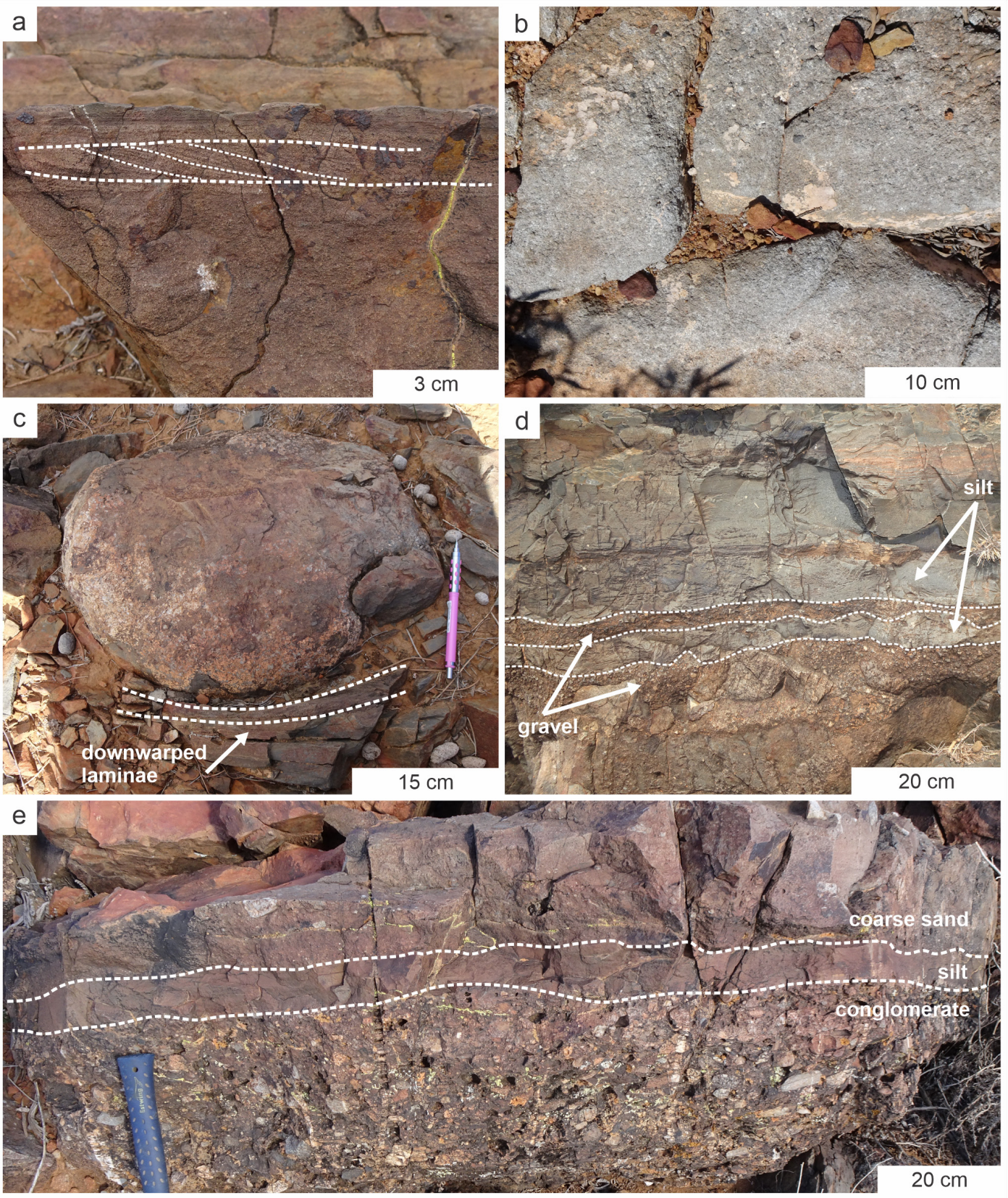

Figure 7 | Key lithofacies and sedimentary structures in proximal proglacial setting. (A) Cross stratified sandstone, LF6. Unidirectional trough cross laminations. Vulkathunha-Gammon Ranges section. (B) Massive sandstone, LF7. Graded bed with angular to sub-rounded clasts. South Copley section. (C) Laminated sandstone, LF5. Rounded boulder dropstone downwarping underlying sandstone laminations. Vulkathunha-Gammon Ranges section. (D) Laminated siltstone and orthoconglomerate, LF2 and LF8. Interbedded laminated siltstone with gravel conglomerate with scoured bases. Vulkathunha-Gammon Ranges section. (E) Laminated siltstone and orthoconglomerate, LF2 and LF8. Interbedded massive siltstone with clast-rich conglomerate and coarse sandstone beds. South Yankaninna section.

and occasionally dolomitic. Stratified diamictite beds are often clast-poor (<15% clasts), comprising gravel to boulder-sized clasts in a siltstone to fine sandstone matrix (Figure 6F).

4.2.5. Proximal proglacial

Proximal proglacial deposits are characterised by laminated siltstone (LF2), laminated sandstone (LF5), ripple and

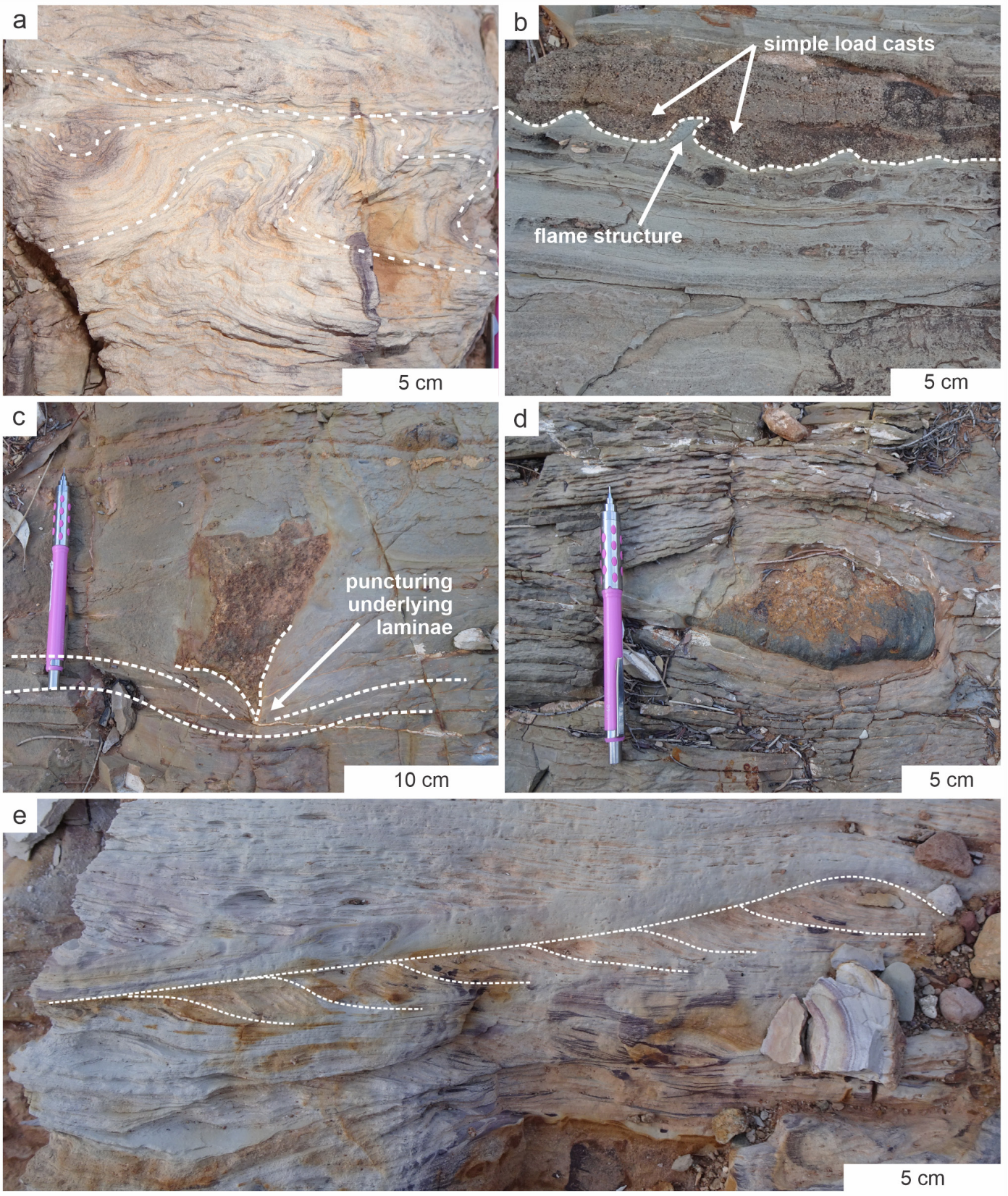

Figure 8 | Key lithofacies and sedimentary structures in distal proglacial setting. (A) Laminated mudstone, LF1. Convolute soft sediment deformation. South Copley section. (B) Laminated mudstone and laminated sandstone, LF1 and LF5. Simple load cast and flame structure soft sediment deformation at contact between sandstone and underlying mudstone bed. South Copley section. (C) Laminated mudstone, LF1. Very angular cobble dropstone that punctures and deforms the underlying mudstone laminations. South Copley section. (D) Laminated mudstone, LF1. Sub-rounded dropstone that downwarps the underlying mudstone laminations and is draped by the overlying mudstone laminations. South Copley section. (E) Laminated mudstone, LF1. Subcritical unidirectional climbing ripples. South Copley section.

cross-stratified sandstone (LF6), massive sandstone (LF7) and massive diamictite (LF10). Minor lithofacies include cross-stratified siltstone, orthoconglomerates (LF8) and stratified diamictites (LF9). Unidirectional, small (<5 cm foresets) ripple cross-stratification is representative of the cross-stratified lithofacies (Figure 7A), where foresets are often comprised of dark, heavy minerals. Massive sandstone beds are frequently graded (inverse and normal) and

immature, characterised by angular to sub-rounded fine sandstone to gravel (Figure 7B). Diamictite lithofacies are marked by frequent clast-poor (<5% to 15%) beds, incorporating sand, quartzite, carbonate and granite gravel to boulder-sized clasts in a siltstone to fine sandstone matrix (Figure 7C). These diamictite beds occasionally have scoured bases. Clast-supported (40% to 80%) orthoconglomerates comprise medium sandstone to boulder-sized, sub- to well-rounded sand, quartz, carbonate and granite clasts. These orthoconglomerate beds are occasionally thinly interbedded with siltstone (Figure 7D, E), graded (inverse and normal), and/or have scoured bases.

4.2.6. Distal proglacial

Fine-grained lithofacies dominate the distal proglacial facies association, including laminated mudstone (LF1), laminated siltstone (LF2) and massive dolostone (LF14). There is a suite of more minor lithofacies, including laminated sandstone (LF5), cross-stratified sandstone (LF6), massive sandstone (LF7), orthoconglomerate (LF8), stratified (LF9) and massive (LF10) diamictite, and laminated dolostone (LF12). A number of fine- and coarse-grained distal proglacial deposits fine-up within beds and in packages. Laminated lithofacies comprise millimetre to centimetre-thick planar and wavy laminations, where mudstone and siltstone are commonly interlaminated. Mudstone beds occasionally contain soft sediment deformation structures, including convolute bedding (Figure 8EA), simple load casts and flame structures (Figure 8B). There are also rare dropstones (Figure 8C, D), ranging from sand, quartzite, carbonate and conglomeratic gravel to boulders, and subcritical (15° climb angle) climbing ripples (Figure 8E). Cross-stratified sands are represented by thin, heavy mineral ripple cross-stratifications. Diamictite lithofacies are commonly clast-poor (<20%), with minor laminated successions in siltstone to very fine-sandstone matrices. Rare orthoconglomerate beds, comprised of up to 70% very coarse sandstone to cobble clasts, pierce overlying fine-grained beds.

5. Discussion

5.1. Facies Association A: Inner platform

5.1.1. Sedimentary processes

The presence of minor wave action is evidenced by the deposition of symmetrical ripples, which were likely deposited from lower flow regime oscillatory flows (Reading, 2009; Boggs, 2014; Counts et al., 2016). Small hummocky and swaley cross-laminations provide evidence for combined waning unidirectional and oscillatory flow (Nøttvedt & Kreisa, 1987; Arnott & Southard, 1990; Cheel, 1991; Duke et al., 1991; Cheel & Leckie, 1993; Dumas & Arnott, 2006; Reading, 2009; Basilici et al., 2012; Boggs, 2014). The suite of unidirectional cross-stratified structures represents downcurrent migration of small sinuous and catenary crested ripples and straight crested dunes from low and high-energy flows, respectively (Ashley, 1990; Colquhoun, 1995; Chakrabarti, 2005; Bridge, 2009; Reading, 2009; Daidu, 2013; Boggs, 2014; Thomson et al., 2014; Momta et al., 2015; Jorissen et al., 2018). The presence of bimodal cross-stratified foresets, reactivation surfaces and mud-drapes indicate tidal influence (Ashley, 1990; Colquhoun, 1995; Reading, 2009; Daidu, 2013; Boggs, 2014; Momta et al., 2015). Further, the presence of heterolithic strata deposited as bedload and suspended load during alternating high and low energy flows are also tidally induced structures (Reineck & Wunderlich, 1968; Bhattacharya, 1997; Daidu, 2013; Boggs, 2014; Maciaszek et al., 2019). Microbialite material likely reflects authigenic precipitation and/or capture, where clastic material was transported under low energy flow regimes, then trapped and bound the microbial layers (Wright, 1984; Tucker & Wright, 2009; O'Connell et al., 2020). This in-situ precipitation could also have been responsible for the accumulation of magnesite mudstone, although developing in more of an evaporative magnesium-rich water column (Mur & Urpinell, 1987; Warren, 1990; Melezhik et al., 2001), and graded, intraformational conglomeratic magnesite beds were likely reworked by secondary current processes (Uppill, 1980; Belperio, 1990; Preiss, 2000; Frank & Fielding, 2003; Counts, 2017). Tepee structures are common in carbonate lithofacies, likely resulting from expansion-related fracturing due to mineral precipitation in peritidal conditions (Asserto & Kendall, 1977; Kendall & Warren, 1987; Belperio, 1990; Frank & Fielding, 2003; Tucker & Wright, 2009; O'Connell et al., 2020). Other desiccation features include branching and polygonal shrinkage cracks (Plummer & Gostin, 1981; Boggs, 2014). However, other branching, polygonal, curlicue, sinuous and spindle cracks were likely developed from subaqueous shrinkage of cohesive sediment caused by compaction during burial (Donovan & Foster, 1972; Plummer & Gostin, 1981; Tanner, 1998; Pflueger, 1999; Gehling, 2000; McMahon et al., 2017).

5.1.2. Environmental interpretations

The mixed carbonate and clastic lithofacies reflect deposition under dominant tidal influence with minor wave energy, and show evidence for evaporative carbonate precipitation and periodic exposure, which is consistent with deposition in an inner carbonate platform (A) setting (Figure 9; e.g., von der Borch & Lock, 1979; Uppill, 1980; Belperio, 1990; Frank and Fielding, 2003). These inner platform deposits can be further classified into packages reflecting deposition in more of a subaerial or subtidal environment based on the presence of desiccation and current features, respectively. Packages comprised of magnesite mudstones, tepee structures and desiccation cracks are interpreted to have been deposited in the supratidal to intertidal zone (A1), while units dominated by current reworking, undisturbed laminations and soft-sediment deformation are characteristic of deposition in the intertidal to subtidal zone (A2), (Figure 9; Belperio, 1990; Powers & Holt, 2000; Frank & Fielding, 2003; Thomson et al., 2014; Kunzmann et al., 2019).

5.2. Facies Association B: Outer platform

5.2.1. Sedimentary processes

Thinly laminated siltstone and mudstone intervals were likely deposited in the lower flow regime, settling out of suspension with a slow sedimentation rate (Boggs, 2014; Yawar & Schieber, 2017), while planar laminated sandstone beds represent deposition under upper flow regime conditions (Cheel, 1990; Bridge, 2009; Boggs, 2014; Jorissen et al., 2018). Convolute soft sediment deformation structures could have developed from seismic activity (Shanmugam, 2017). Less crystalline dolomitic material in dolostone lithofacies likely preserve primary carbonate textures and therefore reflect authigenic precipitation or syn-sedimentary dolomitisation (mimetic replacement). Conversely, more crystalline lithofacies likely reflect secondary diagenetic recrystallisation (non-mimetic replacement) that resulted in the destruction of these primary textures (Tucker, 1985; Tucker & Wright, 2009; Flügel, 2010). Planar and cross-stratified interlaminated clastic material was likely transported as suspended load and deposited from low-energy tidal currents (O'Connell et al., 2020) and higher energy storm activity (Hoffman, 1976; Wanless et al., 1988; Tucker & Wright, 2009; Jahnert & Collins, 2012; Chiarella et al., 2017; Kunzmann et al., 2019; O'Connell et al., 2020), respectively. The same mechanisms were likely responsible for microbialite lithofacies, where microbialite buildups, previously identified as *Baicalia burra* (Preiss, 1973; Belperio, 1990), reflect deposition under lower energy conditions (Hoffman, 1976; Tucker & Wright, 2009; Jahnert & Collins, 2012; Kunzmann et al., 2019).

5.2.2. Environmental interpretations

The deposition of both low-energy fine-grained lithofacies, and higher-energy, inverse-graded carbonate lithofacies are consistent with a setting that experiences both quiescent, subtidal conditions and energetic shoaling (Gómez-Pérez et al., 1999; Grotzinger & James, 2000; Pomar, 2001; Chatalov et al., 2015; Wilmsen et al., 2018; Thorie et al., 2020). This facies association is interpreted as an outer platform (B) (Figure 9), and more specifically a shallow subtidal zone (B1) below fair-weather wave base (e.g., Belperio, 1990; Jahnert & Collins, 2012; Milli et al., 2013; Thomson et al., 2014; Wilmsen et al., 2018; Thorie et al., 2020), and a platform margin reef (B2) where there is evidence for stromatolitic buildups (Figure 9; e.g., Gómez-Pérez et al., 1999; Grotzinger & James, 2000; Pomar, 2001; Chatalov et al., 2015; Thorie et al., 2020). The presence of stromatolitic buildup lithofacies (B2) likely corresponds to a high-relief carbonate platform geometry (Grotzinger, 1988; 1990, 2012; Grotzinger & James, 2000), while outer platform deposits with only shallow subtidal zone lithofacies (B1) may characterise ramp style carbonate platforms (Grotzinger, 1989; Grotzinger & James, 2012).

5.3. Facies Association C: Slope to basin

5.3.1. Sedimentary processes

Soft sediment deformation structures, in particular convolute bedding and load structures, likely resulted from submarine slumping (Stow & Mayall, 2000; Stracchan, 2008) or lateral loading during liquefaction (Postma, 1983; Stromberg & Bluck, 1998; Moretti et al., 2001; Owen, 2003), respectively. Brecciated beds are likely deposited as a debrite from gravitational collapse on an unstable and steep slope (e.g., Talling et al., 2012; Thomson et al., 2014; Wallace et al., 2015).

5.3.2. Environmental interpretations

The prevalence of fine-grained lithofacies, storm reworking, soft sediment deformation and debrite breccias are consistent with a slope to basinal (C) setting (Figure 9; Gómez-Pérez et al., 1999; Grotzinger & James, 2000; Thomson et al., 2014; Wallace et al., 2015; Corkeron & Slezak, 2020). Slumped beds and brecciated beds are consistent with rapid deposition from turbidity and debris flows on an unstable slope (C1) (Talling et al., 2012; Thomson et al., 2014Thorie et al., 2020). From previous literature on slope lithofacies in the north-western Flinders Ranges, the brecciated beds could be forereef debrites that were eroded and transported from a regional reef escarpment (e.g., Giddings & Wallace, 2009a; Hood & Wallace, 2012; Wallace et al., 2015; Corkeron & Slezak, 2020) or resulted from more locally derived topography including those on the margins of minibasins and salt domes (Counts et al., 2016). Conversely, well-laminated fine-grained beds support deposition in more of a basinal (C2) environment under very low energy conditions (Figure 9; Thomson et al., 2014; Kunzmann et al., 2019).

5.4. Facies Association D: Ice margin

5.4.1. Sedimentary processes

The massive, ungraded diamictites of the grounded ice-margin facies association were likely deposited rapidly from meltwater directly from the ice sheet (Link & Gostin, 1981; Young & Gostin, 1988; Preiss et al., 2011). Stratified diamictites and normally graded beds could reflect slower deposition and sorting through clast settling (Anderson, 1989), while inverse grading likely indicates kinetic sieving during flows (Legros, 2002; Talling et al., 2012; Le Heron et al., 2014).

5.4.2. Environmental interpretations

From previous literature, these thick diamictite successions have been interpreted as melt-out at the ice margin (D), (Figure 9; e.g., Link & Gostin, 1981; Young & Gostin, 1988; 1991; Preiss et al., 2011; Le Heron et al., 2014). Massive diamictite packages support deposition as ice-contact till in the terrestrial and/or grounding zone (D1) (Young

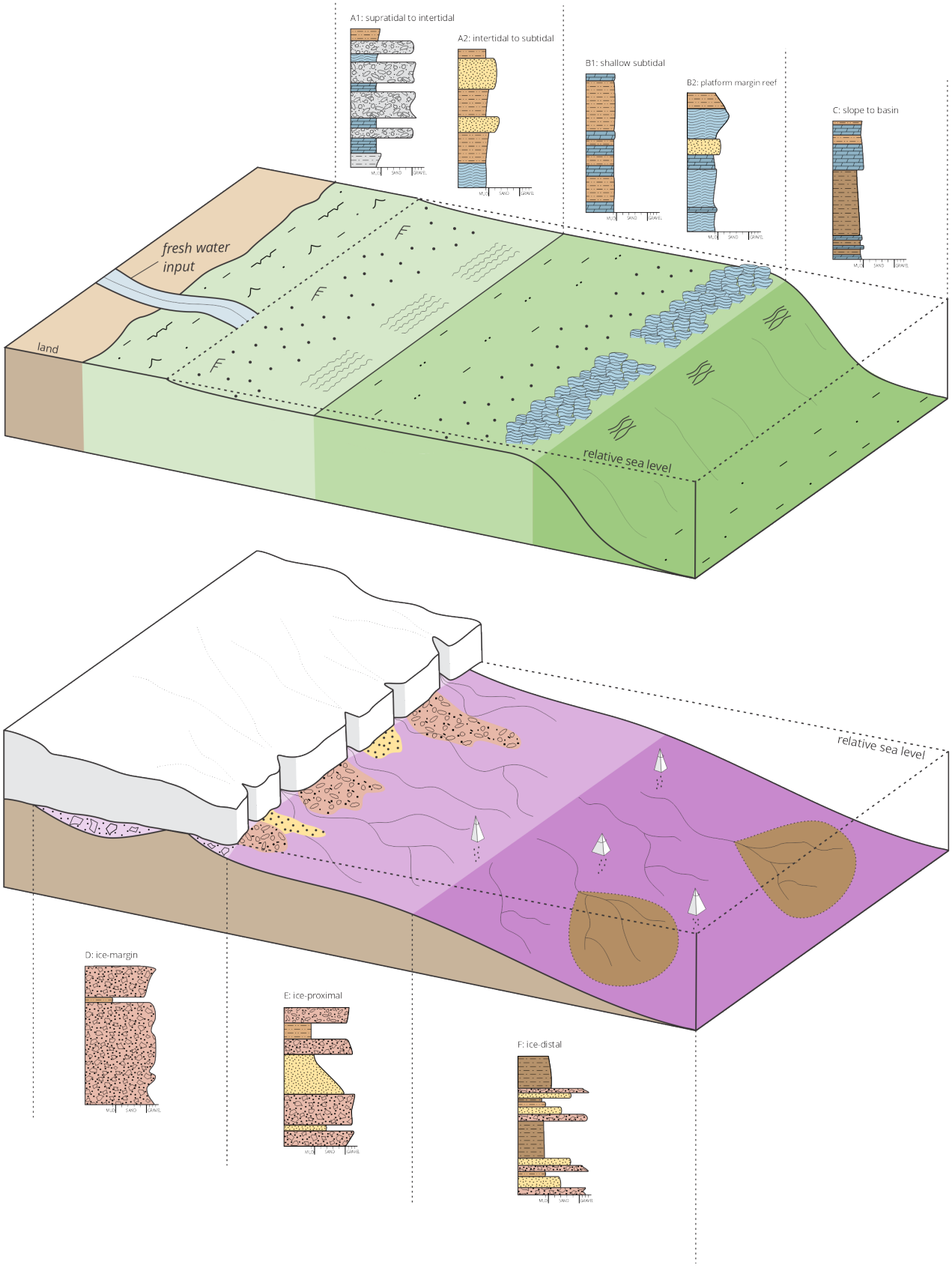

Figure 9 | Depositional models for the two key settings during the Tonian–Cryogenian in the northern Flinders Ranges, with representative sedimentary logs for each depositional environment. Carbonate platforms in this study have been interpreted with both high relief and ramp-style geometries. A high relief carbonate platform model is shown here to demonstrate the platform margin reef (B2). Carbonate platform environments are interpreted for the pre-glacial and post-glacial successions, and glaciomarine environment is interpreted for the syn-glacial succession. Legend for symbology in depositional model and sedimentary logs.

& Gostin, 1988; 1991; Virgo et al., 2021), while packages with evidence for reworking (i.e., sorting and stratification) are more closely associated with subaqueous deposition as proximal proglacial till (D2) (Figure 9; Young & Gostin, 1988; 1990; 1991; Anderson, 1989; Eyles et al., 2007; Boggs, 2014; Busfield & Le Heron, 2013; 2016; Le Heron et al., 2013; 2014; Fleming et al., 2016).

5.5. Facies Association E: Proximal proglacial

5.5.1. Sedimentary processes

Upper plane beds and ripple cross-stratification are likely deposited from a similar process to that outlined in the inner platform setting (Ashley, 1990; Reading, 2009; Boggs, 2014). However, the unimodal current orientation of flows could indicate deposition from low-density turbidity currents rather than a tidal source (Lowe, 1982; Kneller, 1995; Shanmugam, 1997; 2000; Bridge, 2009; Winsemann et al., 2009; Talling et al., 2012; Momta et al., 2015; Jorissen et al., 2018). High-density turbidity currents could have deposited graded sands and orthoconglomerates with internal structure, while more massive beds could reflect deposition from hyperconcentrated debris flows (Lowe, 1982; Kneller, 1995; Shanmugam, 2000; Winsemann et al., 2009; Talling et al., 2012; Le Heron & Busfield, 2016). Similarly, stratified diamictite beds are more consistent with rapid deposition from subaqueous sediment gravity flows (Young & Gostin, 1988; Anderson, 1989; Eyles et al., 2007; Le Heron et al., 2013; 2014), and massive diamictites could indicate moderate to high strength, cohesive debris flow deposits (Talling et al., 2012). Bed forms with rare, scoured bases likely indicate high-velocity flows that eroded the substrate and subsequently filled any new topography during the waning stage of the same flow (Fielding, 2006; Bridge, 2009; Boggs, 2014).

5.5.2. Environmental interpretations

The mix of structured and massive lithofacies was likely deposited in a subaqueous environment from turbidity and debris flows, respectively (Lowe, 1982; Kneller, 1995; Shanmugam, 1997; 2000; Bridge, 2009; Talling et al., 2012; Boggs, 2014). This is consistent with a proximal proglacial setting (E), (Figure 9; e.g., Powell & Domack, 2002; Winsemann et al., 2009; Le Heron et al., 2013; 2014; Busfield & Le Heron, 2013; 2016), which can be further classified based on the abundance of specific lithofacies and the stratigraphic relationship between them. Immature and massive sands, gravels and diamictites are interpreted to represent deposition from debris flows as glacial outwash (E1), (e.g., Young & Gostin, 1988; 1991; Powell & Domack, 2002; Le Heron et al., 2014; Le Heron & Busfield, 2016), while graded beds with scoured bases and unidirectional structures represent subaqueous turbidite channel deposits (E2), (Figure 9; e.g., Lowe, 1982; Reading & Richards, 1994; Le Heron et al., 2014).

5.6. Facies Association F: Distal proglacial

5.6.1. Sedimentary processes

Low-density turbidity currents were likely responsible for depositing fine-grained sediments (Talling et al., 2012; Tinterri et al., 2016). Convolute laminations were likely deposited from bottom current reworking (Dzuynski & Smith, 1963; Shanmugam, 1997), while simple load casts and flame structures reflect liquefaction in response to differential sediment densities or lateral loading (Owen, 2003). Dropstones that deform underlying beds provide evidence for ice-rafted debris that were likely deposited as rainout (e.g., Link & Gostin, 1981; Young & Gostin, 1988; 1991; Powell & Domack, 2002; Eyles et al., 2007; Preiss et al., 2011; Boggs, 2014; Le Heron et al., 2013; 2014; 2021; Le Heron & Busfield, 2016). Subcritical climbing ripples within siltstone beds provide further evidence for decelerating turbidity currents, net deposition and bedform migration (Ashley et al., 1982; Young & Gostin, 1988; Baas et al., 2000; Jobe et al., 2012; Boggs, 2014; Le Heron & Busfield, 2016; Maciaszek et al., 2019).

5.6.2. Environmental interpretations

The repeated emplacement of fine-grained turbidite successions, transitioning from massive sandstone, rippled, cross-stratified and convolute sandstone and siltstone, to laminated mudstone, along with ice-rafted dropstones, have been interpreted as distal proglacial deposits (F), (Figure 9; e.g., Eyles et al., 1983; Powell & Domack, 2002; Le Heron et al., 2014; Busfield & Le Heron, 2016). More specifically, a subaqueous fan (F1) could have provided the large sediment supply and facilitated the slope instability necessary for the development of these turbidity currents (Figure 9; e.g., Bouma, 1964; Middleton & Hampton, 1976; Lowe, 1982; Shanmugam, 1997; 2000; Powell & Domack, 2002; Talling et al., 2012; Boggs, 2014; Le Heron et al., 2014).

5.7. Regional correlation

5.7.1. Sequence 1

5.7.1.1. Sequence 1.1

The base of the Termination Hill section in the north-west corner of the basin is marked by a 350 m thick succession of supratidal to subtidal magnesite and dolostone with minor microbial carbonate, siltstone and sandstone (Sequence 1.1; Figure 10). Although this distinct unit was not logged in the North Copley section, it has been recorded near this location from previous studies (i.e., Frank & Fielding, 2003). Sequence 1.1 can be further traced to the South Copley section (Figure 10), increasing in stratigraphic thickness up to 485 m. Deposition of sedimentary magnesite in the northern Flinders Ranges is restricted to the western margin, extending discontinuously across a strike length of ~130 km.

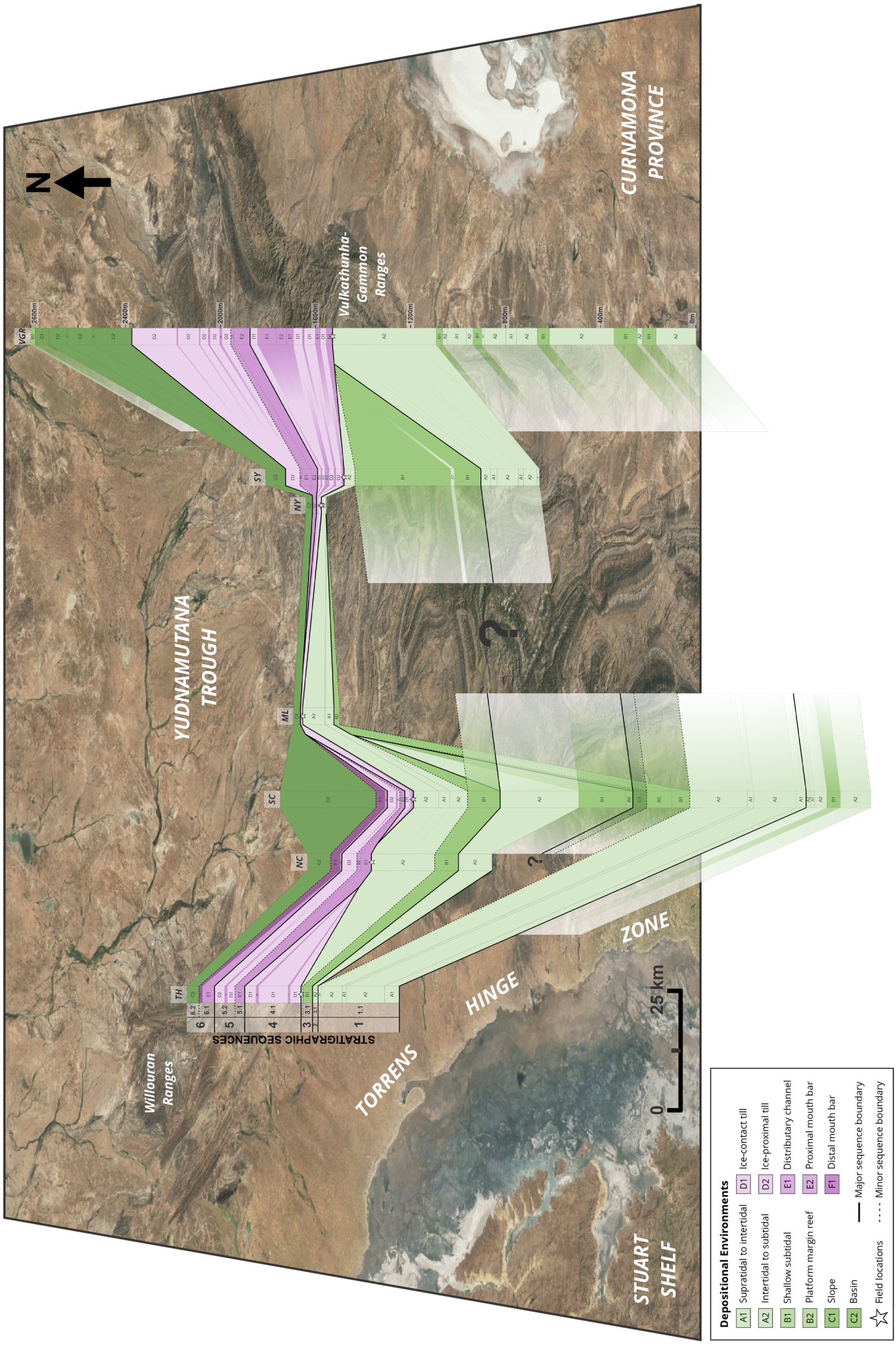
N
CURNAMONA PROVINCE
Vulkathunha-Gammon Ranges
YUDNAMUTANA TROUGH
Willouran Ranges
TORRENS HINGE ZONE
STUART SHELF
STRATIGRAPHIC SEQUENCES
TH
NC
SC
ML
NY
SY
VGR
2600m
2400m
2000m
1600m
1200m
800m
400m
0m
0
25 km
?
?
Depositional Environments
A1 Supratidal to intertidal
A2 Intertidal to subtidal
B1 Shallow subtidal
B2 Platform margin reef
C1 Slope
C2 Basin
D1 Ice-contact till
D2 Ice-proximal till
E1 Distributary channel
E2 Proximal mouth bar
F1 Distal mouth bar
Major sequence boundary
Minor sequence boundary
Field locations

↑ **Figure 10 |** Fence diagram with correlation panels between sections across the northern Flinders Ranges. Stratigraphic columns and panels show temporal and spatial distribution of depositional environments. Semi-transparent panels indicate correlations with uncertainty. Thick black lines indicate major sequence boundaries, dashed lines indicate minor sequence boundaries. TH = Termination Hill, NC = North Copley, SC = South Copley, ML = Mount Lyndhurst, NY = North Yankaninna, SY = South Yankaninna, VGR = Vulkathunha-Gammon Ranges.

5.7.1.2. Sequence 1.2

The overlying unit (Sequence 1.2) was only recorded at the South Copley and Mount Lyndhurst sections (Figure 10), ranging in thickness from 157 m and 33 m, respectively. It is represented by platform margin stromatolitic reefs with minor sandstone, dolostone and layered microbialite. It appears to pinch out north-west towards the Termination Hill section (Figure 10), where the magnesite interval (Sequence 1.1) is directly overlain by Sequence 2. The correlation of this stromatolitic unit to North Copley and Yankannina is uncertain as this part of the stratigraphy was not logged at these locations (Figure 10). However, as stratigraphy appears to be continuous along strike between the South Copley and North Copley sections, it is likely that Sequence 1.2 was also deposited in North Copley.

5.7.1.3. Sequence 1.3

Sequence 1.3 is deposited in the South Copley section and comprises slope to basinal cross-stratified siltstone (60 m thick). Like Sequence 1.2, this interval was not logged in the North Copley and Yankaninna sections, so correlation to these locations is ambiguous (Figure 10). It is evident that this deepwater unit pinches out further north towards Termination Hill and Mount Lyndhurst and east to the Vulkathunha-Gammon Ranges (Figure 10).

Towards the eastern margin of the basin, this sequence totals 1084 m and is characterised by more siliciclastic rocks, which are lithologically dissimilar to the carbonate-dominated rocks along the western margin. At the Vulkathunha-Gammon Ranges section, this interval is represented by supratidal to intertidal clastic (siltstone and sandstone) and carbonate (dolostone and microbial carbonate) lithofacies, and lagoonal siltstone and dolostone. Due to the variability of the lithologies and depositional settings in the Vulkathunha-Gammon Ranges, it is hard to correlate Sequence 1 with certainty to the stratigraphically equivalent successions at other locations in the central and western part of the northern Flinders Ranges (Figure 10).

5.7.2. Sequence 2

At Termination Hill, Sequence 2 is represented by 30 m of intertidal to subtidal dolostone and sandstone (Sequence 1.4; Figure 10). This can be traced along strike to North and South Copley (Figure 10), where it becomes thicker (139 m and 322 m) and includes more clastic lithofacies. In South Yankaninna (Figure 10), Sequence 2 is 254 m thick and includes supratidal layered microbialite and dolostone lithofacies. Although this clastic-rich unit was not logged in North Yankaninna, it has been mapped at this location (Coats, 1973). Sequence 2 can also be correlated to the Vulkathunha-Gammon Ranges (Figure 10), where it is characterised by 476 m of intertidal to subtidal clastics with minor dolostone.

5.7.3. Sequence 3

5.7.3.1. Sequence 3.1

The base of Sequence 3 is characterised by lagoonal siltstone and dolostone (Sequence 3.1) and can be traced across several sections in the northern Flinders Ranges, with varying stratigraphic thicknesses (Figure 10). It increases in thickness from 44 m at Termination Hill, to 100 m at North Copley and 150 m in South Copley, where it includes minor microbial carbonate lithofacies. This lagoonal unit pinches out in the north-central part of the basin at Mount Lyndhurst but can be correlated to the south-central Yankaninna area (Figure 10). In South Yankaninna, the deposition of Sequence 3.1 is considerably thicker (545 m) and is represented by analogous siltstone and dolostone lithofacies to those on the western margin. Like Sequence 2, this interval was not logged in North Yankaninna. However, the correlation is uncertain as it cannot be constrained from the previous mapping. Sequence 3.1 appears to pinch out towards the east in the Vulkathunha-Gammon Ranges section, where Sequence 2 is directly overlain by the Sturtian glaciogenic deposits.

5.7.3.2. Sequence 3.2

The top of Sequence 3 is marked by a microbial-dominated unit that is prevalent in the west and central parts of the northern Flinders Ranges (Sequence 3.2; Figure 10). In North Copley, this 264 m thick interval comprises intertidal to subtidal siltstone, dolostone and microbial carbonates, which can be traced along strike to a 197 m thick succession in South Copley with minor supratidal lithofacies (Figure 10). The unit thins towards Mount Lyndhurst (103 m) and is characterised by comparable inner platform lithofacies, including sandstone interbeds. Sequence 3.2 is the only pre-glacial stratigraphy logged in North Yankaninna (Figure 10), recording a thin (21 m) interval that can be correlated to a thicker (49 m) succession in South Yankaninna.

5.7.4. Sequence 4

At the Termination Hill section, a thick (210 m) basal diamictite unit (Sequence 4.1) with minor conglomeratic interbeds is interpreted to reflect ice-contact till and

proglacial outwash, respectively. Sequence 4 appears to pinch out at the North Copley section, reappearing again in a thinner interval (36 m) at the base of the South Copley section (Figure 10). Similar lithofacies are identified in South Copley but include additional meltwater channel-graded sandstone interbeds. This basal diamictite is the only glaciogenic unit deposited in Mount Lyndhurst, represented by a thin (5 m), massive, graded diamictite bed interpreted as proximal proglacial till. In the Yankaninna sections, Sequence 4 reflects slightly more proglacial deposition of proximal tills and fine-grained, laminated and scoured meltwater channel interbeds. This basal diamictite thickens towards the south from 22 m in North Yankaninna to 116 m thick in the South Yankaninna section (Figure 10). Towards the east, at the Vulkathunha-Gammon Ranges section, Sequence 4 is much thicker (345 m), with frequent sandy interbeds. This marks the return of interpreted ice-contact tills and proglacial outwash analogous to the basal diamictite succession deposited along the western margin.

5.7.5. Sequence 5

5.7.5.1. Sequence 5.1

The overlying heterogenous unit (Sequence 5.1) is deposited in all sections along the north-western margin of the basin, but with varying degrees of thickness and representative lithologies (Figure 10). In the north, at Termination Hill, the unit is 36 m thick and characterised by glacial outwash sands and diamictites. These pass into a 65 m thick succession in North Copley, which includes meltwater channel cross-stratified sands. Along strike, at the South Copley section, Sequence 5.1 is lithologically similar but considerably thinner (20 m). The North and South Yankaninna sections record a 17 m thick succession of turbidite channel deposits and a 77 m thick succession of coarse-grained clastic glacial outwash and meltwater channel lithofacies, respectively. Sequence 5.1 can be correlated east to the Vulkathunha-Gammon Ranges section, represented by an 86 m thick succession of comparable lithofacies to those deposited in the South Yankaninna section.

5.7.5.2. Sequence 5.2

At Termination Hill, Sequence 5.2 is characterised by 77 m of proximal proglacial massive and crudely stratified diamictite till with proglacial outwash sandstone interbeds. At the North Copley section, the unit is thinner (40 m) and lithologically homogenous, depositing only proximal proglacial massive diamictite facies. Along strike at the South Copley section, Sequence 5.2 is 53 m thick and marked by the return of interbedded proximal proglacial sands, comparable to those deposited in the Termination Hill section. This upper diamictite unit appears to pinch out in the North Yankaninna section but can be traced to the top of the South Yankaninna section (Figure 10). Like North Copley, it is lithologically homogenous and represented by a 50 m thick proximal proglacial diamictite. Deposition of Sequence 5.2 can be correlated to a very thick (406 m) succession over to the east at the Vulkathunha-Gammon Ranges section, where it is similar to Termination Hill and South Copley.

5.7.6. Sequence 6

5.7.6.1. Sequence 6.1

Sequence 6.1 appears to have more limited deposition, accumulating only at the top of the sections along the north-western margin of the basin (Figure 10). At the Termination Hill section, this unit is characterised by a 57 m thick succession of proximal outwash sandstone and diamictites, overlain by distal fan mudstone, siltstone and sandstone. Sequence 6.1 is correlated to the North and South Copley sections (Figure 10), where it is represented by 45 m and 41 m thick successions, respectively. Although this upper heterogenous unit was not identified in the other sections, it has been recorded at locations in South Yankaninna from previous studies (i.e., Young & Gostin, 1990; 1991), which were correlated to the sections on the north-western margin of the basin (Figure 10).

5.7.6.2. Sequence 6.2

On the north-western margin in Termination Hill, the bottom of Sequence 6.2 is marked by a 2 m thick dolostone bed, followed by deposition of basinal siltstone and carbonate. The North Copley and South Copley sections are dominated by the deposition of basinal mudstone, with thin (1 m) carbonate beds increasing in number up-section. This succession in South Copley is of particular significance because it contains a 3 cm tuff layer that has provided an accurate geochronological age for the end of the Sturtian glaciation (663.03 ± 0.11 Ma, Cox et al., 2018). The cap carbonate recorded at Termination Hill is also deposited in the north-central Mount Lyndhurst section, represented by a 4 m thick bed that grades into basinal mudstone with minor thin (1m) carbonate interbeds. Sequence 6.2 in North Yankaninna is the only carbonate-dominated interval, where 30 m of basinal dolostone overlie glaciogenic rocks. The South Yankaninna and Vulkathunha-Gammon Ranges sections are comparable to those in Copley, with mudstone-dominated deposition in the bottom, and increasing carbonate deposition up-section.

5.8. Controls on basin architecture

The sequence stratigraphic architecture of the basin, including the variations in depositional environments and stratigraphic thicknesses recorded in this study, results from the interaction of accommodation and sediment input and can be divided into systems tracts (e.g., Catuneanu, 2006; 2017; Embry, 2009; Catuneanu et al., 2009; 2011; Vakarelov & Ainsworth, 2013; Kunzmann et al., 2019; 2020). Accommodation and sedimentation rates

are in turn largely controlled by variations in tectonics (subsidence and uplift), eustasy, and climate. In addition, salt tectonics played a critical role in the production of syndepositional topography. This was largely through the formation of salt withdrawal minibasins and diapirs, which correspond to topographic lows and highs, respectively (Rowan et al., 2020).

5.8.1. Sequence 1

5.8.1.1. Sequence 1.1

The distinctive magnesite succession (Sequence 1.1) is interpreted to have been deposited during a slow transgression (Figure 11) in an arid, low-energy, inner platform environment that was sheltered from marine reworking by barrier reefs (O'Connell et al., 2020). This is evidenced by the limited clastic input and aggradation of shallow water carbonate deposits (Figure 11). Eustatic sea level rise was likely driving the increase in accommodation during a time of relative tectonic quiescence, demonstrated by the prevalence of fine-grained, carbonate-rich material and lack of source area clastics (Figure 11; Preiss, 1987; Catuneanu, 2006). Due to the tabular geometry of the platform, minor fluctuations in sea level would result in near instantaneous flooding (Preiss, 2000), and it is marked by current-reworked intraclastic magnesite and third-order flooding surfaces (Figure 11). Sequence 1.1 is confined to the western margin of the northern Flinders Ranges because it was restricted to a major rift shoulder on this western boundary of the Adelaide Rift Complex (Lloyd et al., 2020). This resulted in a littoral depositional setting and higher relief relative to other parts of the basin.

5.8.1.2. Sequence 1.2

The stromatolitic buildup of Sequence 1.2 indicates deposition as a platform margin microbialite reef during a highstand systems tract (Figure 11), where the reefal growth kept pace with the newly created accommodation space. This accumulation of carbonate material was likely facilitated by earlier transgressions that flooded the rift shoulder platform margins, creating a sediment-starved distal area relative to clastic source areas in the northwest (Catuneanu, 2006; Lloyd et al., 2020). Deposition of these Tonian reefs was recorded in the north-western margin and north central part of the basin (Figure 11), and coincides with the location of later Cryogenian reef complexes (e.g., Balcanoona Formation, Wallace et al., 2015; Corkeron and Slezak, 2020). These likely correspond to long-lasting topographic highs, which were influenced by normal faults along the basin margin in the north-west (Preiss, 2000) and large salt diapirs in Mount Lyndhursrt (Rowan et al., 2020). Further, the deposition of Sequence 1.2 at Copley and Mount Lyndhurst likely corresponds to carbonate platforms with high relief geometries (Wallace et al., 2015), while locations that do not record this sequence (e.g., Yankaninna) probably developed more of a ramp-style geometry.

In contrast, the Vulkathunha-Gammon Ranges section in the north-eastern part of the basin was likely deposited under a very different set of conditions. The thick, clastic-rich succession (Figure 11) is consistent with fault-controlled deposition and proximity to uplifted source areas at the rim of the basin. This is supported by detrital zircon provenance data that demonstrates restricted eastern detrital sources (Lloyd et al., 2020). Deposition likely occurred during a highstand systems tract (Figure 11), as the high supply of clastic material prograded basinward into the high accommodation area generated by tectonic subsidence. Not only could these tectonics be related to the ongoing rifting in the basin, but the nearby formation of the allochthonous salt (e.g., Arkaroola and Tourmaline Hill diapirs) may have also been responsible for the generation of uplifted material and subsidence-induced accommodation. The Arkaroola diapir to the east is defined by a gentler ramp geometry, while the Tourmaline Hill diapir to the north is very steep and continued into the overlying Umberatana Group (Rowan et al., 2020). The latter would have created significant topography and is likely, in part, responsible for the generated uplift and subsidence recognised in the deposition of this sequence in the Vulkathunha-Gammon Ranges section.

5.8.1.3. Sequence 1.3

The deep-water siltstone succession of Sequence 1.3 was likely deposited during rapid transgression (Figure 11), resulting in the drowning of the carbonate platform and the shutdown of carbonate productivity. This is represented by backstepping (retrogradational) geometries and is capped by a major flooding surface (MFS; Figure 11). On the western margin, this unit pinches out towards the north, suggesting a more distal setting in Copley (Figure 11). Further, Sequence 1.3 was not deposited in the north-central and eastern sections, supporting a more proximal, shallow environment in these parts of the basin.

5.8.2. Sequence 2

The overlying sandstone succession (Sequence 2) is consistent with a highstand systems tract and is capped by a major regressive surface (MRS; Figure 11), reflecting deposition in a proximal clastic-dominated setting with high sediment input. This was likely in response to pulses of rifting and newly uplift of source regions (Preiss, 1987), which resulted in basinward progradation of clastics and burial of the platform carbonates. The uplift interpreted during the deposition of this unit may also have developed from salt diapirism actively forming across the basin during this time. Complex diapirism in the Willouran Ranges (Hearon et al., 2015; 2015a; Rowan et al., 2020), may have eroded areas close to the diapir (e.g., Termination Hill), which in turn created the lateral thickness variation of Sequence 2 along the western margin. The Burr diapir to the west of the Yankaninnna Anticline formed an apparent flat (Rowan et al., 2020), which would have created the

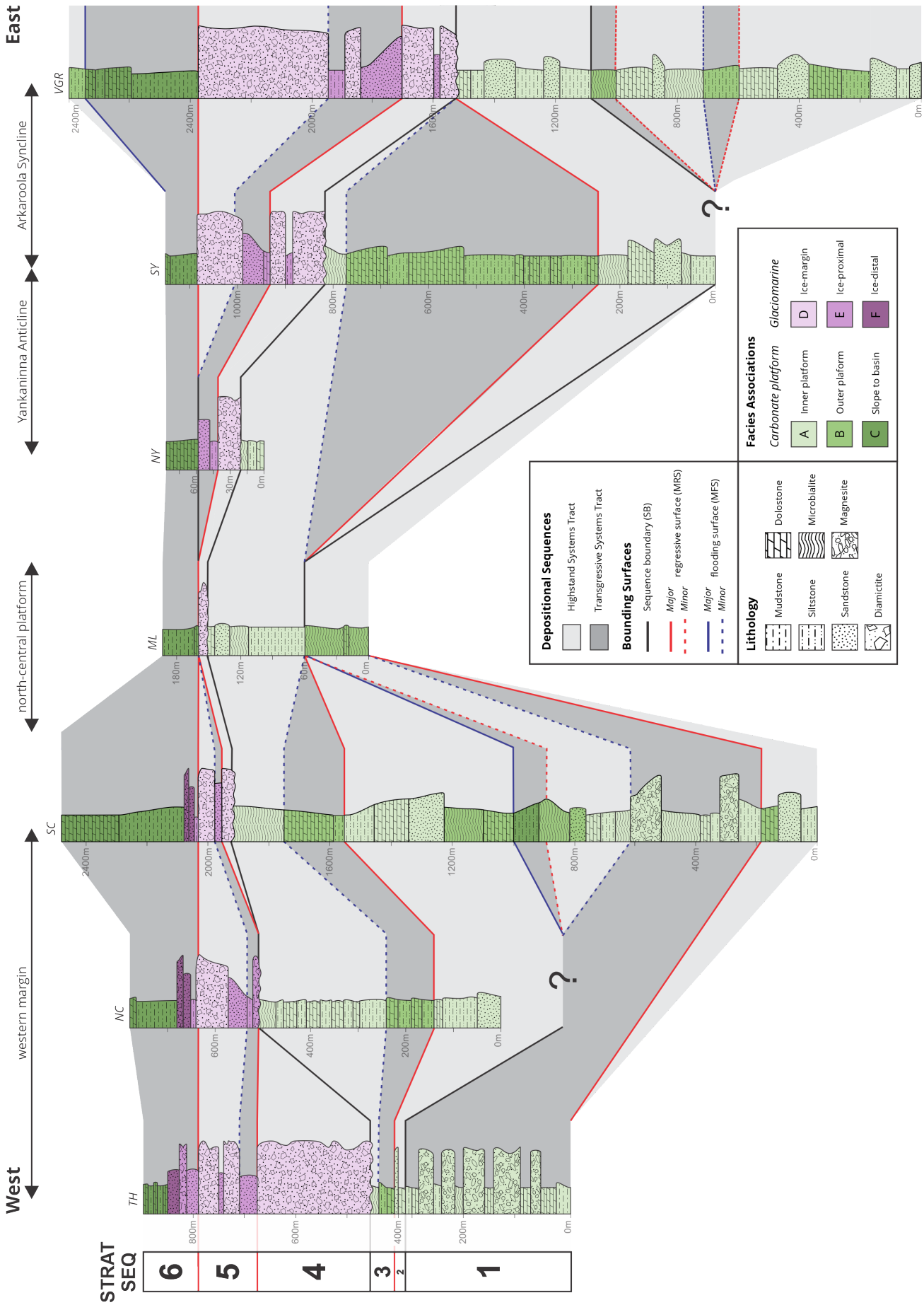

Figure 11 | Generalised sedimentary logs through Tonian-Cryogenian sections across the northern Flinders Ranges, South Australia. Colour of logs corresponds to facies associations. Grey panels indicate correlation of systems tracts between sections. Coloured dashed lines indicate correlation of sequence stratigraphic surfaces between sections. STRAT SEQ = Stratigraphic Sequences. TH = Termination Hill, NC = North Copley, SC = South Copley, ML = Mount Lyndhurst, NY = North Yankaninna, SY = South Yankaninna, VGR = Vulkathunha-Gammon Ranges.

high topography responsible for highstand deposition. This succession is recorded across most of the northern Flinders Ranges, except in the Mt Lyndhurst section (Figure 11). There are several possibilities as to why Sequence 2 is not present in the north central portion of the basin. The first is that these locations were too proximal and topographically high to be affected by the rise in base level. The second possibility is that they were restricted from the fluvial sources of sediment input. Thirdly, sediments in these locations may have been subaerially exposed and eroded during the subsequent drop in base level.

5.8.3. Sequence 3

5.8.3.1. Sequence 3.1

The widespread siltstone and dolostone unit (Sequence 3.1) that succeeds Sequence 2 is consistent with a low energy, lagoonal outer platform setting deposited during a transgression (Figure 11). This rise in base level creates a backstepping geometry as the mixed clastic and carbonate material retrograde over the underlying sandstone unit. The increase in accommodation was largely tectonically controlled (Preiss, 1987), but could also be in part eustatic due to the prevalent deposition of fine-grained sediment across the basin (Figure 11).

5.8.3.2. Sequence 3.2

The inner platform microbial succession at the top of Sequence 3 represents deposition during a highstand systems tract (Figure 11), where the accumulated sediment outpaced base-level rise and the carbonate platform aggraded and prograded basinward (Catuneanu, 2006). Like the rest of the pre-glacial succession, the transgressive-regressive cycle likely formed due to pulses of rift-related subsidence (Figure 11; Preiss, 1987). The widespread deposition of this particular succession across the basin could represent a eustatically driven fluctuation in base level. Sequence 3.2 may not have been deposited in the east in the Vulkathunha-Gammon Ranges section because that area was physically separated from the rest of the basin and dominated by the deposition of clastic material (Figure 11).

5.8.4. Sequence 4

The basal diamictite in the bottom of Sequence 4 unconformably overlies the pre-glacial successions, which is represented by a sequence boundary (SB; Figure 11). Sequence 4 could have been deposited during a lowstand systems tract and would be capped by an MRS (Figure 11). This was likely driven by climatic fluctuations and glacio-eustatic fall and marked by widespread deposition across the basin during a glacial maximum. Although sediment is typically eroded during drops in eustacy, the predominance of climatic control on deposition during the glaciation prompted a decrease in fluvial discharge and resulted in glacio-fluvial aggradation (e.g., Blum, 1994; 2001; Catuneanu, 2006). Le Heron et al. (2014) suggests that a tectonic mechanism for topography generation may not have been required. However, the extreme thickness variations of Sequence 4 across the basin (Figure 11), and in particular across the Paralana Fault in Arkaroola (Lloyd et al., 2022), suggests that faulting was active during deposition and impacted the topography. Combined glacial scour and coeval faulting was likely the cause for these thickness and lithological variations (Young & Gostin, 1991, Preiss, 2000). The considerably thinner exposure of this unit at Mt Lyndhurst (Figure 11) may have been influenced by contemporaneous uplift of the Lyndhurst Diapir (Preiss, 1987), although Rowan et al. (2020) suggested that allochthonous salt transport was initiated later during the deposition of the overlying Tapley Hill Formation. The complex geometry of this diapir, where it displays evidence of both allochthonous and thrust structures, makes it difficult to unravel both the nature and timing of emplacement (Rowan et al., 2020). On the western margin, a platform geometry may have influenced the deposition of more proximal ice-contact diamictites (Figure 11), where localised deposition in Termination Hill and South Copley may correspond to palaeovalleys that channelled ice flow (Young & Gostin, 1988, 1991). Further, the pronounced variability in depositional thickness between the South Yankaninna and North Yankaninna sections (Figure 11) was likely due to topography generated from contemporaneous faulting (Young & Gostin, 1990) and/or allochthonous salt diapirism associated with the Burr Diapir (Rowan et al., 2020). This diapir occurred less than 10 km to the west within the underlying Skillogalee Dolomite (Sequence 1), where the geometry of its eastern extent was largely influenced by a pre-existing anticlinorium (Rowan et al., 2020), referred to in this study as the Yankaninna Anticline. Uneven glacial incision further to the east could have resulted from active tectonic faulting that created uplift and increased glacial erosion relative to other parts of the basin (Young & Gostin, 1991).

5.8.5. Sequence 5

5.8.5.1. Sequence 5.1

The overlying fine-grained unit (Sequence 5.1) is consistent with deposition during a transgression (Figure 11), which would similarly have been driven by eustacy and climate. The implication of this sequence is that the Sturtian glaciation likely reflects more of a "slushball" than a hard "snowball" earth (Lewis et al., 2007). As the grounded ice margin retreated, the increased fluvial discharge from melting ice would have outpaced the rise in sea level, resulting in fluvial erosion (e.g., Blum, 1994; 2001; Catuneanu, 2006). From palaeocurrent data, glacier movement was from the south (Young & Gostin, 1991), producing a backstepping geometry from the Termination Hill section to the South Copley section (Figure 11). Sequence 5.1, and subsequent glaciogenic units, are not present in the north-central zone in Mt Lyndhurst (Figure 11). This was likely due to the topographic high in this area

and the possible erosion during the subsequent glacial advance. Coarse deposits included in this lower heterogenous unit in South Yankaninna could reflect local uplift and resedimentation of shedding material related to diapiric movements (Young & Gostin, 1990). Areas that were previously dominated by glacial scour, particularly those in the east, received significant amounts of sediment and resulted in thick deposition (Figure 11; Young & Gostin, 1991). Sequence 5.1 is exposed at the Vulkathunha-Gammon Ranges section and is lithologically dissimilar to other sections in the basin, likely due to its proximal proglacial location where coarse material continued to deposit despite the glacial recession.

5.8.5.2. Sequence 5.2

The ice proximal till of Sequence 5.2 represents deposition during a second basinward prograding package that represents either a highstand and/or lowstand systems tract, capped by an MRS (Figure 11). Like the lower diamictite (Sequence 4), this coincides with a glacial advance and an eustatic sea-level fall. However, this represents slightly more distal, subaqueous deposition relative to the first glacial advance (Young & Gostin, 1988; 1990; 1991). This unit does not appear in the Mt Lyndhurst and North Yankaninna sections (Figure 11). As these sections correlate with a central high (horst) in the basin, Sequence 5.2 may not have been deposited or was potentially eroded.

5.8.6. Sequence 6

5.8.6.1. Sequence 6.1

Like the lower heterogenous unit (Sequence 5.1), Sequence 6.1 is characterised by transgressive, fine-grained lithofacies (Figure 11), although deposited during widespread deglaciation rather than an ice retreat. This was probably driven by climatic warming following the glacial maximum and eustatic sea level rise, where fine-grained subaqueous sediment backstepped and retrograded landward. Sequence 6.1 is only recorded along the western margin (Figure 11), which could correspond to the tabular geometry here and subsequent susceptibility to flooding.

5.8.6.2. Sequence 6.2

The slope to basinal succession of Sequence 6.2 is consistent with deposition during a widespread transgression (Figure 11), where postglacial sediments backstepped over the continental margin. Consequently, this succession is recorded on the adjacent Stuart Shelf in the west and right over the Curnamona province to the Barrier Ranges in New South Wales to the east (Preiss, 1987). The predominance of fine-grained material (Figure 11), and depositional spread and synchronicity across the basin have been used to suggest that post-rift thermal subsidence likely assisted the eustatic rise (Preiss, 1987; Powell, 1994). Deglaciation delivered large amounts of detritus into the marine environment, which resulted in considerable stratigraphic thicknesses of this postglacial succession in the Adelaide Superbasin (Lloyd et al., 2020). This has been hypothesised to have stimulated eukaryote evolution through the flux of detrital bio-essential nutrients (Brocks et al., 2017).

Carbonate rocks ("cap carbonates") at the base of Sequence 6.2 are recorded in the northern most sections of this study (Figure 11), which could be due to their more restricted setting relative to other locations in the basin. These more restricted settings provide an optimal environment for cap carbonate precipitation due to the increased effect of ocean stratification, low salinity, and greater alkalinity production (Yu et al., 2020). This was likely due to their relative proximity to continental weathering sources.

5.9. Global context

5.9.1. Stratigraphy

5.9.1.1. Pre-glacial

The pre-glacial succession in South Australia was marked by active rifting that created topographic variability and varying sediment supply across the basin. Subsurface allochthonous salt movement during Skillogalee Dolomite Formation (Sequence 1 and 2) times is also documented to have a role in topography creation (Rowan et al., 2020). This regional tectonic control during Tonian deposition has been shown in other sections globally, including key sites in Namibia, Canada, China, Svalbard, Scotland and Ethiopia (Figure 12).

Namibia and northern Canada both underwent episodic cratonic rifting during the Tonian (Figure 12; Narbonne & Aitken, 1995; Frimmel et al., 1996; Hoffman & Halverson, 2008; Miller, 2013; Hood et al., 2015; Milton et al., 2017; Lamothe et al., 2019). These were characterised by deposition of up to 5800 m and 3500 m of coarse clastics, evaporitic to subtidal carbonates, and deep water shales, representing multiple regressive-transgressive cycles (Chartrand & Brown, 1985; Park & Jefferson, 1991; Narbonne & Aitken, 1995; Batten et al., 2004; Long & Turner, 2013; Hood et al., 2015; Lamothe et al., 2019). In South China, rifting was more consistently active throughout the Tonian (Figure 12; Zhang et al., 2011; Lan et al., 2015; Busigny et al., 2018), and resulted in 200 m to 3500 m thick (Zhang et al., 2008) successions characterised by fine-grained clastic turbidites and minor platform carbonates (Wang & Li, 2001).

Conversely, Svalbard and Scotland appear to be in a post-rift thermal subsidence phase during the Tonian (Figure 12; Smith et al., 1999; Maloof et al., 2006; Stephenson et al., 2013; Halverson et al., 2017). This resulted in the deposition of 1000 m of transgressive-regressive sequences in a carbonate platform setting (Halverson et al., 2017) and up to 15,500 m of cyclical clastics and carbonates in deep to shallow water settings, respectively (Glover & Winchester,

1989; Smith et al., 1999; Stephenson et al., 2013; Fairchild et al., 2017).

The pre-glacial succession in northern Ethiopia developed in an intra-oceanic back-arc basin (Figure 12; Alene et al., 2006; Miller et al., 2009; 2011; Swanson-Hysell et al., 2015; Park et al., 2020), where slab rollback followed by thermal isostatic subsidence facilitated the deposition of up to 5 km of intertidal carbonate and siliciclastics and subtidal, micritic carbonates, respectively (Alene et al., 2006; Miller et al., 2009; 2011; Swanson-Hysell et al., 2015; Park et al., 2020).

5.9.1.2. Syn-glacial

The syn-glacial succession in Australia is characterised by two glacial advance and retreat cycles in a glaciomarine setting, reflecting climatically driven eustatic changes in base level, and coeval faulting that impacted the thickness distribution of the glacial unit across the basin.

Sections in northern Canada (Eisbacher, 1985; Narbonne et al., 1994), California (Busfield & Le Heron, 2016; Le Heron & Busfield, 2016), Idaho and Utah (Crittenden et al., 1983; Link & Christie-Blick, 2011) all preserve two diamictite packages with interbedded carbonate and clastic units, representing glacial advance and retreat phases in glaciomarine environments, respectively. Although there were significant climate-driven eustatic sea-level fluctuations during the Sturtian glaciation, the deposition of sections in USA and Canada were still largely fault controlled in response to continental rifting (Figure 12; Eisbacher, 1985; Link et al., 1994; Narbonne et al., 1994; Fairchild & Kennedy, 2007; Link & Christie-Blick, 2011; Keeley et al., 2012).

The <2000 m thick syn-glacial successions in South China and Namibia have very thin (20 m and 30 m thick) intervals of mudstone and sandstone between thicker diamictite packages (Zhang et al., 2011; Le Heron et al., 2013; Lan et al., 2015; Buechi et al., 2017; Hoffman et al., 2017a). These have been interpreted as representing a sub-glacial to glaciomarine environment, influenced by both fluctuations in climate-controlled eustasy (Zhang et al., 2011; Le Heron et al., 2013) and tectonic phases (Zhang et al., 2011; Hoffman et al., 2017a; Busigny et al., 2018).

In Scotland, the syn-glacial succession is ~1100 m thick, depositing diamictites with interbedded clastics that represent a glaciomarine environment (Ali et al., 2018; Fairchild et al., 2017). This climatically dynamic succession is interpreted to result from tectonic subsidence, eustatic changes, ice loading and extreme seasonal fluxes (Ali et al., 2018; Fairchild et al., 2017).

Conversely, the deposition of glaciomarine diamictites with shale interbeds in Svalbard is incredibly thin (average 10 m) (Halverson et al., 2011; 2017; 2022; Hoffman et al., 2012; Kunzmann et al., 2015; Fairchild et al., 2016). This was likely due to the decreased accommodation space and/or erosion from reduced subsidence during deposition in the Cryogenian (Halverson et al., 2022), resulting in an unconformity of approximately 10 million years (Millikin et al., 2022).

The syn-glacial succession in northern Ethiopia is consistent with a subglacial to glaciomarine setting (Park et al., 2020). This is represented by ~750 m of massive diamictites with interbedded sandstone, siltstone, micritic carbonate and carbonate breccia (Park et al., 2020), which accumulated during thermal subsidence (Alene et al., 2006). In this scenario, the sediment was able to keep pace with the increasing accommodation space (Park et al., 2020), which maintained a relatively proximal setting.

5.9.1.3. Post-glacial

The post-glacial succession in Australia is represented by widespread transgressive to basinal shales and carbonates, a result of de-glacial eustatic sea level rise coupled with thermal sag after rifting (Figure 12).

A transgression to deeper water argillite, carbonates and turbidites has been recorded in North America, where between 200 m and 1000 m of material accumulated in northern Canada (Eisbacher, 1985; Narbonne et al., 1994), California (Nelson et al., 2020; 2021), Idaho (Fanning & Link, 2004; Lund et al., 2003; Link & Christie-Blick, 2011; Keeley et al., 2012), and Utah (Crittenden et al., 1971; Link & Christie-Blick, 2011; Balgord et al., 2013). The accommodation space increase was likely controlled by a combination of eustatic and tectonic factors associated with the developing Pacific margin (Figure 12; Eisbacher, 1985; Narbonne et al., 1994; Link & Christie-Blick, 2011; Keeley et al., 2012; Balgord et al., 2013).

Deep-water successions were also deposited after the Sturtian glaciation in South China and Svalbard. Sections in South China are 12–500 m thick, and deposit basinal muddy clastics and carbonaceous shales (Zhang et al., 2011), while Svalbard is characterised by up to 215 m of offshore marine dolomitic shales and siltstones (Hoffman et al., 2012; 2017a; Fairchild et al., 2016; 2016a). South China was marked by persistent rift-induced subsidence, and deposition transgressed into a restricted shelf setting (Zhang et al., 2011). Conversely, Svalbard was already in a post-rift setting (Figure 12) and exhibited no apparent changes in relative sea level with the underlying diamictite (Halverson et al., 2004; 2011).

Namibia and Scotland form a sharp contrast to the aforementioned post-glacial successions, and record deposition in much shallower settings. The <450 m thick unit in Namibia is characterised by laminated dolostone, turbidites and microbial carbonates, deposited in a shallow water, platform environment (Hoffman et al., 2017a; 2021). Meanwhile, the post-glacial unit in Scotland is represented by 350 m of shallow subtidal to intertidal clastics

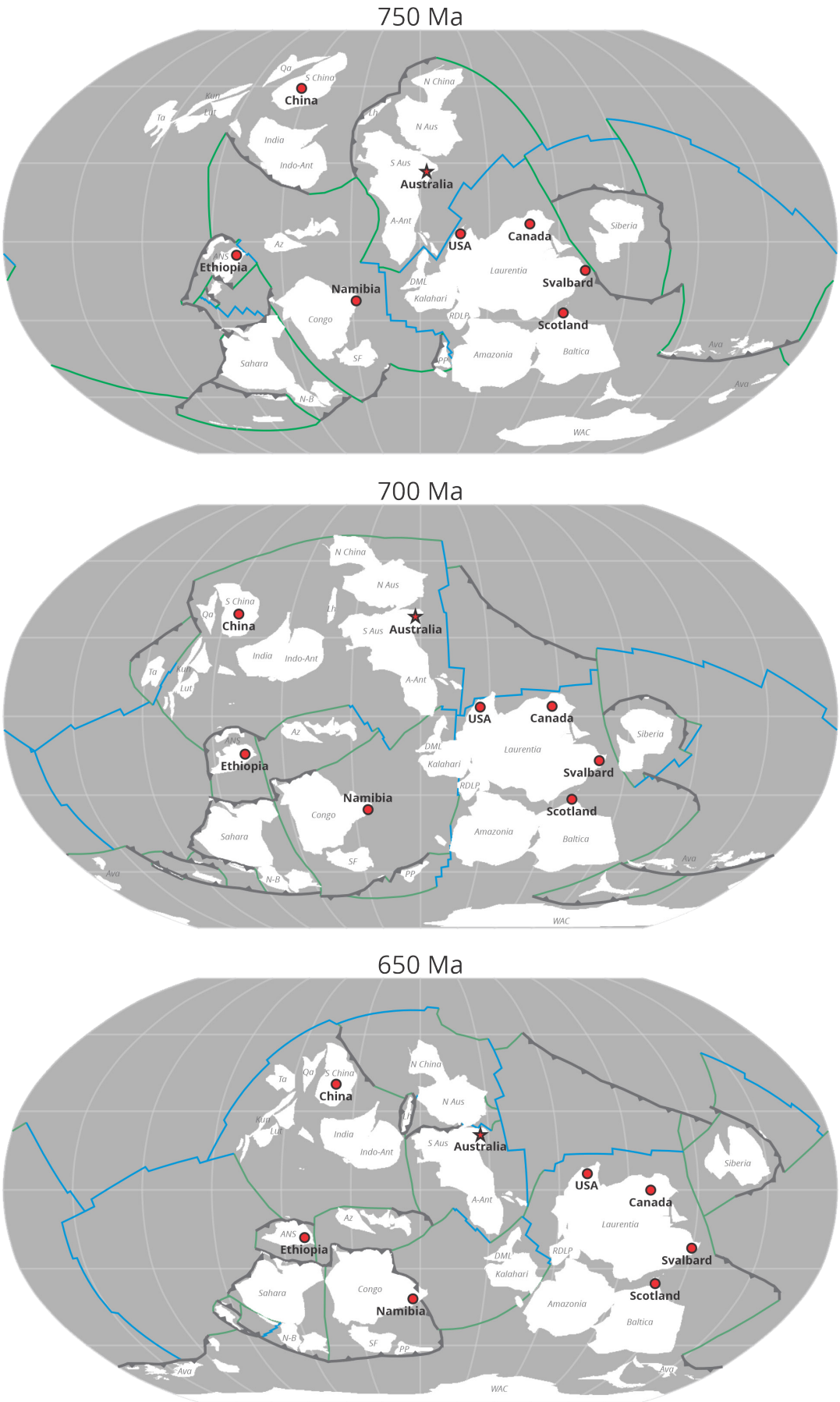

Figure 12 | Global plate models with evolving plate boundaries. Models were produced using G-Plates software and files from Merdith et al. (2021). Each model corresponds to key time slice in Tonian or Cryogenian. 750 Ma = pre-glacial. 700 Ma = syn-glacial. 650 Ma = post-glacial. Transform boundary = green line. Divergent boundary = blue line. Convergent boundary = grey line (arrows indicate direction). Key sites marked by red circles. This study marked by red star. Cratons and continents labelled in grey. ANS = Arabian Nubian Shield, Ant = Antarctica, A-Ant = Austral-Antarctica, Aus = Australia, Ava = Avalonia, Az = Azania, DML = Dronning Maud Land, Kun = Kunlun, N-B = Nigeria-Benin, Qa = Qaidam, Lh = Lhasa, PP = Parana Panema, RDLP = Rio de la Plata, SF = Sao Francisco, Ta = Tarim, WAC = West African Craton.

and carbonates (Spencer & Spencer, 1972; Anderson et al., 2013; Stephenson et al., 2013; Fairchild et al., 2017; Ali et al., 2018). The shallow platform setting in Namibia was the result of active uplift during deposition at the edge of the basin (Hoffman et al., 2017a; 2021), while Scotland was experiencing steady subsidence that was balanced by high sediment supply (Ali et al., 2018).

5.9.2. Correlation and significance

5.9.2.1. Pre-glacial

An overall increase in accommodation space and deposition of marginal marine, interbedded clastic and carbonate successions characterise Tonian deposits globally, including those in Australia, Namibia, northern Canada, South China, Svalbard, Scotland and Ethiopia. The widespread extent of these comparable depositional settings is likely to reflect global signatures, which were then modified by local tectonically driven effects.

The abundant platform carbonates recorded at these locations suggest that the climate during this time was stable, and despite the variability in palaeolatitudes (Figure 12), promoted deposition in warm, shallow seas globally (MacLennan et al., 2020). Further, the correlation of isotopic signatures recorded in these Tonian rocks has often been used to justify that the basins developing during this time were globally connected (Halverson et al., 2005; 2010; Park et al., 2020). As the $\delta^{13}C$ signature in carbonates and organic-rich shales is used as a measure of bioproductivity (Knoll et al., 1986; Schidlowski, 1988), and the Proterozoic ocean is widely accepted to have been stratified (i.e., oxic shallow water and anoxic deep water; Preiss, 1987; Giddings & Wallace, 2009a; Hood & Wallace, 2015; Counts, 2017), excursions in the isotope record may correspond to shifts from bioproductive, oxic, shallow water (positive $\delta^{13}C$ values) to biologically inactive, anoxic deep water (negative $\delta^{13}C$ values). Consequently, the preservation and correlation of negative excursions at multiple sites globally could reflect widespread transgressions that, on that scale, likely resulted from eustatic sea level rise.

With that said, the development of basins during the Tonian largely resulted from active tectonism associated with the breakup of supercontinent Rodinia (Merdith et al., 2021), and corresponds to a suite of local tectonic conditions (e.g., rifting, subsidence and slab rollback) that would have influenced the production of accommodation space. These local tectonic controls may modify the lithostratigraphic trends recorded in Tonian successions, and by extension, the chemostratigraphic record.

5.9.2.2. Syn-glacial

The Sturtian glaciation is recognised in the stratigraphic record through the deposition of distinct diamictite intervals capped by carbonate rocks, which, accompanied by palaeomagnetic and geochemical data, facilitated the correlation of these deposits globally (Hoffman & Schrag, 2002). However, the stratigraphic thicknesses of these units and the presence or absence of finer-grained interbeds have resulted in contention surrounding the extent and cyclicity of the icehouse.

Although the glacial successions in North America appear to record a very similar two-fold glacial advance-retreat cycle to that in South Australia (Eisbacher, 1985; Link et al., 1994), Le Heron et al. (2020) suggested that these instead represent regional, diachronous glacial cycles. In fact, Le Heron et al. (2020) makes a controversial suggestion that because there have been no direct ages from the Sturtian cryochron in Australia, just ages that bracket the glacial rocks, then perhaps there was no glaciation in Australia between ca. 716 and 663 Ma. However, recent laser Rb–Sr dating of shales in the lower heterogenous unit (Sequence 3.2) in a borehole from the Stuart Shelf yields an age of 684 ± 37 Ma (Lloyd et al. 2023), and instead suggests that the Sturtian cryochron of South Australia had a ca. 58 Ma time span, and represents two major ice advances, one before ca. 684 Ma and a second between ca. 684 and 663 Ma. These data agree with the syn-glacial volcanic ages from Idaho of Lund et al. (2003), demonstrating that the glaciations in North America and Australia were likely synchronous.

Like in Australia and North America, the glacial successions in South China and Namibia have been interpreted as reflecting a glacial retreat phase between two glacial advance episodes in a glaciomarine setting (Zhang et al., 2011; Le Heron et al., 2013; Lan et al., 2015), which was largely controlled by climatic sea level changes (Zhang et al., 2011; Le Heron et al., 2013). However, these sections have also been interpreted to reflect sub-ice deposition during a singular glacial event (Lechte and Wallace, 2016; Buechi et al., 2017; Hoffman et al., 2017a; Busigny et al., 2018), with more emphasis on the influence of changing tectonic phases (Figure 12; Zhang et al., 2011; Hoffman et al., 2017a; Busigny et al., 2018). Further, the thick interbedded diamictite and clastic successions in Scotland have been interpreted to represent up to 28 glacial cycles (Ali et al., 2018; Fairchild et al., 2017).

For these reasons, although age constraints and detailed paleoenvironmental interpretations are improving, it is still uncertain whether the Sturtian glacial cycle advances were global (eustatically driven) or happening at different times and at more local scales (tectonically driven).

5.9.2.3. Post-glacial

The transgression at the end of the Sturtian glaciation is observed globally and is widely accepted to be a consequence of eustatic sea level rise driven by melting of continental ice sheets (Kaufman et al., 1997; Kennedy et al., 1998; Bold et al., 2016). Not only was there significant eustatic sea level rise and climatic warming, but there is

a notable tectonic shift to post-rift subsidence at almost all the sites discussed above, which would further increase accommodation in basins globally. Further, the distinct carbonate cap unit that overlies glaciogenic rocks has been documented at many localities and records a sharp negative $\delta^{13}C$ excursion that has long been used as a chemostratigraphic tool to correlate this horizon (Halverson et al., 2005; 2010; Park et al., 2020). Consequently, the post Sturtian-glacial interval is one of the most well constrained and reliably correlated of the Neoproterozoic..

6. Conclusions

The Adelaide Superbasin was a dynamic basin influenced by syn-sedimentary tectonics, and climate and environmental changes throughout the Tonian and Cryogenian. This study presents over 8,350 m of measured sedimentary logs through seven sections in an approximately 150 km east–west transect across the northern Flinders Ranges. This includes sites in Termination Hill, Copley, Mount Lyndhurst, Yankaninna and Vulkathunha-Gammon Ranges. From these, 18 lithofacies, 6 facies associations and 11 depositional environments have been classified.

Facies and sequence stratigraphic analyses reveal deposition in a carbonate platform setting for the preglacial succession, where in the western margin a mixed carbonate succession of dolostone and magnesite accumulated under the influence of fluctuations in sea level. A topographic high in the north central portion of the basin at Mount Lyndhurst is characterised by a high-relief platform margin microbialite reef. To the east, at Yankaninna, the preglacial succession is represented by more equal volumes of fine-grained clastic and carbonate facies that were deposited in a ramp-style platform environment. Further east again, clastic rocks dominate the succession. These were sourced locally from contemporaneous fault-created topography, with some possible topography created by salt tectonics. The syn-glacial sequence coincides with a climatically driven regression. This succession is represented by two tillite units and two fine-grained heterogenous units, that represent glacial advance and retreat phases, respectively. The platform geometry of the western margin and subsequent susceptibility to flooding promoted the deposition of ice-contact till and distal fine-grained clastics. Conversely, the central part of the basin was characterised by a number of topographic highs and palaeovalleys, which were marked by a lack of glacial deposition, and a mix of proximal proglacial till and fine-grained sediment, respectively. On the eastern side of the basin, thick tillites and coarse interbedded deposits are interpreted to result from increased glacial erosion in response to syn-depositional fault-created accommodation space and proximity to uplift source areas relative to other parts of the basin. The post-glacial succession in the northern Flinders Ranges is represented by a widespread transgression following the Sturtian glaciation that was driven by the large volume of melting ice. This promoted the deposition of slope to basinal fine-grained siltstone and dolostone facies at all locations in the study area, with varying proportions of clastic and carbonate deposits.

The lithostratigraphic and sequence stratigraphic correlation of Tonian to Cryogenian successions globally provides insights into the scale and impact of tectonic, eustatic and climate conditions, highlighting whether these changes were occurring on a local level or influencing the global system. Tonian successions in Australia, Ethiopia, Namibia, South China, Canada, Svalbard (Norway), and Scotland are all represented by the deposition of marginal marine clastics and carbonates, indicating stable climatic conditions. Further, these sites have been correlated through chemostratigraphy based on the shared record of carbon isotope excursions, implying global connections between these developing basins. However, the impact of tectonics complicates this correlation, as local tectonic regimes superimpose on litho- and chemo-stratigraphic signatures. Locations in North America (northern Canada, California, Idaho and Utah) are comparable to South Australia during the Sturtian glaciation, as they also preserve two distinct glacial advance-retreat cycles that were deposited during faulting and rifting. However, uncertainty surrounding the timing of these glaciations calls into question the synchronicity of the Sturtian. Further, glacial cyclicity at these sites ranges from one to several dozen, which convolutes our understanding of the global extent of this glaciation. Conversely, the post-glacial transgression is more consistent globally. This interval is marked by distinct litho- chemo- and sequence stratigraphic shifts to deep water carbonates that record a negative carbon isotope excursion and demonstrate the widespread nature of the Sturtian deglaciation.

This comprehensive sedimentological and sequence stratigraphic analysis presents a facies architecture and stratigraphic framework for the Tonian to Cryogenian across the Adelaide Rift Complex in the northern Flinders Ranges. The study elucidates the temporal and spatial distribution of depositional environments before, during and after the global Sturtian glaciation, and correlates the stratigraphic framework of this basin with others that were developing across the globe during this unique time in Earth's history.

Acknowledgments

We acknowledge that this research is conducted on the ancestral lands for the Adnyamathanha people. We acknowledge and respect their deep feelings of attachment and spiritual relationship to Country, and that their cultural and heritage beliefs are still as important to the living people today. We thank reviewers Paula Castillo and John Counts, executive editor Giovanna Della Porta, and associate editor Or Bialik for their valuable insight, comments and advice that greatly improved the quality of this manuscript. This project was supported by funding from the Geological Survey of South Australia, and an Australian Government Research Training Program (RTP)

Scholarship awarded to Virgo. We are very grateful to Jack Ward (The University of Queensland) and Jarred Lloyd (The University of Adelaide) for their field assistance in 2018 and 2019, respectively. We would also like to thank the Department for Energy and Water (DEW) for granting us a permit to undertake scientific research in Witchelina (Permit Number: Q26796-1).

Authors contribution

Georgina M. Virgo: Investigation, Methodology, Formal analysis, Writing – original draft, Writing - review & editing, Visualization. Alan S. Collins: Supervision, Investigation, Writing - review & editing, Funding acquisition. Morgan L. Blades: Methodology, Investigation, Writing - review & editing. Kathryn J. Amos: Supervision, Writing - review & editing, Funding acquisition.

Data availability

The authors confirm that the data supporting the findings of this study are available within the article and its supplementary material.

Conflict of interest

The authors declare that they have no known competing financial interests or personal relationships that could have appeared to influence the work reported in this paper.

References

Alene, M., Jenkin, G. R., Leng, M. J. & Darbyshire, D. F. (2006). The Tambien Group, Ethiopia: an early Cryogenian (ca. 800–735 Ma) neoproterozoic sequence in the Arabian–Nubian shield. Precambrian Research 147(1-2): 79-99. https://doi.org/10.1016/j.precamres.2006.02.002

Ali, D. O., Spencer, A. M., Fairchild, I. J., Chew, K. J., Anderton, R., Levell, B. K., Hambrey, M. J., Dove, D. & Le Heron, D. P. (2018). Indicators of relative completeness of the glacial record of the Port Askaig Formation, Garvellach Islands, Scotland. Precambrian Research 319: 65-78. https://doi.org/10.1016/j.precamres.2017.12.005

Anderson, J. B. (1989). Antarctica's glacial setting. Glacial-Marine Sedimentation. Short course in Geology (9): 11-57.

Anderson, R. P., Fairchild, I. J., Tosca, N. J. & Knoll, A. H. (2013). Microstructures in metasedimentary rocks from the Neoproterozoic Bonahaven Formation, Scotland: Microconcretions, impact spherules, or microfossils? Precambrian Research 233: 59-72. https://doi.org/10.1016/j.precamres.2013.04.016

Armistead, S. E., Collins, A. S., Buckman, S. & Atkins, R. (2020). Age and geochemistry of the Boucaut Volcanics in the Neoproterozoic Adelaide Rift Complex, South Australia. Australian Journal of Earth Sciences 68(4): 1-10. https://doi.org/10.1080/08120099.2021.1840435

Arnott, R. W. & Southard, J.B. (1990). Exploratory flow-duct experiments on combined-flow bed configurations, and some implications for interpreting storm-event stratification. Journal of Sedimentary Research 60(2): 211-219. https://doi.org/10.1306/212F9156-2B24-11D7-8648000102C1865D

Ashley, G. M. (1990). Classification of large-scale subaqueous bedforms; a new look at an old problem. Journal of Sedimentary Research 60(1): 160-172. https://doi.org/10.2110/jsr.60.160

Ashley, G. M., Southard, J. B. & BoothRoyd, J. C. (1982). Deposition of climbing-ripple beds: a flume simulation. Sedimentology, 29(1), 67-79. https://doi.org/10.1111/j.1365-3091.1982.tb01709.x

Assereto, R. L. & Kendall, C. G. ST C. (1977). Nature, origin and classification of peritidal tepee structures and related breccias. Sedimentology 24(2): 153-210. https://doi.org/10.1111/j.1365-3091.1977.tb00254.x

Avigad, D., Stern, R. J., Beyth, M., Miller, N. & McWilliams, M. O. (2007). Detrital zircon U–Pb geochronology of Cryogenian diamictites and Lower Paleozoic sandstone in Ethiopia (Tigrai): age constraints on Neoproterozoic glaciation and crustal evolution of the southern Arabian–Nubian Shield. Precambrian Research 154(1-2): 88-106. https://doi.org/10.1016/j.precamres.2006.12.004

Baas, J. H., Van Dam, R. L. & Storms, J. E. A. (2000). Duration of deposition from decelerating high-density turbidity currents. Sedimentary Geology 136(1-2): 71-88. https://doi.org/10.1016/S0037-0738(00)00088-9

Balgord, E. A., Yonkee, W. A., Link, P. K. & Fanning, C. M. (2013). Stratigraphic, geochronologic, and geochemical record of the Cryogenian Perry Canyon Formation, northern Utah: Implications for Rodinia rifting and snowball Earth glaciation. Bulletin 125(9-10): 1442-1467. https://doi.org/10.1130/B30860.1

Basilici, G., de Luca, P. H. V. & Poiré, D. G. (2012). Hummocky cross-stratification-like structures and combined-flow ripples in the Punta Negra Formation (Lower-Middle Devonian, Argentine Precordillera): a turbiditic deep-water or storm-dominated prodelta inner-shelf system? Sedimentary Geology 267: 73-92.

Batten, K. L., Narbonne, G. M. & James, N. P. (2004). Paleoenvironments and growth of early Neoproterozoic calcimicrobial reefs: platformal Little Dal Group, northwestern Canada. Precambrian Research 133(3-4): 249-269. https://doi.org/10.1016/j.precamres.2004.05.003

Belperio, A. (1990). Palaeoenvironmental interpretations of the Late Proterozoic Skillogalee Dolomite in the Willouran Ranges, South Australia. The Evolution of a Late Precambrian–Early Palaeozoic Rift Complex: The Adelaide Geosyncline. Geol. Soc. Aust. Spec. Publ 16: 85-104.

Bhattacharya, A. (1997). On the origin of non-tidal flaser bedding in point bar deposits of the river Ajay, Bihar and West Bengal, NE India. Sedimentology 44(6): 973-975. https://doi.org/10.1111/j.1365-3091.1997.tb02172.x

Blum, M. (2001). Importance of falling stage fluvial deposition: Quaternary examples from the Texas Gulf Coastal Plain and Western Europe. Seventh International Conference on Fluvial Sedimentology, Lincoln, August.

Blum, M. D. (1993). Genesis and architecture of incised valley fill sequences: a Late Quaternary example from the Colorado River, Gulf Coastal Plain of Texas: Chapter 10: Recent applications of siliciclastic sequence stratigraphy. M 58: Siliciclastic Sequence Stratigraphy: Recent Developments and Applications: 259-283.

Boggs Jr, S. (2014). Principles of sedimentology and stratigraphy. Pearson Education.

Bold, U., Smith, E. F., Rooney, A. D., Bowring, S. A., Buchwaldt, R., Dudás, F. Ő., Ramezani, J., Crowley, J. L., Schrag, D. P. & Macdonald, F. A. (2016). Neoproterozoic stratigraphy of the

Zavkhan terrane of Mongolia: The backbone for Cryogenian and early Ediacaran chemostratigraphic records. American Journal of Science 316(1): 1-63. https://doi.org/10.2475/01.2016.01

Bouma, A. (1964). Turbidites. Developments in Sedimentology, Elsevier. 3: 247-256. https://doi.org/10.1016/S0070-4571(08)70967-1

Bridge, J. S. (2009). Rivers and floodplains: forms, processes, and sedimentary record. John Wiley & Sons.

Brocks, J. J., Jarrett, A. J., Sirantoine, E., Hallmann, C., Hoshino, Y. & Liyanage, T. (2017). The rise of algae in Cryogenian oceans and the emergence of animals. Nature 548(7669): 578-581. https://doi.org/10.1038/nature23457

Buechi, M. W., Frank, S. M., Graf, H. R., Menzies, J. & Anselmetti, F. S. (2017). Subglacial emplacement of tills and meltwater deposits at the base of overdeepened bedrock troughs. Sedimentology 64(3): 658-685. https://doi.org/10.1111/sed.12319

Busfield, M. & Le Heron, D. (2014). Sequencing the Sturtian icehouse: dynamic ice behaviour in South Australia. Journal of the Geological Society 171(3): 443-456. https://doi.org/10.1144/jgs2013-067

Busfield, M. E. & Le Heron, D. P. (2013). Glacitectonic deformation in the Chuos Formation of northern Namibia: implications for Neoproterozoic ice dynamics. Proceedings of the Geologists' Association 124(5): 778-789. https://doi.org/10.1016/j.pgeola.2012.10.005

Busfield, M. E. & Le Heron, D. P. (2016). A Neoproterozoic ice advance sequence, Sperry Wash, California. Sedimentology 63(2): 307-330. https://doi.org/10.1111/sed.12210

Busigny, V., Planavsky, N. J., Goldbaum, E., Lechte, M. A., Feng, L. & Lyons, T. W. (2018). Origin of the Neoproterozoic Fulu iron formation, South China: Insights from iron isotopes and rare earth element patterns. Geochimica et Cosmochimica Acta 242: 123-142. https://doi.org/10.1016/j.gca.2018.09.006

Butterfield, N. J. (2011). Animals and the invention of the Phanerozoic Earth system. Trends in ecology & evolution 26(2): 81-87. https://doi.org/10.1016/j.tree.2010.11.012

Catuneanu, O. (2006). Principles of sequence stratigraphy. Elsevier.

Catuneanu, O., Abreu, V., Bhattacharya, J. P., Blum, M. D., Dalrymple, R. W., Eriksson, P. G., Fielding, C. R., Fisher, W. L., Galloway, W. E., Gibling, M. R. & Giles, K. A. (2009). Towards the standardization of sequence stratigraphy. Earth-Science Reviews 92(1-2): 1-33. https://doi.org/10.1016/j.earscirev.2008.10.003

Catuneanu, O., Galloway, W. E., Kendall, C. G. St C., Miall, A. D., Posamentier, H. W., Strasser, A. & Tucker M. E. (2011). Sequence stratigraphy: methodology and nomenclature. Newsletters on stratigraphy 44(3): 173-245.

Catuneanu, O. (2017). Sequence stratigraphy: Guidelines for a standard methodology. Stratigraphy & timescales, Elsevier. 2: 1-57. https://doi.org/10.1016/bs.sats.2017.07.003

Chakrabarti, A. (2005). Sedimentary structures of tidal flats: A journey from coast to inner estuarine region of eastern India. Journal of earth system science 114(3): 353-368. https://doi.org/10.1007/BF02702954

Chartrand, F. & Brown, A. (1985). The diagenetic origin of stratiform copper mineralization, Coates Lake, Redstone copper belt, NWT, Canada. Economic Geology 80(2): 325-343. https://doi.org/10.2113/gsecongeo.80.2.325

Cheel, R. J. (1990). Horizontal lamination and the sequence of bed phases and stratification under upper-flow-regime conditions. Sedimentology 37(3): 517-529. https://doi.org/10.1111/j.1365-3091.1990.tb00151.x

Cheel, R. J. (1991). Grain fabric in hummocky cross-stratified storm beds; genetic implications. Journal of Sedimentary Research 61(1): 102-110. https://doi.org/10.1306/D426769A-2B26-11D7-8648000102C1865D

Cheel, R. J. & Leckie, D. A. (1993). Hummocky cross-stratification. Sedimentology review 1, Blackwell Scientific Publications Oxford. 1: 103-122.

Chiarella, D., Longhitano, S. G. & Tropeano, M. (2017). Types of mixing and heterogeneities in siliciclastic-carbonate sediments. Marine and Petroleum Geology 88: 617-627. https://doi.org/10.1016/j.marpetgeo.2017.09.010

Coats, R. (1973). Geological Atlas 1:250 000 Series: Sheet 54-9, Copley [Map].

Collins, A. S., Blades, M. L., Merdith, A. S. & Foden, J. D. (2021). Closure of the Proterozoic Mozambique Ocean was instigated by a late Tonian plate reorganization event. Communications Earth & Environment 2(1): 75 https://doi.org/10.1038/s43247-021-00149-z

Colquhoun, G. P. (1995). Siliciclastic sedimentation on a storm-and tide-influenced shelf and shoreline: the Early Devonian Roxburgh Formation, NE Lachlan Fold Belt, south-eastern Australia. Sedimentary Geology 97(1-2): 69-98. https://doi.org/10.1016/0037-0738(94)00142-H

Corkeron, M. L. & Slezak, P. R. (2020). Stromatolite framework builders: ecosystems in a Cryogenian interglacial reef. Australian Journal of Earth Sciences, 67(6), 833-856. https://doi.org/10.1080/08120099.2020.1732464

Counts, J. W., Rarity, F., Ainsworth, R. B., Amos, K. J., Lane, T., Moron, S., Trainor, J., Valenti, C. & Nanson, R. (2016). Sedimentological interpretation of an Ediacaran delta: Bonney Sandstone, South Australia. Australian Journal of Earth Sciences, 63(3), 257-273. https://doi.org/10.1080/08120099.2016.1180322

Counts, J. W. (2017). The Adelaide Rift Complex in the Flinders Ranges: Geologic history, past investigations and relevant analogues. Department of the Premier and Cabinet, South Australia, Adelaide, Report Book 16: 42.

Cox, G. M., Isakson, V., Hoffman, P. F., Gernon, T. M., Schmitz, M. D., Shahin, S., Collins, A. S., Preiss, W., Blades, M. L., Mitchell, R. N. & Nordsvan, A. (2018). South Australian U-Pb zircon (CA-ID-TIMS) age supports globally synchronous Sturtian deglaciation. Precambrian Research 315: 257-263. https://doi.org/10.1016/j.precamres.2018.07.007

Crittenden Jr, M. D., Christie-Blick, N. & Karl Link, P. (1983). Evidence for two pulses of glaciation during the late Proterozoic in northern Utah and southeastern Idaho. Geological Society of America Bulletin 94(4): 437-450. https://doi.org/10.1130/0016-7606(1983)94<437:EFTPOG>2.0.CO;2

Crittenden Jr, M. D., Schaeffer, F. E., Trimble, D. E. & Woodward, L. A. (1971). Nomenclature and correlation of some upper Precambrian and basal Cambrian sequences in western Utah and southeastern Idaho. Geological Society of America Bulletin 82(3): 581-602. https://doi.org/10.1130/0016-7606(1971)82[581:NACOSU]2.0.CO;2

Daidu, F., Yuan, W. & Min, L. (2013). Classifications, sedimentary features and facies associations of tidal flats. Journal of Palaeogeography 2(1): 66-80. https://doi.org/10.3724/SP.J.1261.2013.00018

Donovan, R. N. & Foster, R. J. (1972). Subaqueous shrinkage cracks from the Caithness Flagstone Series (middle Devonian) of northeast Scotland. Journal of Sedimentary Research 42(2): 309-317. https://doi.org/10.1306/74D72531-2B21-11D7-8648000102C1865D

Duke, W. L., Arnott, R. W. C. & Cheel, R. J. (1991). Shelf sandstones and hummocky cross-stratification: new insights on a stormy debate. Geology 19(6): 625-628. https://doi.org/10.1130/0091-7613(1991)019<0625:SSAHCS>2.3.CO;2

Dumas, S. & Arnott, R. (2006). Origin of hummocky and swaley cross-stratification—The controlling influence of unidirectional current strength and aggradation rate. Geology 34(12): 1073-1076. https://doi.org/10.1130/G22930A.1

Dzuynski, S. & Smith, A. J. (1963). Convolute lamination, its origin, preservation, and directional significance. Journal of Sedimentary Research 33(3): 616-627. https://doi.org/10.1306/74D70ED4-2B21-11D7-8648000102C1865D

Eisbacher, G. (1985). Late Proterozoic rifting, glacial sedimentation, and sedimentary cycles in the light of Windermere deposition, western Canada. Palaeogeography, Palaeoclimatology, Palaeoecology 51(1-4): 231-254. https://doi.org/10.1016/0031-0182(85)90087-2

Embry, A. (2009). Practical sequence stratigraphy. Canadian Society of Petroleum Geologists 81: 79.

Eyles, C. H., Eyles, N. & Grey, K. (2007). Palaeoclimate implications from deep drilling of Neoproterozoic strata in the Officer Basin and Adelaide Rift Complex of Australia; a marine record of wet-based glaciers. Palaeogeography, Palaeoclimatology, Palaeoecology 248(3-4): 291-312. https://doi.org/10.1016/j.palaeo.2006.12.008

Fairchild, I. J., Bonnand, P., Davies, T., Fleming, E. J., Grassineau, N., Halverson, G. P., Hambrey, M. J., McMillan, E. M., McKay, E., Parkinson, I. J. & Stevenson, C. T. (2016). The Late Cryogenian warm interval, NE Svalbard: chemostratigraphy and genesis. Precambrian Research 281: 128-154. https://doi.org/10.1016/j.precamres.2016.05.013

Fairchild, I. J., Fleming, E. J., Bao, H., Benn, D. I., Boomer, I., Dublyansky, Y. V., Halverson, G. P., Hambrey, M. J., Hendy, C., McMillan, E. A. & Spötl, C. (2016a). Continental carbonate facies of a Neoproterozoic panglaciation, north-east Svalbard. Sedimentology 63(2): 443-497. https://doi.org/10.1111/sed.12252

Fairchild, I. J. & Kennedy, M. J. (2007). Neoproterozoic glaciation in the Earth System. Journal of the Geological Society 164(5): 895-921. https://doi.org/10.1144/0016-76492006-191

Fairchild, I. J., Spencer, A. M., Ali, D. O., Anderson, R. P., Anderton, R., Boomer, I., Dove, D., Evans, J. D., Hambrey, M. J., Howe, J. & Sawaki, Y. (2017). Tonian-Cryogenian boundary sections of Argyll, Scotland. Precambrian Research 319: 37-64. https://doi.org/10.1016/j.precamres.2017.09.020

Fanning, C. M., Ludwig, K. R., Forbes, B. G. & Preiss, W. V. (1986). Single and multiple grain U–Pb zircon analyses for the early Adelaidean Rook Tuff, Willouran Ranges, South Australia. Geological Society of Australia Abstracts 15: 71-72.

Fanning, C. M. & Link, P. K. (2004). U-Pb SHRIMP ages of Neoproterozoic (Sturtian) glaciogenic Pocatello Formation, southeastern Idaho. Geology, 32(10), 881-884. https://doi.org/10.1130/G20609.1

Fielding, C. R. (2006). Upper flow regime sheets, lenses and scour fills: extending the range of architectural elements for fluvial sediment bodies. Sedimentary Geology 190(1-4): 227-240. https://doi.org/10.1016/j.sedgeo.2006.05.009

Fleming, E. J., Benn, D. I., Stevenson, C. T., Petronis, M. S., Hambrey, M. J. & Fairchild, I. J. (2016). Glacitectonism, subglacial and glacilacustrine processes during a Neoproterozoic panglaciation, north-east Svalbard. Sedimentology 63(2): 411-442. https://doi.org/10.1111/sed.12251

Flügel, E. (2010). Microfacies of carbonate rocks: analysis, interpretation and application. Springer Science & Business Media.

Foden, J., Elburg, M., Turner, S., Clark, C., Blades, M. L., Cox, G., Collins, A. S., Wolff, K. & George, C. (2020). Cambro-Ordovician magmatism in the Delamerian orogeny: Implications for tectonic development of the southern Gondwanan margin. Gondwana Research 81: 490-521. https://doi.org/10.1016/j.gr.2019.12.006

Foden, J., Elburg, M. A., Dougherty-Page, J. & Burtt, A. (2006). The timing and duration of the Delamerian Orogeny: correlation with the Ross Orogen and implications for Gondwana assembly. The Journal of Geology 114(2): 189-210. https://doi.org/10.1086/499570

Frank, T. D. & Fielding, C. R. (2003). Marine origin for Precambrian, carbonate-hosted magnesite? Geology 31(12): 1101-1104. https://doi.org/10.1130/G20101.1

Frimmel, H. E., Klötzli, U. S. & Siegfried, P. R. (1996). New Pb-Pb single zircon age constraints on the timing of Neoproterozoic glaciation and continental break-up in Namibia. The Journal of Geology 104(4): 459-469. https://doi.org/10.1086/629839

Fromhold, T. & Wallace, M. (2011). Nature and significance of the Neoproterozoic Sturtian–Marinoan Boundary, Northern Adelaide Geosyncline, South Australia. Australian Journal of Earth Sciences 58(6): 599-613. https://doi.org/10.1080/08120099.2011.579624

Fromhold, T. & Wallace, M. (2012). Regional recognition of the Neoproterozoic Sturtian–Marinoan boundary, northern and central Adelaide Geosyncline, South Australia. Australian Journal of Earth Sciences 59(4): 527-546. https://doi.org/10.1080/08120099.2012.673507

Gehling, J. (2000). Environmental interpretation and a sequence stratigraphic framework for the terminal Proterozoic Ediacara Member within the Rawnsley Quartzite, South Australia. Precambrian Research 100(1-3): 65-95. https://doi.org/10.1016/S0301-9268(99)00069-8

Giddings, J. A., Wallace, M. W. & Woon, E. M. (2009). Interglacial carbonates of the Cryogenian Umberatana Group, northern Flinders Ranges, South Australia. Australian Journal of Earth Sciences 56(7): 907-925. https://doi.org/10.1080/08120090903005378

Giddings, J. A. & Wallace, M. W. (2009a). Facies-dependent δ13C variation from a Cryogenian platform margin, South Australia: Evidence for stratified Neoproterozoic oceans? Palaeogeography, Palaeoclimatology, Palaeoecology 271(3-4): 196-214. https://doi.org/10.1016/j.palaeo.2008.10.011

Giddings, J. A. & Wallace, M. W. (2009b). Sedimentology and C-isotope geochemistry of the 'Sturtian'cap carbonate, South Australia. Sedimentary Geology 216(1-2): 1-14. https://doi.org/10.1016/j.sedgeo.2009.01.007

Gough, A. (2020). Sedimentary Structures. In D. Alderton, & N. Lancaster (Eds.), Encyclopaedia of Geology Elsevier.

Glover, B. & Winchester, J. (1989). The Grampian group: a major Late Proterozoic clastic sequence in the Central Highlands of Scotland. Journal of the Geological Society 146(1): 85-96. https://doi.org/10.1144/gsjgs.146.1.0085

Gómez-Pérez, I., Fernández-Mendiola, P. A. & García-Mondéjar, J. (1999). Depositional architecture of a rimmed carbonate platform

(Albian, Gorbea, western Pyrenees). Sedimentology 46(2): 337-356. https://doi.org/10.1046/j.1365-3091.1999.00217.x

Grey, K., Hill, A. C. & Calver, C. (2011). Biostratigraphy and stratigraphic subdivision of Cryogenian successions of Australia in a global context. Geological Society, London, Memoirs 36(1): 113-134. https://doi.org/10.1144/M36.8

Grotzinger, J. P. & James, N. P. (2000). Precambrian carbonates: evolution of understanding. SEPM Special Publication 67: 3-20.

Grotzinger, J. P. (1990). Geochemical model for Proterozoic stromatolite decline. American Journal of Science, v 290-A, p 80-103

Grotzinger, J. P. (1989). Facies and evolution of Precambrian carbonate depositional systems emergence ofthe modern platform archetype. Controls on Carbonate Platform and Basin Development, SEPM Special Publication 44: 79-106. https://doi.org/10.2110/pec.89.44.0079

Grotzinger, J. P. (1988). Introduction to Precambrian reefs. Reefs Canada and Adjacent Areas Canadian Society of Petroleum Geologists Memoir 13: 30-37

Halverson, G. P., Shen, C., Davies, J. H. & Wu, L. (2022). A Bayesian Approach to Inferring Depositional Ages Applied to a Late Tonian Reference Section in Svalbard. Front. Earth Sci 10: 798739. https://doi.org/10.3389/feart.2022.798739

Halverson, G. P. (2011). Glacial sediments and associated strata of the Polarisbreen Group, northeastern Svalbard. Geological Society, London, Memoirs 36(1): 571-579. http://hdl.handle.net/10214/9436

Halverson, G. P., Kunzmann, M., Strauss, J. V. & Maloof, A. C. (2017). The Tonian-Cryogenian transition in Northeastern Svalbard. Precambrian Research 319: 79-95. https://doi.org/10.1016/j.precamres.2017.12.010

Halverson, G. P., Wade, B. P., Hurtgen, M. T. & Barovich, K. M. (2010). Neoproterozoic chemostratigraphy. Precambrian Research 182(4): 337-350. https://doi.org/10.1016/j.precamres.2010.04.007

Halverson, G. P., Hurtgen, M. T., Porter, S. M. & Collins, A. S. (2009). Neoproterozoic-Cambrian biogeochemical evolution. Developments in Precambrian geology 16: 351-365. https://doi.org/10.1016/S0166-2635(09)01625-9

Halverson, G. P., Hoffman, P. F., Schrag, D. P., Maloof, A. C. & Rice, A. H. N. (2005). Toward a Neoproterozoic composite carbon-isotope record. GSA bulletin 117(9-10): 1181-1207. https://doi.org/10.1130/B25630.1

Halverson, G. P., Maloof, A. C. & Hoffman, P. F. (2004). The Marinoan glaciation (Neoproterozoic) in northeast Svalbard. Basin Research 16(3): 297-324. https://doi.org/10.1111/j.1365-2117.2004.00234.x

Hearon IV, T. E., Rowan, M. G., Lawton, T. G., Hannah, P. T. & Giles, K. A. (2015). Geology and tectonics of Neoproterozoic salt diapirs and salt sheets in the eastern Willouran Ranges, South Australia. Basin Research 27(2): 183–207. https://doi.org/10.1111/bre.12067

Hearon IV, T. E., Rowan, M. G., Giles, K. A., Kernen, R. A., Gannaway, C. E., Lawton, T. F. & Fiduk, J. C. (2015a). Allochthonous salt initiation and advance in the northern Flinders and eastern Willouran ranges, South Australia: Using outcrops to test subsurface-based models from the northern Gulf of Mexico. AAPG Bulletin 99: 293–331. https://doi.org/10.1306/08111414022

Hill, A. & Walter, M. (2000). Mid-Neoproterozoic (~830–750 Ma) isotope stratigraphy of Australia and global correlation. Precambrian Research 100(1-3): 181-211. https://doi.org/10.1016/S0301-9268(99)00074-1

Hoffman, P. (1976). Environmental diversity of Middle Precambrian stromatolites. Developments in Sedimentology, Elsevier. 20: 599-611. https://doi.org/10.1016/S0070-4571(08)71161-0

Hoffman, P. F., Kaufman, A. J., Halverson, G. P. & Schrag, D. P. (1998). A Neoproterozoic snowball earth. Science 281(5381): 1342-1346. 10.1126/science.281.5381.1342

Hoffman, P. F. & Schrag, D. P. (2002). The snowball Earth hypothesis: testing the limits of global change. Terra nova 14(3): 129-155. https://doi.org/10.1046/j.1365-3121.2002.00408.x

Hoffman, P. & Halverson, G. (2008). Otvi Group of the Western Northern Platform, the Eastern Kaoko Zone and the Western Northern Margin Zone. The Geology of Namibia 2008: 69-136. https://hdl.handle.net/2440/54299

Hoffman, P. F., Halverson, G. P., Domack, E. W., Maloof, A. C., Swanson-Hysell, N. L. & Cox, G. M. (2012). Cryogenian glaciations on the southern tropical paleomargin of Laurentia (NE Svalbard and East Greenland), and a primary origin for the upper Russøya (Islay) carbon isotope excursion. Precambrian Research 206: 137-158. https://doi.org/10.1016/j.precamres.2012.02.018

Hoffman, P. F., Lamothe, K. G., LoBianco, S. J., Hodgskiss, M. S., Bellefroid, E. J., Johnson, B. W., Hodgin, E. B. & Halverson, G. P. (2017a). Sedimentary depocenters on snowball Earth: Case studies from the Sturtian Chuos Formation in northern Namibia. Geosphere 13(3): 811-837. https://doi.org/10.1130/GES01457.1

Hoffman, P. F., Abbot, D. S., Ashkenazy, Y., Benn, D. I., Brocks, J. J., Cohen, P. A., Cox, G. M., Creveling, J. R., Donnadieu, Y., Erwin, D. H. & Fairchild, I. J. (2017b). Snowball Earth climate dynamics and Cryogenian geology-geobiology. Science Advances 3(11): e1600983. 10.1126/sciadv.1600983

Hoffman, P. F., Halverson, G. P., Schrag, D. P., Higgins, J. A., Domack, E. W., Macdonald, F. A., Pruss, S. B., Blättler, C. L., Crockford, P. W., Hodgin, E. B. & Bellefroid, E. J. (2021). Snowballs in Africa: sectioning a long-lived Neoproterozoic carbonate platform and its bathyal foreslope (NW Namibia). Earth-Science Reviews 219: 103616. https://doi.org/10.1016/j.earscirev.2021.103616

Hood, A. v.S, Wallace, M. W. & Drysdale, R. N. (2011). Neoproterozoic aragonite-dolomite seas? Widespread marine dolomite precipitation in Cryogenian reef complexes. Geology 39(9): 871-874. https://doi.org/10.1130/G32119.1

Hood, A. v.S, Wallace, M. W., Reed, C. P., Hoffmann, K. H. & Freyer, E. E. (2015). Enigmatic carbonates of the Ombombo Subgroup, Otavi Fold Belt, Namibia: a prelude to extreme Cryogenian anoxia? Sedimentary Geology 324: 12-31. https://doi.org/10.1016/j.sedgeo.2015.04.007

Hood, A. v.S, Planavsky, N. J., Wallace, M. W., Wang, X., Bellefroid, E. J., Gueguen, B. & Cole, D. B. (2016). Integrated geochemical-petrographic insights from component-selective δ238U of Cryogenian marine carbonates. Geology 44(11): 935-938. https://doi.org/10.1130/G38533.1

Hood, A. v.S., Planavsky, N. J., Wallace, M. W. & Wang, X. (2018). The effects of diagenesis on geochemical paleoredox proxies in sedimentary carbonates. Geochimica et Cosmochimica Acta, 232, 265-287. https://doi.org/10.1016/j.gca.2018.04.022

Hood, A. v.S. & Wallace, M. W. (2012). Synsedimentary diagenesis in a Cryogenian reef complex: Ubiquitous marine dolomite precipitation. Sedimentary Geology 255: 56-71. https://doi.org/10.1016/j.sedgeo.2012.02.004

Hood, A. v.S. & Wallace, M. W. (2014). Marine cements reveal the structure of an anoxic, ferruginous Neoproterozoic ocean. Journal of the Geological Society 171(6): 741-744. https://doi.org/10.1144/jgs2013-099

Howchin, W. (1929). Geology of South Australia, Govt. Printer, Adelaide.

Jahnert, R. J. & Collins, L. B. (2012). Characteristics, distribution and morphogenesis of subtidal microbial systems in Shark Bay, Australia. Marine Geology 303: 115-136. https://doi.org/10.1016/j.margeo.2012.02.009

Jobe, Z. R., Lowe, D. R. & Morris, W. R. (2012). Climbing-ripple successions in turbidite systems: depositional environments, sedimentation rates and accumulation times. Sedimentology 59(3): 867-898. https://doi.org/10.1111/j.1365-3091.2011.01283.x

Jorissen, E. L., de Leeuw, A., van Baak, C. G., Mandic, O., Stoica, M., Abels, H. A. & Krijgsman, W. (2018). Sedimentary architecture and depositional controls of a Pliocene river-dominated delta in the semi-isolated Dacian Basin, Black Sea. Sedimentary Geology 368: 1-23. https://doi.org/10.1016/j.sedgeo.2018.03.001

Kaufman, A. J., Knoll, A. H. & Narbonne, G. M. (1997). Isotopes, ice ages, and terminal Proterozoic earth history. Proceedings of the National Academy of Sciences 94(13): 6600-6605. https://doi.org/10.1073/pnas.94.13.6600

Keeley, J. A., Link, P. K., Fanning, C. M. & Schmitz, M. D. (2013). Pre-to synglacial rift-related volcanism in the Neoproterozoic (Cryogenian) Pocatello Formation, SE Idaho: New SHRIMP and CA-ID-TIMS constraints. Lithosphere 5(1): 128-150. https://doi.org/10.1130/L226.1

Kendall, C. G. S. C. & Warren, J. (1987). A review of the origin and setting of tepees and their associated fabrics. Sedimentology 34(6): 1007-1027.

Kennedy, M. J., Runnegar, B., Prave, A. R., Hoffmann, K. H. & Arthur, M. A. (1998). Two or four Neoproterozoic glaciations? Geology 26(12): 1059-1063. https://doi.org/10.1111/j.1365-3091.1987.tb00590.x

Kirschvink, J. L. (1992). Late Proterozoic low-latitude global glaciation: the snowball Earth. The Proterozoic biosphere : a multidisciplinary study. Cambridge University Press , New York, pp. 51-52. ISBN 9780521366151. https://resolver.caltech.edu/CaltechAUTHORS:20130117-100718783

Kneller, B. (1995). Beyond the turbidite paradigm: physical models for deposition of turbidites and their implications for reservoir prediction. Geological Society, London, Special Publications 94(1): 31-49. https://doi.org/10.1144/GSL.SP.1995.094.01.04

Knoll, A. H., Hayes, J. M., Kaufman, A. J., Swett, K. & Lambert, I. B. (1986). Secular variation in carbon isotope ratios from Upper Proterozoic successions of Svalbard and East Greenland. Nature 321(6073): 832-838. https://doi.org/10.1038/321832a0

Kunzmann, M., Crombez, V., Catuneanu, O., Blaikie, T. N., Barth, G. & Collins, A. S. (2020). Sequence stratigraphy of the ca. 1730 Ma Wollogorang Formation, McArthur Basin, Australia. Marine and Petroleum Geology 116: 104297. https://doi.org/10.1016/j.marpetgeo.2020.104297

Kunzmann, M., Halverson, G. P., Scott, C., Minarik, W. G. & Wing, B. A. (2015). Geochemistry of Neoproterozoic black shales from Svalbard: Implications for oceanic redox conditions spanning Cryogenian glaciations. Chemical Geology 417: 383-393. https://doi.org/10.1016/j.chemgeo.2015.10.022

Kunzmann, M., Schmid, S., Blaikie, T. N. & Halverson, G. P. (2019). Facies analysis, sequence stratigraphy, and carbon isotope chemostratigraphy of a classic Zn-Pb host succession: The Proterozoic middle McArthur Group, McArthur Basin, Australia. Ore Geology Reviews 106: 150-175. https://doi.org/10.1016/j.oregeorev.2019.01.011

Lamothe, K. G., Hoffman, P. F., Greenman, J. W. & Halverson, G. P. (2019). Stratigraphy and isotope geochemistry of the pre-Sturtian Ugab Subgroup, Otavi/Swakop Group, northwestern Namibia. Precambrian Research 332: 105387. https://doi.org/10.1016/j.precamres.2019.105387

Lan, Z., Li, X. H., Zhang, Q. & Li, Q. L. (2015). Global synchronous initiation of the 2nd episode of Sturtian glaciation: SIMS zircon U–Pb and O isotope evidence from the Jiangkou Group, South China. Precambrian Research 267: 28-38. https://doi.org/10.1016/j.precamres.2015.06.002

Le Heron, D. P., Busfield, M. E. & Kettler, C. (2021). Ice-rafted dropstones in "postglacial" Cryogenian cap carbonates. Geology 49(3): 263-267. https://doi.org/10.1130/G48208.1

Le Heron, D. P. & Busfield, M. E. (2016). Pulsed iceberg delivery driven by Sturtian ice sheet dynamics: An example from Death Valley, California. Sedimentology 63(2): 331-349. https://doi.org/10.1111/sed.12225

Le Heron, D. P., Busfield, M. E. & Collins, A. S. (2014). Bolla Bollana boulder beds: A Neoproterozoic trough mouth fan in South Australia? Sedimentology 61(4): 978-995. https://doi.org/10.1111/sed.12082

Le Heron, D. P., Busfield, M. E. & Kamona, F. (2013). An interglacial on snowball Earth? Dynamic ice behaviour revealed in the Chuos Formation, Namibia. Sedimentology 60(2): 411-427. https://doi.org/10.1111/j.1365-3091.2012.01346.x

Le Heron, D. P., Cox, G., Trundley, A. & Collins, A. (2011). Sea ice– free conditions during the Sturtian glaciation (early Cryogenian), South Australia. Geology 39(1): 31-34. https://doi.org/10.1130/G31547.1

Le Heron, D. P., Cox, G., Trundley, A. & Collins, A. S. (2011a). Two Cryogenian glacial successions compared: Aspects of the Sturt and Elatina sediment records of South Australia. Precambrian Research 186(1-4): 147-168. https://doi.org/10.1016/j.precamres.2011.01.014

Le Heron, D. P., Eyles, N. & Busfield, M. E. (2020). The Laurentian Neoproterozoic Glacial Interval: reappraising the extent and timing of glaciation. Austrian Journal of Earth Sciences 113(1): 59-70. https://doi.org/10.17738/ajes.2020.0004

Lechte, M. & Wallace M. (2016). Sub–ice shelf ironstone deposition during the Neoproterozoic Sturtian glaciation. Geology 44(11): 891-894. https://doi.org/10.1130/G38495.1

Lechte, M. A. & Wallace M. (2015). Sedimentary and tectonic history of the Holowilena Ironstone, a Neoproterozoic iron formation in South Australia. Sedimentary Geology 329: 211-224. https://doi.org/10.1016/j.sedgeo.2015.09.014

Legros, F. (2002). Can dispersive pressure cause inverse grading in grain flows? Journal of Sedimentary Research 72(1): 166-170. https://doi.org/10.1306/041301720166

Lenton, T. M., Boyle, R. A., Poulton, S. W., Shields-Zhou, G. A. & Butterfield, N. J. (2014). Co-evolution of eukaryotes and ocean oxygenation in the Neoproterozoic era. Nature Geoscience 7(4): 257-265. https://doi.org/10.1038/ngeo2108

Lewis, J. P., Weaver, A. J. & Eby, M. (2007). Snowball versus slushball Earth: Dynamic versus nondynamic sea ice?. Journal of Geophysical Research: Oceans, 112(C11): 1-8. https://doi.org/10.1029/2006JC004037

Li, Z. X., Bogdanova, S., Collins, A. S., Davidson, A., De Waele, B., Ernst, R. E., Fitzsimons, I. C. W., Fuck, R. A., Gladkochub,

D. P., Jacobs, J. & Karlstrom, K. E. (2008). Assembly, configuration, and break-up history of Rodinia: a synthesis. Precambrian Research 160(1-2): 179-210. https://doi.org/10.1016/j.precamres.2007.04.021

Li, Z. X., Li, X., Kinny, P., Wang, J., Zhang, S. & Zhou, H. (2003). Geochronology of Neoproterozoic syn-rift magmatism in the Yangtze Craton, South China and correlations with other continents: evidence for a mantle superplume that broke up Rodinia. Precambrian Research 122(1-4): 85-109. https://doi.org/10.1016/S0301-9268(02)00208-5

Link, P. K. & Gostin, V. A. (1981). Facies and paleogeography of Sturtian glacial strata (late Precambrian), South Australia. American Journal of Science 281(4): 353-374. https://doi.org/10.2475/ajs.281.4.353

Link, P. K. (1994). Glacial-marine facies in a continental rift environment: Neoproterozoic rocks of the western United States Cordillera. Earth's Glacial Record: 29-46.

Lloyd, J. C., Blades, M. L., Counts, J. W., Collins, A. S., Amos, K. J., Wade, B. P., Hall, J. W., Hore, S., Ball, A. L., Shahin, S. & Drabsch, M. (2020). Neoproterozoic geochronology and provenance of the Adelaide Superbasin. Precambrian Research 350: 105849. https://doi.org/10.1016/j.precamres.2020.105849

Lloyd, J. C., Collins, A. S., Blades, M. L., Gilbert, S. E. & Amos, K. J. (2022). Early Evolution of the Adelaide Superbasin. Geosciences 12(4): 154. https://doi.org/10.3390/geosciences12040154

Lloyd, J. C., Preiss, W. V., Collins, A. S., Virgo, G. M., Blades, M. L., Gilbert, S. E. & Amos, K. J. (2023). Geochronology and formal stratigraphy of the Sturtian Glaciation in the Adelaide Superbasin. Geological Magazine: 1-24. https://doi.org/10.1017/S0016756823000390

Long, D. & Turner, E. (2013). Formal definition of the Neoproterozoic Mackenzie Mountains Supergroup (Northwest Territories), and formal stratigraphic nomenclature for terrigenous clastic units of the Katherine Group. Geological Survey of Canada.

Lowe, D. R. (1982). Sediment gravity flows; II, Depositional models with special reference to the deposits of high-density turbidity currents. Journal of Sedimentary Research 52(1): 279-297. https://doi.org/10.1306/212F7F31-2B24-11D7-8648000102C1865D

Lund, K., Aleinikoff, J. N., Evans, K. V. & Fanning, C. M. (2003). SHRIMP U-Pb geochronology of Neoproterozoic Windermere Supergroup, central Idaho: Implications for rifting of western Laurentia and synchroneity of Sturtian glacial deposits. Geological Society of America Bulletin 115(3): 349-372. https://doi.org/10.1130/0016-7606(2003)115<0349:SUPGON>2.0.CO;2

Maciaszek, P., Chomiak, L., Wachocki, R. & Widera, M. (2019). The interpretative significance of ripple-derived sedimentary structures within an upper Neogene fluvial succession of central Poland. Geologos 25: 1-13. 10.2478/logos-2019-0001

Maloof, A. C., Halverson, G. P., Kirschvink, J. L., Schrag, D. P., Weiss, B. P. & Hoffman, P. F. (2006). Combined paleomagnetic, isotopic, and stratigraphic evidence for true polar wander from the Neoproterozoic Akademikerbreen Group, Svalbard, Norway. Geological Society of America Bulletin 118(9-10): 1099-1124. https://doi.org/10.1130/B25892.1

Mawson, D. & Sprigg, R. (1950). Subdivision of the Adelaide system. Australian Journal of Science 13(3): 69-72.

McKirdy, D. M., Burgess, J. M., Lemon, N. M., Yu, X., Cooper, A. M., Gostin, V. A., Jenkins, R. J. & Both, R. A. (2001). A chemostratigraphic overview of the late Cryogenian interglacial sequence in the Adelaide Fold-Thrust Belt, South Australia. Precambrian Research 106(1-2): 149-186. https://doi.org/10.1016/S0301-9268(00)00130-3

McMahon, Hood, A. v.S. & McIlroy, D. (2017). The origin and occurrence of subaqueous sedimentary cracks. Geological Society, London, Special Publications 448(1): 285-309. https://doi.org/10.1144/SP448.15

Melezhik, V. A., Fallick, A. E., Medvedev, P. V. & Makarikhin, V. V. (2001). Palaeoproterozoic magnesite: lithological and isotopic evidence for playa/sabkha environments. Sedimentology 48(2): 379-397. https://doi.org/10.1046/j.1365-3091.2001.00369.x

Merdith, A. S., Collins, A. S., Williams, S. E., Pisarevsky, S., Foden, J. D., Archibald, D. B., Blades, M. L., Alessio, B. L., Armistead, S., Plavsa, D. & Clark, C. (2017). A full-plate global reconstruction of the Neoproterozoic. Gondwana Research 50: 84-134. https://doi.org/10.1016/j.gr.2017.04.001

Merdith, A. S., Williams, S. E., Brune, S., Collins, A. S. & Müller, R. D. (2019). Rift and plate boundary evolution across two supercontinent cycles. Global and planetary change 173: 1-14. https://doi.org/10.1016/j.gloplacha.2018.11.006

Merdith, A. S., Williams, S. E., Collins, A. S., Tetley, M. G., Mulder, J. A., Blades, M. L., Young, A., Armistead, S. E., Cannon, J., Zahirovic, S. & Müller, R. D. (2021). Extending full-plate tectonic models into deep time: Linking the Neoproterozoic and the Phanerozoic. Earth-Science Reviews 214: 103477. https://doi.org/10.1016/j.earscirev.2020.103477

Middleton, G. V. (1976). Subaqueous sediment transport and deposition by sediment gravity flows. Marine sediment transport and environment management.

Miller, N. R., Avigad, D., Stern, R. J. & Beyth, M. (2011). The Tambien Group, Northern Ethiopia (Tigre). Geological Society, London, Memoirs 36(1): 263-276. https://doi.org/10.1144/M36.21

Miller, N. R., Stern, R. J., Avigad, D., Beyth, M. & Schilman, B. (2009). Cryogenian slate-carbonate sequences of the Tambien Group, Northern Ethiopia (I): Pre-"Sturtian" chemostratigraphy and regional correlations. Precambrian Research 170(3-4): 129-156. https://doi.org/10.1016/j.precamres.2008.12.004

Miller, R. M. (2013). Comparative stratigraphic and geochronological evolution of the Northern Damara Supergroup in Namibia and the Katanga Supergroup in the Lufilian Arc of Central Africa. Geoscience Canada 40(2): 118-140. http://dx.doi.org/10.12789/geocanj.2013.40.007

Millikin, A. E., Strauss, J. V., Halverson, G. P., Bergmann, K. D., Tosca, N. J. & Rooney, A. D. (2022). Calibrating the Russøya excursion in Svalbard, Norway, and implications for Neoproterozoic chronology. Geology: 50(40), 506-510. https://doi.org/10.1130/G49593.1

Milton, J. E., Hickey, K. A., Gleeson, S. A. & Friedman, R. M. (2017). New U-Pb constraints on the age of the Little Dal Basalts and Gunbarrel-related volcanism in Rodinia. Precambrian Research 296: 168-180. https://doi.org/10.1016/j.precamres.2017.04.030

Momta, P. S., Omoboh, J. O. & Odigi, M. I. (2015). Sedimentology and depositional environment of D2 sand in part of greater ughelli depobelt, onshore Niger Delta, Nigeria. American Journal of Engineering and Applied Sciences 8(4): 556.

Moretti, M., Soria, J. M., Alfaro, P. & Walsh, N. (2001). Asymmetrical soft-sediment deformation structures triggered by rapid sedimentation in turbiditic deposits (Late Miocene, Guadix Basin, Southern Spain). Facies, 44(1), 283-294. https://doi.org/10.1007/BF02668179

De Mowbray, T. & Visser, M. J. (1984). Reactivation surfaces in subtidal channel deposits, Oosterschelde, southwest Netherlands.

Journal of Sedimentary Research, 54(3), 811-824. https://doi.org/10.1306/212F8503-2B24-11D7-8648000102C1865D

Mur, J. P. & Urpinell, M. I. (1987). Magnesite formation in recent playa lakes, Los Monegros, Spain. Geological Society, London, Special Publications 36(1): 119-122. https://doi.org/10.1144/GSL.SP.1987.036.01.10

Narbonne, G. M., Kaufman, A. J. & Knoll, A. H. (1994). Integrated chemostratigraphy and biostratigraphy of the Windermere Supergroup, northwestern Canada: Implications for Neoproterozoic correlations and the early evolution of animals. Geological Society of America Bulletin 106(10): 1281-1292. https://doi.org/10.1130/0016-7606(1994)106<1281:ICABOT>2.3.CO;2

Narbonne, G. M. & Aitken, J. D. (1995). Neoproterozoic of the mackenzie mountains, Northwestern Canada. Precambrian Research 73(1-4): 101-121. https://doi.org/10.1016/0301-9268(94)00073-Z

Nelson, L. L., Smith, E. F., Hodgin, E. B., Crowley, J. L., Schmitz, M. D. & Macdonald, F. A. (2020). Geochronological constraints on Neoproterozoic rifting and onset of the Marinoan glaciation from the Kingston Peak Formation in Death Valley, California (USA). Geology 48(11): 1083-1087. https://doi.org/10.1130/G47668.1

Nelson, L. L., Ahm, A. S. C., Macdonald, F. A., Higgins, J. A. & Smith, E. F. (2021). Fingerprinting local controls on the Neoproterozoic carbon cycle with the isotopic record of Cryogenian carbonates in the Panamint Range, California. Earth and Planetary Science Letters 566: 116956. https://doi.org/10.1016/j.epsl.2021.116956

Nelson, T. R. & Voulgaris, G. (2014). Temporal and spatial evolution of wave-induced ripple geometry: Regular versus irregular ripples. Journal of Geophysical Research: Oceans, 119(2): 664-688. https://doi.org/10.1002/2013JC009020

Nøttvedt, A. & Kreisa, R. (1987). Model for the combined-flow origin of hummocky cross-stratification. Geology 15(4): 357-361. https://doi.org/10.1130/0091-7613(1987)15<357:MFTCOO>2.0.CO;2

O'Connell, B., Wallace, M. W., Hood, A. v.S, Lechte, M. A. & Planavsky, N. J. (2020). Iron-rich carbonate tidal deposits, Angepena Formation, South Australia: A redox-stratified Cryogenian basin. Precambrian Research, 342, 105668. https://doi.org/10.1016/j.precamres.2020.105668

Owen, G. (2003). Load structures: gravity-driven sediment mobilization in the shallow subsurface. Geological Society, London, Special Publications, 216(1), 21-34. https://doi.org/10.1144/GSL.SP.2003.216.01.03

Park, J. K. & Jefferson, C. W. (1991). Magnetic and tectonic history of the Late Proterozoic Upper Little Dal and Coates Lake groups of northwestern Canada. Precambrian Research 52(1-2): 1-35. https://doi.org/10.1016/0301-9268(91)90011-X

Park, Y., Swanson-Hysell, N. L., MacLennan, S. A., Maloof, A. C., Gebreslassie, M., Tremblay, M. M., Schoene, B., Alene, M., Anttila, E. S., Tesema, T. & Haileab, B. (2020). The lead-up to the Sturtian Snowball Earth: Neoproterozoic chemostratigraphy time-calibrated by the Tambien Group of Ethiopia. Bulletin 132(5-6): 1119-1149. https://doi.org/10.1130/B35178.1

Pflueger, F. (1999). Matground structures and redox facies. Palaios 14(1): 25-39. https://doi.org/10.2307/3515359

Plummer, P. & Gostin, V. (1981). Shrinkage cracks; desiccation or synaeresis? Journal of Sedimentary Research 51(4): 1147-1156. https://doi.org/10.1306/212F7E4B-2B24-11D7-8648000102C1865D

Pomar, L. (2001). Types of carbonate platforms: a genetic approach. Basin Research 13(3): 313-334. https://doi.org/10.1046/j.0950-091x.2001.00152.x

Postma, G. (1983). Water escape structures in the context of a depositional model of a mass flow dominated conglomeratic fan-delta (Abrioja Formation, Pliocene, Almeria Basin, SE Spain). Sedimentology, 30(1), 91-103. https://doi.org/10.1111/j.1365-3091.1983.tb00652.x

Powell, C. M., Preiss, W. V., Gatehouse, C. G., Krapez, B. & Li, Z. X. (1994). South Australian record of a Rodinian epicontinental basin and its mid-Neoproterozoic breakup (~700 Ma) to form the Palaeo-Pacific Ocean. Tectonophysics 237(3-4): 113-140. https://doi.org/10.1016/0040-1951(94)90250-X

Powell, R. & Domack, G. W. (2002). Modern glaciomarine environments. Modern and past glacial environments, Elsevier: 361-389. https://doi.org/10.1016/B978-075064226-2/50015-5

Powers, D. W. & Holt, R. M. (2000). The salt that wasn't there: Mudflat facies equivalents to halite of the Permian Rustler Formation, southeastern New Mexico. Journal of Sedimentary Research 70(1): 29-36. https://doi.org/10.1306/2DC408FB-0E47-11D7-8643000102C1865D

Preiss, W. V. (1973). Palaeoecological interpretations of South Australian Precambrian stromatolites. Journal of the Geological Society of Australia 19(4): 501-532. https://doi.org/10.1080/00167617308728820

Preiss, W. V. (1987). The Adelaide Geosyncline: Late Proterozoic stratigraphy, sedimentation, palaeontology and tectonics. Department of Mines and Energy.

Preiss, W. V., Drexel, J. F. & Parker, A. J. (1993). The Geology of South Australia: The Precambrian (Vol. 1): Mines and Energy, South Australia, Geological Survey of South Australia.

Preiss, W., Dyson, I., Reid, P. & Cowley, W. (1998). Revision of lithostratigraphic classification of the Umberatana Group. MESA Journal, 9, 36-42.

Preiss, W. & Cowley, W. (1999). Genetic stratigraphy and revised lithostratigraphic classification of the Burra Group in the Adelaide Geosyncline. MESA Journal 14: 30-40.

Preiss, W. (2000). The Adelaide Geosyncline of South Australia and its significance in Neoproterozoic continental reconstruction. Precambrian Research 100(1-3): 21-63. https://doi.org/10.1016/S0301-9268(99)00068-6

Preiss, W. V., Drexel, J. F. & Reid, A. J. (2009). Definition and age of the Kooringa Member of the Skillogalee Dolomite: host for Neoproterozoic (c. 790 Ma) porphyry related copper mineralisation at Burra. MESA Journal 55: 19-33.

Preiss, W. V., Gostin, V. A., McKirdy, D. M., Ashley, P. M., Williams, G. E. & Schmidt, P. W. (2011). Chapter 69 The glacial succession of Sturtian age in South Australia: the Yudnamutana Subgroup. Geological Society, London, Memoirs 36(1): 701-712. https://doi.org/10.1144/M36.69

Reading, H. G. (2009). Sedimentary environments: processes, facies and stratigraphy. John Wiley & Sons.

Reading, H. G. & Richards, M. (1994). Turbidite systems in deep-water basin margins classified by grain size and feeder system. AAPG bulletin 78(5): 792-822. https://doi.org/10.1306/A25FE3BF-171B-11D7-8645000102C1865D

Reineck, H. E. & Wunderlich, F. (1968). Classification and origin of flaser and lenticular bedding. Sedimentology 11(1-2): 99-104. https://doi.org/10.1111/j.1365-3091.1968.tb00843.x

Rowan, M. G., Hearon IV, T. E., Kernen, R. A., Giles, K. A., Gannaway-Dalton, C. E., Williams, N. J., Fiduk, J. C., Lawton,

T. F., Hannah, P. T. & Fischer, M. P. (2020). A review of allochthonous salt tectonics in the Flinders and Willouran ranges, South Australia. Australian Journal of Earth Sciences 67(6): 787-813. https://doi.org/10.1080/08120099.2018.1553063

Schidlowski, M. (1988). A 3,800-million-year isotopic record of life from carbon in sedimentary rocks. Nature 333(6171): 313-318. https://doi.org/10.1038/333313a0

Segnit, R. W. (1939). The Pre-Cambrian-Cambrian Succession: The General and Economic Geology of These Systems, in Portions of South Australia. Frank Trigg, government printer. 10.1086/624923

Shanmugam, G. (1997). The Bouma sequence and the turbidite mind set. Earth-Science Reviews 42(4): 201-229. https://doi.org/10.1016/S0012-8252(97)81858-2

Shanmugam, G. (2000). 50 years of the turbidite paradigm (1950s—1990s): deep-water processes and facies models—a critical perspective. Marine and Petroleum Geology 17(2): 285-342. https://doi.org/10.1016/S0264-8172(99)00011-2

Shanmugam, G. (2017). Global case studies of soft-sediment deformation structures (SSDS): Definitions, classifications, advances, origins, and problems. Journal of Palaeogeography 6(4): 251-320. https://doi.org/10.1016/j.jop.2017.06.004

Shields-Zhou, G. & Och, L. (2011). The case for a Neoproterozoic oxygenation event: geochemical evidence and biological consequences. GSA Today 21(3): 4-11. http://dx.doi.org/10.1130/GSATG102A.1

Shinn, E. A. (1969). Submarine lithification of Holocene carbonate sediments in the Persian Gulf. Sedimentology 12(1-2): 109-144. https://doi.org/10.1111/j.1365-3091.1969.tb00166.x

Shuster, A. M., Wallace, M. W., van Smeerdijk Hood, A. & Jiang, G. (2018). The Tonian Beck Spring Dolomite: Marine dolomitization in a shallow, anoxic sea. Sedimentary Geology 368: 83-104. https://doi.org/10.1016/j.sedgeo.2018.03.003

Smith, M., Robertson, S. & Rollin, K. E. (1999). Rift basin architecture and stratigraphical implications for basement-cover relationships in the Neoproterozoic Grampian Group of the Scottish Caledonides. Journal of the Geological Society 156(6): 1163-1173. https://doi.org/10.1144/gsjgs.156.6.1163

Spencer, A. M. & Spencer, M. O. (1972). The Late Precambrian/Lower Cambrian Bonahaven Dolomite of Islay and its stromatolites. Scottish Journal of Geology 8(3): 269-282. https://doi.org/10.1144/sjg08030269

Stephenson, D., Mendum, J. R., Fettes, D. J. & Leslie, A. G. (2013). The Dalradian rocks of Scotland: an introduction. Proceedings of the Geologists' Association 124(1-2): 3-82. https://doi.org/10.1016/j.pgeola.2012.06.002

Stow, D. A. & Mayall, M. (2000). Deep-water sedimentary systems: New models for the 21st century. Marine and Petroleum Geology 17(2): 125-135. https://doi.org/10.1016/S0264-8172(99)00064-1

Strachan, L. J. (2008). Flow transformations in slumps: a case study from the Waitemata Basin, New Zealand. Sedimentology, 55(5), 1311-1332. https://doi.org/10.1111/j.1365-3091.2007.00947.x

Stromberg, S. G. & Bluck, B. (1998). Turbidite facies, fluid-escape structures and mechanisms of emplacement of the Oligo-Miocene Aljibe Flysch, Gibraltar Arc, Betics, southern Spain. Sedimentary Geology 115(1-4): 267-288. https://doi.org/10.1016/S0037-0738(97)00096-1

Swanson-Hysell, N. L., Maloof, A. C., Condon, D. J., Jenkin, G. R., Alene, M., Tremblay, M. M., Tesema, T., Rooney, A. D. & Haileab, B. (2015). Stratigraphy and geochronology of the Tambien Group, Ethiopia: Evidence for globally synchronous carbon isotope change in the Neoproterozoic. Geology 43(4): 323-326. https://doi.org/10.1130/G36347.1

Talling, P. J., Masson, D. G., Sumner, E. J. & Malgesini, G. (2012). Subaqueous sediment density flows: Depositional processes and deposit types. Sedimentology 59(7): 1937-2003. https://doi.org/10.1111/j.1365-3091.2012.01353.x

Tanner, P. (1998). Interstratal dewatering origin for polygonal patterns of sand-filled cracks: a case study from late Proterozoic metasediments of Islay, Scotland. Sedimentology 45(1): 71-89. https://doi.org/10.1046/j.1365-3091.1998.00135.x

Thomson, B. P., Coats, R. P., Mirams, R. C., Forbes, B. G., Dalgarno, C. R. & Johnson, J. E. (1964). Precambrian rock groups in the Adelaide Geosyncline: a new subdivision. Quarterly Journal of the Geological Survey of South Australia 9: 1-19.

Thomson, D., Rainbird, R. H. & Dix, G. (2014). Architecture of a Neoproterozoic intracratonic carbonate ramp succession: Wynniatt Formation, Amundsen basin, Arctic Canada. Sedimentary Geology 299: 119-138. https://doi.org/10.1016/j.sedgeo.2013.11.005

Thorie, A., Mukhopadhyay, A., Mazumdar, P. & Banerjee, T. (2020). Characteristics of a Tonian reef rimmed shelf before the onset of Cryogenian: Insights from Neoproterozoic Kunihar Formation, Simla Group, Lesser Himalaya. Marine and Petroleum Geology 117: 104393. https://doi.org/10.1016/j.marpetgeo.2020.104393

Tinterri, R., Magalhaes, P. M., Tagliaferri, A. & Cunha, R. S. (2016). Convolute laminations and load structures in turbidites as indicators of flow reflections and decelerations against bounding slopes. Examples from the Marnoso-arenacea Formation (northern Italy) and Annot Sandstones (south eastern France). Sedimentary Geology 344: 382-407. https://doi.org/10.1016/j.sedgeo.2016.01.023

Tucker, M. E. (1982). Precambrian dolomites: petrographic and isotopic evidence that they differ from Phanerozoic dolomites. Geology 10(1): 7-12. https://doi.org/10.1130/0091-7613(1982)10<7:PDPAIE>2.0.CO;2

Tucker, M. (1985). Shallow-marine carbonate facies and facies models. Geological Society, London, Special Publications 18(1): 147-169. https://doi.org/10.1144/GSL.SP.1985.018.01.08

Tucker, M. E. & Wright, V. P. (2009). Carbonate sedimentology. John Wiley & Sons.

Uppill, R. K. (1980). Sedimentology of the late Precambrian Mundallio Subgroup: a clastic-carbonate (Dolomite, Magnesite) sequence in the Mt. Lofty and Flinders Ranges, South Australia. Doctoral dissertation. https://hdl.handle.net/2440/37784

Vakarelov, B. K. & Ainsworth, R. B. (2013). A hierarchical approach to architectural classification in marginal-marine systems: Bridging the gap between sedimentology and sequence stratigraphyHierarchical Marginal-Marine Architectural Classification. AAPG bulletin 97(7): 1121-1161. https://doi.org/10.1306/11011212024

Virgo, G. M., Collins, A. S., Amos, K. J., Farkaš, J., Blades, M. L. & Subarkah, D. (2021). Descending into the "snowball": High resolution sedimentological and geochemical analysis across the Tonian to Cryogenian boundary in South Australia. Precambrian Research 367: 106449. https://doi.org/10.1016/j.precamres.2021.106449

Von der Borch, C. & Lock, D. (1979). Geological significance of Coorong dolomites. Sedimentology 26: 813-824. https://doi.org/10.1111/j.1365-3091.1979.tb00974.x

Wallace, M. W., Hood, A. v.S, Woon, E. M., Giddings, J. A. & Fromhold, T. A. (2015). The Cryogenian Balcanoona reef complexes of the Northern Flinders Ranges: implications for Neoproterozoic ocean chemistry. Palaeogeography, Palaeoclimatology, Palaeoecology 417: 320-336. https://doi.org/10.1016/j.palaeo.2014.09.028

Wang, J. & Li, Z. X. (2001). Sequence stratigraphy and evolution of the Neoproterozoic marginal basins along southeastern Yangtze Craton, South China. Gondwana Research 4(1): 17-26. https://doi.org/10.1016/S1342-937X(05)70651-1

Wanless, H. R., Tedesco, L. P. & Tyrrell, K. M. (1988). Production of subtidal tubular and surficial tempestites by hurricane Kate, Caicos Platform, British West Indies. Journal of Sedimentary Research 58(4): 739-750. https://doi.org/10.1306/212F8E31-2B24-11D7-8648000102C1865D

Warren, J. K. (1990). Sedimentology and mineralogy of dolomitic Coorong lakes, South Australia. Journal of Sedimentary Research 60(6): 843-858. https://doi.org/10.1306/212F929B-2B24-11D7-8648000102C1865D

Wilmsen, M., Berensmeier, M., Fürsich, F. T., Majidifard, M. R. & Schlagintweit, F. (2018). A Late Cretaceous epeiric carbonate platform: the Haftoman Formation of central Iran. Facies 64(2): 11. https://doi.org/10.1007/s10347-018-0523-6

Winsemann, J., Hornung, J. J., Meinsen, J., Asprion, U., Polom, U., Brandes, C., Bußmann, M. & Weber, C. (2009). Anatomy of a subaqueous ice-contact fan and delta complex, Middle Pleistocene, North-west Germany. Sedimentology 56(4): 1041-1076. https://doi.org/10.1111/j.1365-3091.2008.01018.x

Wright, V. (1984). Peritidal carbonate facies models: a review. Geological Journal 19(4): 309-325. https://doi.org/10.1002/gj.3350190402

Yawar, Z. & Schieber, J. (2017). On the origin of silt laminae in laminated shales. Sedimentary Geology 360: 22-34. https://doi.org/10.1016/j.sedgeo.2017.09.001

Young, G. & Gostin, V. (1988). Stratigraphy and sedimentology of Sturtian glacigenic deposits in the western part of the North Flinders Basin, South Australia. Precambrian Research 39(3): 151-170. https://doi.org/10.1016/0301-9268(88)90040-X

Young, G. & Gostin, V. (1990). Sturtian glacial deposition in the vicinity of the Yankaninna Anticline, north Flinders Basin, south Australia. Australian Journal of Earth Sciences 37(4): 447-458. https://doi.org/10.1080/08120099008727944

Young, G. & Gostin, V. (1991). Late Proterozoic (Sturtian) succession of the North Flinders Basin, South Australia: an example of temperate glaciation in an active rift setting. Glacial Marine Sedimentation: Paleoclimatic Significance 261: 207-222.

Yu, W., Algeo, T. J., Zhou, Q., Du, Y. & Wang, P. (2020). Cryogenian cap carbonate models: A review and critical assessment. Palaeogeography, Palaeoclimatology, Palaeoecology 552: 109727. https://doi.org/10.1016/j.palaeo.2020.109727

Zhang, Q. R., Chu, X. L. & Feng, L. J. (2011). Neoproterozoic glacial records in the Yangtze Region, China. Geological Society, London, Memoirs 36(1): 357-366.

Zhang, S., Jiang, G. & Han, Y. (2008). The age of the Nantuo Formation and Nantuo glaciation in South China. Terra Nova 20(4): 289-294. https://doi.org/10.1111/j.1365-3121.2008.00819.x

How to cite: Virgo, G. M., Collins, A. S., Blades, M. L., & Amos, K. J. (2023). Tectonic, eustatic and climate controls on facies architecture during the transition to the Neoproterozoic icehouse in the Adelaide Superbasin, Australia. Sedimentologika, 1(1), 1-38. https://doi.org/10.57035/journals/sdk.2023.e11.1083